The Atmospheric Response to Arctic Sea Ice Loss in the Coupled Climate System

by

Russell Blackport

A thesis submitted in conformity with the requirements
for the degree of Doctor of Philosophy

Department of Physics
University of Toronto

The Atmospheric Response to Arctic Sea Ice Loss in the Coupled Climate System

Russell Blackport

Doctor of Philosophy

Department of Physics
University of Toronto

2017

Abstract

Arctic sea ice loss is expected to have a large impact on the atmosphere, both in the Arctic and potentially outside the Arctic, through changing the atmospheric circulation. In this thesis, the impact of sea ice loss in the climate system is studied using multi-century coupled Earth system model simulations that include dynamical coupling between oceans, atmosphere, and sea ice. In these simulations, sea ice is artificially melted by reducing its albedo. This framework allows for adequate sampling of the isolated impacts of sea ice loss when potentially important ocean feedbacks are included. It is shown that in response to sea ice loss, the atmospheric circulation response is weak compared with internal variability. There is a large reduction in temperature variability on all timescales over the Arctic Ocean. Smaller magnitude reductions in variability are also seen in mid-latitude temperature, sea level pressure and mid-tropospheric geopotential height.

The impacts of sea ice loss are isolated from the impacts of warming at low-latitudes in the sea ice albedo forced simulations and simulations forced by projected greenhouse-dominated radiative forcing using a pattern scaling method. It is found that many of the wintertime atmospheric circulation responses that occur in response to sea ice loss are opposed and at least partially cancelled out by the impacts of low-latitude warming. However, both sea ice loss and

low-latitude surface warming act in concert to reduce subseasonal temperature variability throughout the mid and high latitudes.

Finally, the cause of the previously documented amplified response to sea ice loss in the coupled climate system is investigated. Atmospheric general circulation modelling (AGCM) experiments are performed that show that ocean warming in the mid-to-high latitudes induced by sea ice loss amplifies the atmospheric circulation response. The impact of the ocean warming that occurs in regions away from the sea ice loss region is similar in magnitude and structure to the impacts of sea ice loss itself, indicating modelling experiments that do not include ocean feedbacks will underestimate the response.

Acknowledgments

I am particularly grateful to my supervisor Prof Paul Kushner. Paul has always been willing to provide advice and guidance that has made the research in this thesis possible and aided me in becoming a better scientist. He has also generously supported me to attend conferences and workshops to present my work and meet other researchers from around the world.

I am also grateful to my committee members, Prof Dylan Jones and Prof Kimberly Strong for their thoughtful suggestions at the regular committee meetings. I would also like to thank my external examiner, Marika Holland, for providing constructive criticism that improved this thesis.

I would like to thank the many fellow students and postdocs in the Atmospheric Physics group for making my time at University of Toronto productive and enjoyable. I am particularly grateful to Lawrence Mudryk, for his help with CESM and SciNet. I am also thankful towards Oliver Watt-Meyer, Melanie Cooke, Robert Fajber, Fred Laliberte, Neil Tandon, Ellen Dyer and others for their thoughtful discussions at group meetings, around the department, or at the pub.

Finally, thanks to my parents Ray and Joanne, and my brothers, Darryl and Graham for their support. In particular, I would like to thank my father for instilling in me my love for science.

Table of Contents

List of Tables

List of Figures

Chapter 1
Introduction

1.1 Preface

The rapidly melting sea ice in the Arctic (Stroeve et al. 2012) is one of the most iconic impacts of the warming climate. Not only is the melting ice an indicator of climate change, it also impacts the atmosphere by profoundly changing many aspects of the surface energy budget. Sea ice loss is one of the primary causes of Arctic amplification – the greater warming of the Arctic compared to the global average (Holland and Bitz 2003; Screen and Simmonds 2010; Screen et al. 2012). While the impacts in the Arctic are expected to be large, sea ice loss also has the potential to impact the climate and weather outside the Arctic through changing the atmospheric circulation. There has been some evidence that circulation changes resulting from sea ice loss has already had impacts on extreme weather events in North America, Europe and Asia (Francis and Vavrus 2012; Cohen et al. 2014), however this evidence is controversial (Screen and Simmonds 2013; Barnes 2013; Barnes and Screen 2015). It is difficult to understand these impacts from observations alone as the amount of internal variability in the atmosphere is large, the observational record is short, and it is difficult to isolate the impacts of sea ice loss from other processes. These issues can be overcome by performing modelling experiments using models with various levels of complexity. Typically, this is done by forcing an Atmospheric General Circulation Model (AGCM) with fixed sea surface temperatures (SSTs) and fixed high and low sea ice concentrations (SICs) and examining the differences (e.g. Deser et al. 2010; Screen et al. 2013; Peings and Magnusdottir 2014). By fixing the SSTs, however, these experiments ignore potentially important thermodynamic and dynamic feedbacks with the ocean. Only a few studies have been performed that look at how the atmosphere responds to sea ice when coupling to the ocean is included (Scinocca et al. 2009; Deser et al. 2015,2016).

This thesis expands our understanding of how the atmosphere responds to sea ice loss by using very long (multi-centennial) simulations of a coupled model (i.e. a climate model that uses a full dynamical ocean and sea ice model coupled to an atmosphere and land model). The impacts of sea ice loss are isolated by artificially reducing the sea ice albedo, allowing the ice to absorb more sunlight, while keeping other parameters and boundary conditions constant. Observational analysis looking for some of the proposed changes in atmospheric variability due

to sea ice loss have significant uncertainties owing to internal variability, so these very long simulations allow for a clean, detailed, and well sampled quantitative analysis. It is shown in Chapter 2 that there is a general reduction of variability throughout the atmosphere on all timescales, which contradicts what some previous studies have suggested. Chapter 2 also utilises a number of shorter simulations with reduced sea ice to examine how the response differs from the initial transient period to the final equilibrated period.

In Chapter 3, the reduced sea ice albedo simulations are used in conjunction with additional simulations using the same models, but in this case forced with the projected effects of climate change, which are dominated by increases in greenhouse gas concentrations. One of the impacts of forcing sea ice loss in the coupled climate system that is not seen in prescribed sea ice and SST experiments is that there is modest tropical warming that is part of a "mini" global warming response (Deser et al. 2015). A pattern scaling technique is developed that separates the impacts of sea ice loss from the impacts that are due to warming at low-latitudes. It is found that the atmospheric circulation response to sea ice loss and low-latitude warming generally oppose each other and at least partially cancel. Many of the atmospheric circulation responses that are seen in the sea ice albedo forcing experiments are not seen in the simulations that are forced with projected greenhouse gas increase due to these cancellation effects.

Finally, Chapter 4 addresses the cause of some of the differences in the extratropical response between the coupled and prescribed sea ice and SST experiments. From the results of Chapter 3, it may be expected that the tropical warming seen in coupled model sea ice loss experiments helps to cancel out the atmospheric circulation response, resulting in a weaker response than in the prescribed sea ice and SST experiments. However, Deser et al. (2015,2016), find in fact that coupling to the ocean enhances the circulation response, suggesting that other mechanisms are at play. In Chapter 4, using AGCM experiments with prescribed sea ice and SST experiments, it is shown that the extratropical ocean warming that occurs in response to sea ice loss enhances the atmospheric circulation response in the coupled climate system.

The atmospheric response to sea ice loss is a complex and well-studied issue, and the following sections will review some of the sizeable literature to summarize the current understanding. Section 1.2 outlines the mechanisms and evidence for how sea ice loss can impact the mean atmospheric response. Next, in Section 1.3, how sea ice could potentially impact the

atmospheric variability is discussed. Also included in this section is a discussion of the "tug of war" that has been posited between the warming at high latitudes caused by sea ice loss and the warming at low-latitudes caused by increased greenhouse gas concentrations. Section 1.4 discusses how the atmosphere responds to sea ice in the coupled climate system. Next, Section 1.5 outlines the models that are used throughout this thesis. Finally, Section 1.6 identifies the outstanding issues that are addressed in the following chapters.

1.2 The Mean Atmospheric Response to Arctic Sea Ice Loss

Arctic sea ice levels have been declining at a rapid pace since the modern satellite record began in 1979 (Stroeve et al. 2012). The largest changes have been since the late 1990s, especially during late summer and fall. The sea ice extent in September, when the ice is at its minimum, has decreased by over 13% per decade over the satellite record (Fig. 1.1). Observations of sea ice thickness and volume, though more uncertain than extent or area, also show large reductions (Schweiger et al. 2011; Laxon et al. 2013). With continued emissions of greenhouse gases and rising temperatures, the reduction of sea ice is expected to continue, as most climate models from the Coupled Model Intercomparison Project phase 5 (CMIP5) are predicting an ice-free September sometime in the mid-21st century (Stroeve et al. 2012; Overland and Wang 2013).

Sea ice loss impacts the atmosphere through altering the surface energy budget. By replacing the high albedo sea ice surface with the low albedo ocean, the shortwave absorption increases at the surface. In addition, sea ice acts as an insulator between the ocean and the atmosphere, so decreasing sea ice area and thickness increases the sensible and latent heat flux from the ocean to the atmosphere. All of these processes directly lead to a warmer atmosphere above the sea ice in the Arctic lower troposphere. Because of this, sea ice loss is likely one of the primary mechanisms that lead to Arctic amplification (Holland and Bitz 2003; Screen et al. 2010; Screen et al. 2012).These thermally direct processes can also lead to changes away from the Arctic by changing the large-scale atmospheric circulation.

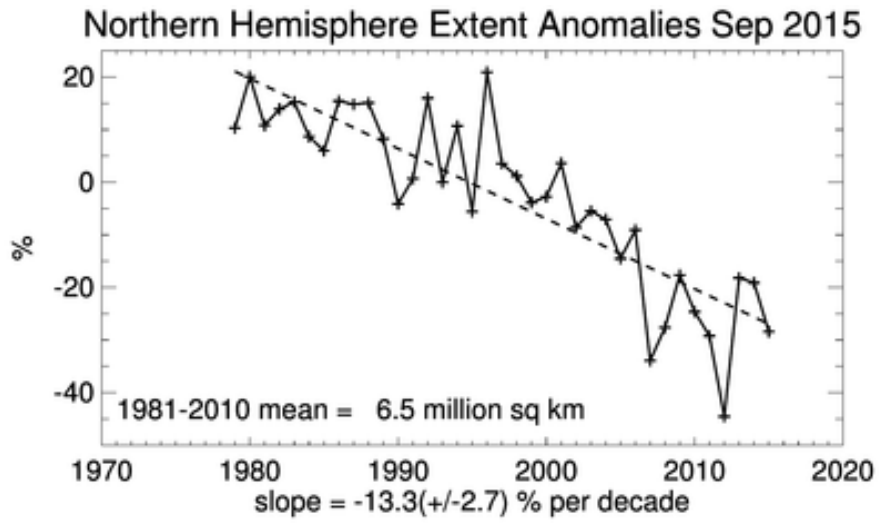

Figure 1.1: Time series of the Northern Hemisphere September sea ice extent anomalies (% difference from the 1981-2010 mean) from 1979 to 2015 (from NSIDC: https://nsidc.org/data/seaice_index/).

Studying these changes from observations is difficult due to sparse observations over the Arctic, a short observational record with large internal variability, and the difficulty in isolating sea ice loss from other effects. Because of this, climate models are used to understand how the atmosphere responds to sea ice loss in isolation. This is typically done by using an AGCM and forcing it with prescribed high and low sea ice concentrations, while keeping everything else constant and examining the response. The direct thermal responses are in general agreement regardless of the model used or how the experiment is designed. Common responses include increased heat flux into the atmosphere, warming and moistening near the surface, and increased clouds and precipitation over regions of sea ice loss (e.g. Deser et al. 2004, 2010; Screen et al. 2013, 2014; Peings and Magnusdottir 2014). One such experiment was done by Deser et al. (2010) who investigated the atmospheric response to projected 21st century sea ice loss in an AGCM. The authors started with a control simulation with prescribed sea ice and SSTs for the late 20th century, obtained from the average of an ensemble of coupled climate model experiments forced with historical greenhouse gas and aerosol forcing. Next, a perturbed simulation was performed that had the same SSTs, but had sea ice from the late 21st century, obtained from coupled model simulations forced with projected anthropogenic emissions. The difference between these two simulations represents the response to sea ice loss in isolation. Fig.

1.2 shows the heat flux and temperature response that Deser et al. (2010) found. The bars in Fig. 1.2a show the prescribed change in SIC that was derived from the coupled model and the thick solid line represents the total heat flux response. There is increased heat flux into the atmosphere in response to sea ice loss most of the year, with a peak response in November that lags behind the changes in sea ice concentrations. This lag occurs as a result of the large temperature difference between the atmosphere and surface in winter. This heat flux results in a large increase in temperature in the lowest part of the Arctic lower-troposphere (Fig. 1.2b) during winter.

While the direct thermodynamic response to sea ice loss is well understood, how the atmospheric circulation may respond is more uncertain. There are a number of mechanisms through which sea ice loss, and the warming it causes, may impact the circulation. One such mechanism is the impact that it may have on the modes of variability, particularly the North Atlantic Oscillation (NAO), Arctic Oscillation (AO) or Northern Annular Mode (NAM). These are related forms of the leading modes of variability in the extratropical atmosphere and they describe a seesaw in sea level pressure (SLP) from the high-latitudes to mid-latitudes, and a latitudinal shift of the tropospheric jet (Walker and Bliss 1932; Wallace and Gutzler 1981; Thompson and Wallace 1998). A number of modelling studies have examined how these modes of variability are affected by reduced sea ice cover using AGCM experiments, starting with Newson (1973), who found a weakening and southward shift of the westerly winds in response to a complete removal of wintertime sea ice. In more recent terms, this corresponds to a shift towards the negative phase of the NAM. More recent studies using improved and higher resolution models also tend to show a negative NAM response to sea ice loss. For example, Magnusdottir et al. (2004) and Deser et al. (2004) forced an AGCM with observed trends of North Atlantic sea ice and SSTs and found a response that projected onto the negative phase of the NAO/NAM. The observed sea ice pattern that was used was associated with the positive phase of the NAO, indicating a negative feedback between the atmospheric circulation and sea ice. This negative feedback has also been seen in observations by Strong et al. (2009). Many other modelling studies also find a response that resembles a negative NAO/AO/NAM in response to either localized or pan-Arctic sea ice decreases (e.g. Alexander et al. 2004; Seierstad and Bader 2009; Petoukhov and Semenov 2010; Deser et al. 2010; Liptak and Strong 2014; Peings and Magnusdottir 2014). While this negative NAO/AO/NAM response is common, it is

not completely robust, as some experiments find no projection onto these modes, or a projection onto the positive phase (e.g. Screen et al. 2013, Screen et al. 2014).

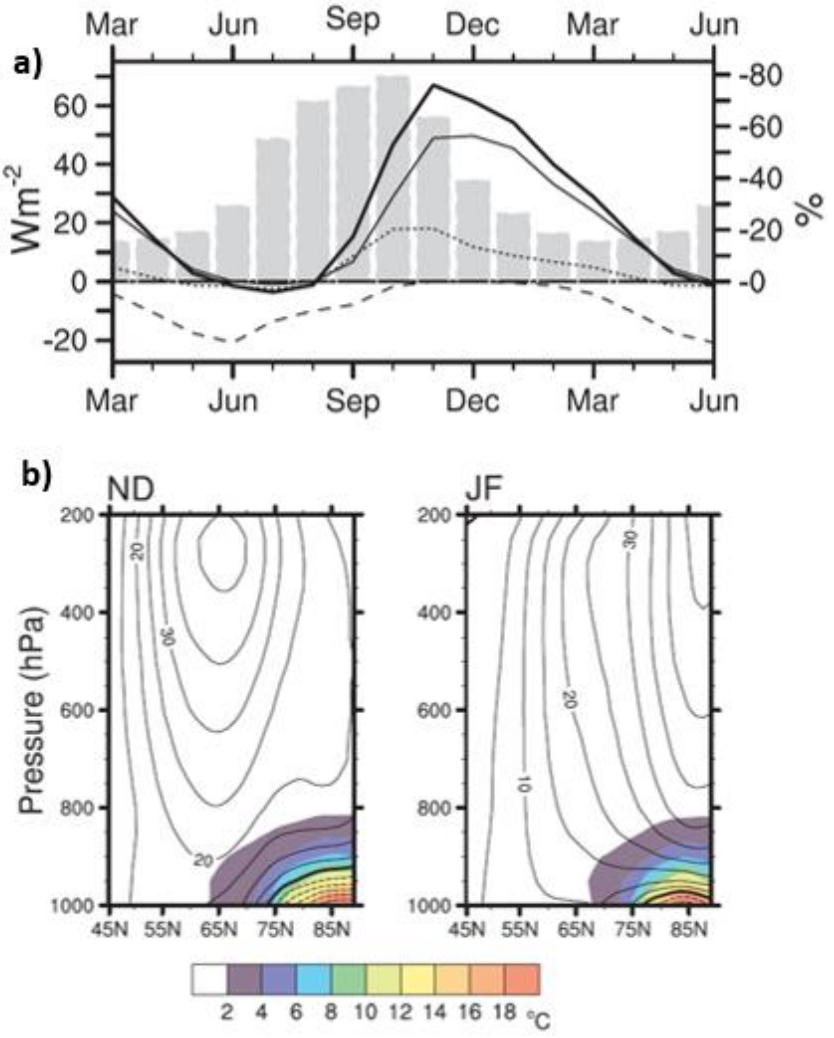

Figure 1.2: (a) Seasonal cycle of the turbulent energy flux (Wm^{-2}; ΔSH + LH; thin solid curve), longwave radiative flux (ΔLW; dotted curve), and shortwave radiative flux (ΔSW; dashed curve) responses (low ice – high ice) area averaged over the Arctic Ocean. The net surface energy flux response is given by the thick solid curve, and the SIC changes (%) are indicated by the gray bars (note the inverted scale). Fluxes are positive upward. (b) Vertical structures of the geopotential height (m; contours) and temperature (°C; color shading) responses along 90°E in (left) November–December and (right) January–February (from Deser et al. 2010).

The lack of robustness in the atmospheric response to sea ice loss was examined in detail by Screen et al. (2014), who used two independent AGCMs to quantify signal-to-noise ratios and calculate how large of an ensemble (and how many simulated years) were needed to get

statistically robust atmospheric responses to observed sea ice loss. The authors find that while variables like temperature and precipitation, particularly in the vicinity of the sea ice loss, have signals that are easy to detect, variables related to the circulation such as SLP or geopotential height have responses with much lower signal-to-noise ratios. The minimum number of years needed to detect statistically significant 500 hPa geopotential height (Z500) responses are calculated to be more than 70 years, which incidentally is more than what is used as an analysis period in most studies. The authors speculate that the small signal to noise ratio is responsible for some of the disagreements in the circulation responses between studies. For example, Liu et al. (2012) and Screen et al. (2014) found opposite SLP responses to sea ice loss despite using the same model and very similar forcing (Fig. 1.3), but Liu et al. (2012) only ran the simulation for 20 years, while Screen et al. (2014) used 60 years.

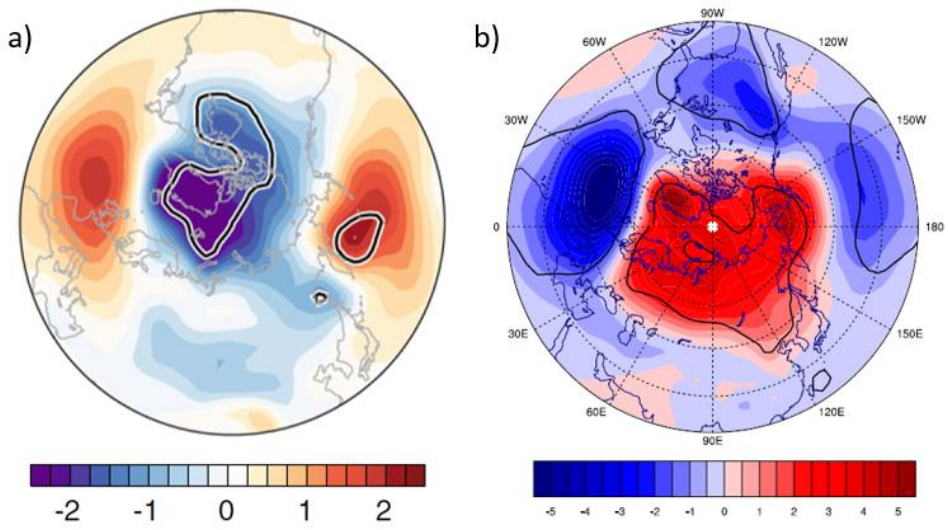

Figure 1.3: (a) The wintertime SLP (hPa) response to sea ice loss in CAM3 (from Screen et al. 2014). (b) The wintertime SLP (hPa) response to sea ice loss in CAM3 (from Liu et al. 2012).

One possible mechanisms for the sea ice loss to impact the NAO/AO/NAM and the atmospheric circulation in general is through the stratosphere. This was shown by Peings and Magnusdottir (2014) who forced an AGCM with past, present and future sea ice conditions and found that wintertime Northern Hemisphere climatological planetary waves were enhanced by the anomalous waves forced by the sea ice perturbation, weakening the stratosphere polar vortex.

This weakening of the vortex then propagated downward into the troposphere causing a negative NAM response at the surface in late winter. Kim et al. (2014), Wu and Smith (2016) and Nakamura et al. (2016) also found that a weakening of the stratospheric polar vortex by sea ice loss or Arctic amplification plays an important role in the tropospheric response. Further work by Sun et al. (2015) examined the role of the stratosphere in the atmospheric response to sea ice loss, by comparing the response between a typical low-top model and a high-top model with a better representations of the stratosphere. The high-top model had a stronger circulation response to sea ice loss in the troposphere, possibly due to differences in the stratospheric response. Another key result from Sun et al. (2015) was that sea ice loss in the Pacific and Atlantic sectors were found to have opposite responses in the stratosphere, which cancel out to produce only a weak response. As previous studies discussed use different magnitudes and spatial patterns of sea ice loss, this sensitivity to where the reduction in sea ice loss is prescribed could potentially explain some of the lack of robustness seen.

One of the more common circulation responses to sea ice loss that has been seen in both modelling studies and observations is an amplification of the Siberian high in winter which causes a cooling response in East Asia. This was first studied by Honda et al. (2009) who found a correlation between September SIC along the Siberian coast (from the Barents to East Siberian Seas) and cold winters in East Asia. They were able to reproduce this in an AGCM experiment by examining the difference between high and low SIC simulations. The warming over the sea ice loss region causes a thermally generated stationary Rossby wave which amplifies the Siberian high, and causes cold air advection into East Asia. Petoukhov and Semenov (2010) also found a connection between the SIC in the Barents-Kara Seas and cooling in Asia in an AGCM experiment, but they note that the response was non-linearly related to the SIC concentration. Going from 80% to 40% SIC saw cooling over much of the Eurasian continent related to an anticyclonic anomaly over the Arctic Ocean, however going from 100% to 80% or from 40% to 1% in the same region failed to reproduce this result. One thing to note is that while this connection between sea ice in the Barents and Kara Seas and cold temperatures over East Asia is found in observations and other modelling studies (e.g. Mori et al. 2014; Peings and Magnusdottir 2014; Nakamura et al. 2015), the connection is significantly weaker in models. For example, Mori et al. (2014) find that a composite of low minus high years produces a cold temperature anomaly that is over six times larger in magnitude and much more widespread over

Asia than AGCM experiments forced with the same low and high SIC that was found in composite. Sun et al. (2016) have argued that these cold East Asian wintertime temperatures may be a result of internal variability, as they were able to simulate cold temperature trends over East Asia in some members of a large ensemble and were unable to make the connection with sea ice loss (though this would require that what has been seen in the observations to be a low probability event).

In summary, sea ice loss impacts the atmosphere through increased heat fluxes into the atmosphere which causes warming in the lower Arctic troposphere. This can impact the atmospheric circulation through a number of mechanisms. The current literature suggests that sea ice loss may lead to a wintertime shift towards the negative phase of the NAO/AO/NAM, a weakening of the stratospheric polar vortex, and an amplification of the Siberian high, however these results are not robust across all studies. Reasons for the lack of robustness may include a large amount of internal variably that overwhelms the relatively weak signal, sensitivity to the model used (including its representation of the stratosphere), or sensitivity to the exact forcing (e.g. location or magnitude of the prescribed sea ice changes). In the next subsection how sea ice loss may impact the weather and temperature variability will be discussed.

1.3 Impact of Sea Ice Loss on Atmospheric Variability

In addition to its effect on the mean atmospheric response, some studies have suggested that sea ice loss and its associated warming may impact atmosphere variability. Changes in atmospheric variability will potentially have a greater human impact than mean changes, as events on the tails of distributions (e.g. heat waves, floods, and drought) tend to have the biggest impact on society, the economy and ecosystems (Katz et al. 1992).

Francis and Vavrus (2012) first proposed that Arctic amplification, in which sea ice loss plays a major role, could increase the severity of extreme weather events through modifying the jet-stream. The authors proposed that the reduction of the North-South temperature gradients is decreasing the strength of the zonal winds, which could increase the amplitude and decrease the speed of waves in the jet-stream, leading to more extreme and persistent weather. They showed that the maximum latitude of 500 hPa ridge peaks have moved northward over the observational

record in summer, fall and winter and conclude that this is related to sea ice loss and snow melt causing Arctic amplification. Follow-on work shows evidence that the atmospheric flow has become more meridional at mid-latitudes in the most recent observations compared to past observations (Francis and Vavrus 2015). These results lead the authors to conclude that the jet-stream has become "wavier", which has been posited to lead to more extreme weather events (Screen and Simmonds 2014).

The idea that the jet-stream has been getting wavier and that it is caused by sea ice loss or Arctic amplification has been a controversial issue. Screen and Simmonds (2013) attempted to reproduce the results of Francis and Vavrus (2012), by using two different, but equally valid ways of measuring the wave amplitude. One measure, called the meridional amplitude (A_M), calculates the amplitude of waves of particular Z500 isopleths (lines of constant geopotential height), similar to Francis and Vavrus's (2012) diagnostic, and another, called zonal amplitude (A_Z) calculates the amplitude of the depths and heights of Z500 troughs and ridges around a latitude circle. Figure 1.4 shows the trends in A_M and A_Z at different wave numbers and the total amplitude (T) for different seasons in observations. Overall, there are very few statistically significant trends, and most of those that are significant are decreasing in amplitude. Barnes (2013) also examined the trends in wave amplitudes and speed using different methods and also find a lack of change, and showed that the results of Francis and Vavrus (2012) may have been an artifact of the methodology chosen.

While the observations do not appear to show any robust trends in wave amplitude of the jet-stream, it could be that the observed record is too short and internal variability is too large for the signal to emerge over the internal variability. Barnes and Polvani (2015) attempted to find evidence of the mechanism proposed by Francis and Vavrus (2012) in CMIP5 projections under the strongest greenhouse gas forcing (RCP8.5), in order to obtain a large signal-to-noise ratio. The authors found that while nearly all models have significant Arctic amplification, there is little evidence of the changes that Francis and Vavrus (2012) proposed. In the model mean, there is no change in the strength of the zonal wind or jet speed, an increase in wave speed, and a decrease in wave extent. The latter two impacts contradict what Francis and Vavrus (2012) predict. There was, however considerable model spread in the results and some of this spread could be explained by the amount of Arctic amplification. Models that had more Arctic

amplification saw more of a decrease in zonal wind speed, jet speed and wave speed, with correlations being weak but still statistically significant.

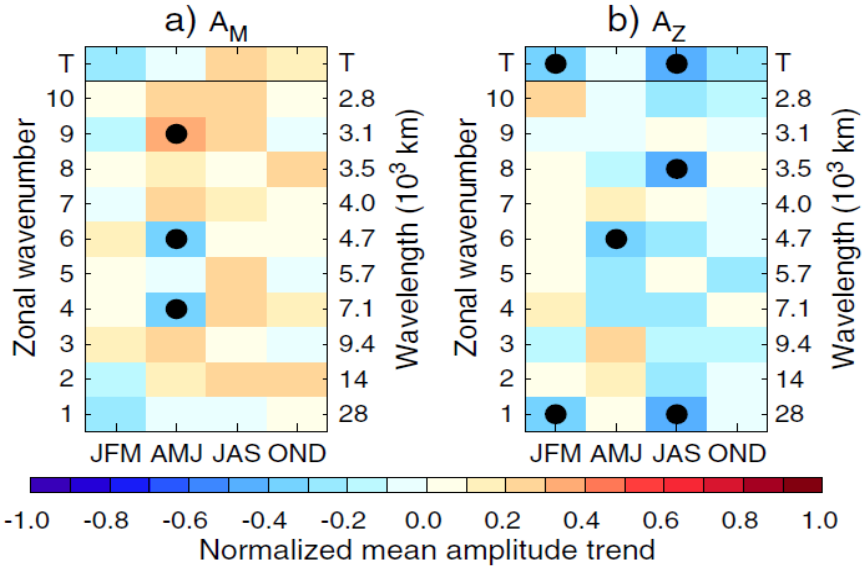

Figure 1.4: (a) Trends in meridional amplitude as a function of season and wavelength for the hemispheric domain. "T" denotes the combination of wavenumbers 1 to 10 (AM). Trends significant at the $p \leq 0.05$ level are shown by black dots. The units are σ per decade. (b) Same as (a), but for zonal amplitude (from Screen and Simmonds 2013).

Barnes and Polvani (2015) also discuss an important reason why it is not surprising that there is little observational evidence of the hypothesized impacts of Arctic amplification. Sea ice loss and Arctic amplification are occurring in response to global warming, which can impact the weather and climate in many other ways. Under global warming, while the largest increases in temperature are in the Arctic lower troposphere, likely mostly due to sea ice loss, there is also a large peak in warming in the tropical upper troposphere. From thermal wind balance, decreasing the temperature gradient in the lower troposphere should decrease the zonal wind speeds, while the increased temperature gradients in the upper troposphere should increase the speed of the zonal winds. Because of this it may be expected that there will be some cancellation of some of the effects of the sea ice loss on circulation. This has been called a "tug of war" between the warming in the tropics and the poles, and it is not clear which one has the stronger effect.

This "tug of war" was also seen in Butler et al. (2010) who examined how thermal heating in different regions, including the tropical upper troposphere and the Arctic lower

troposphere, impact the atmospheric circulation in a simplified atmospheric general circulation model. The authors found that tropical upper troposphere heating produced a poleward shift in the jet and storm tracks and the Arctic lower troposphere heating induced a weaker equatorward shift in the jet and storm tracks, attenuating the response to tropical warming. Using the CMIP5 model projections, Harvey et al. (2014) also found competing influences of Arctic and tropical warming on the wintertime storm tracks. The authors correlated upper and lower troposphere temperature gradients with the response in storm tracks in each model. In both cases, storm track strength generally increases with increased temperature gradients, but they do have different spatial structures, which gives rise to the spread in storm track responses across models. Similar results were seen by Harvey et al. (2015) using AGCM experiments forced with sea ice loss or a uniform SST warming to reflect the spread in upper and lower troposphere temperature gradients seen in CMIP3 models. The authors found that in response to sea ice loss there was a decrease in the strength of the storm tracks, while there was smaller increase in strength in response to uniform SST forcing. They concluded that the spread in lower troposphere temperature gradients has more influence on the spread in storm track responses.

To test whether it is possible for sea ice loss or Arctic amplification in isolation to influence the amplitude of waves in the atmosphere, Hassanzadeh et al. (2014) imposed different near-surface temperature gradients in an idealized dry, general circulation model. They found that while there were reductions in zonal wind speed and meridional Z500 gradients, the waviness and number of blocks actually decreased with a reduction of temperature gradient. The decrease in waviness was found to be due to the anomalies in Z500 decreasing with the decrease in gradient. Hassanzadeh and Kuang (2015) expanded on this work by examining the relationship between Arctic amplification, the AO and blocking. Because blocking becomes more common under the negative phase of the AO, and because Arctic amplification likely leads to a shift in circulation resembling the negative phase of the AO, it has led some to suggest that Arctic amplification will cause more blocking and weather extremes (Cohen et al. 2014). Hassanzadeh and Kuang (2015), however, find that in idealized modelling experiments, while a shift to a negative AO driven by internal dynamics of the atmosphere resulted in more blocking, a shift to a negative AO forced by Arctic amplification caused a decrease in blocking. The authors concluded that caution must be used in using observed AO blocking relationships to predict the response to external forcing.

While understanding how atmospheric variability will change in response to sea ice loss and Arctic amplification is difficult in part due to the difficulty in defining the metrics used to describe it, quantifying how the temperature variability might change is easier. Francis and Vavrus (2012, 2015) have suggested that due to changes in the jet-stream, prolonged cold periods in winter may become more common despite rising mean temperatures, due to an increase in variability. In addition Coumou et al. (2015) predict that the weakening of the circulation could decrease the temperature variability on short time scales (less than a week), but increase variability on longer time scales. How the subseasonal temperature variability has changed in the observational record and in the CMIP5 projections was examined by Screen (2014) who found that there was a detectable decrease in wintertime temperature variability in the high and mid latitudes in the observational record and in model projections. The decrease in variability seen in the future model projections is highly robust as it was seen in every model. This decrease in temperature variability is explained by the fact that under Arctic amplification, the cold air advected from the north is warming faster than the warm air that is advected from south. This means that unusually cold days are warming faster than unusually warm days. This decrease in temperature variability was also found in sea ice perturbation experiments in two different models by Screen et al. (2015) and in idealized general circulation models (Schneider et al. 2015).

In summary, in response to sea ice loss and Arctic amplification, some studies have suggested that the jet-stream will become "wavier" and slower moving, leading to more extreme weather. This however, is not a robust result, as other studies have shown that the changes in the "waviness" depend on the metric being used and that overall there seems to be little change in observations. There also appears to be a "tug of war" between the impacts of warming at the poles and warming in the tropics that lead to very little circulation response in both observations and in model projections under greenhouse gas warming. Idealized modelling studies also show little change or even a decrease in atmospheric variability in response to Arctic amplification. Wintertime subseasonal temperature variability has been shown to decrease in observations and in model experiments forced with sea ice loss or greenhouse gas increases.

1.4 Atmospheric Response to Sea Ice loss in the Coupled Climate System

Most studies that have used models to isolate the atmospheric response to sea ice loss use an AGCM with prescribed sea ice and SST. This method has the advantage that it is easy to design and set up experiments. It is also computationally inexpensive, in relative terms. However it also results in potentially unrealistic heat fluxes and ignores potential feedbacks with the ocean. For example, in response to sea ice loss, the atmosphere warms (Fig. 1.1b) and this heat can be transported to nearby regions, where it gets transferred into the ocean through downward vertical turbulent heat fluxes. In an AGCM experiment, as the ocean cannot respond, this heat gets removed from the system, while in the coupled system, the ocean will warm, changing the air-sea temperature gradients and heat fluxes. There have been only a few studies that have investigated the atmospheric response to sea ice loss in coupled climate models, despite it being more realistic. The rest of this section outlines these studies that have investigated the atmospheric response to sea ice loss while ocean feedbacks with various levels of complexity are included.

Chiang and Bitz (2005) coupled an AGCM to a slab ocean mixed layer model, and examined the response to an expanded sea ice cover, using conditions representing the Last Glacial Maximum. The slab ocean model is intermediate between using a prescribed SST and a full dynamical ocean, as it is able to capture the thermodynamic processes (i.e. the ocean is allowed to change temperature), but it does not include dynamical processes (i.e. there are no ocean currents). Chiang and Bitz (2005) found that the response propagated into the tropics as there was a shift in the Intertropical Convergence Zone (ITCZ) away from the hemisphere with the increase in sea ice. Experiments with a more complete representation of ocean feedbacks were performed by Scinnoca et al. (2009), who used an ocean general circulation model coupled to a chemistry climate model to examine the stratospheric ozone response to a reduction in sea ice albedo. The authors found a springtime cooling of the stratosphere and a decrease in stratospheric ozone due to reduced wave forcing from the troposphere.

More recent studies done in parallel to this thesis by Deser et al. (2015, 2016) examined the atmospheric response to sea ice loss in the coupled climate system in more detail, including a comparison of how the different levels of ocean complexities (prescribed SST, slab ocean,

dynamical ocean) impact the response. The authors melted the sea ice in the coupled model by imposing a seasonally varying longwave forcing over the Arctic sea ice to match sea ice conditions from the late 20th century in simulations forced by historical greenhouse gas and aerosol forcing and the late 21st century from the RCP8.5 projected forcing simulations. By using a seasonally varying longwave forcing, a more realistic seasonal cycle of the sea ice response is obtained compared to simulations that melt the ice using reduced albedo similar to Scinocca et al. (2009), as the albedo forcing simulations favour more sea ice melt in summer and less in winter. Figure 1.5 shows the response in annual, zonal mean temperature and wind speeds for the experiments using prescribed sea ice and SST (ΔICE_NOM; top), slab ocean model (ΔICE_SOM; middle) and full dynamical ocean (ΔICE_FOM; bottom). In the prescribed sea ice and SST experiments the temperature response is confined to the lower Arctic troposphere, while in the slab and full ocean simulations, there is a small amount of warming throughout the troposphere. This warming in the dynamical ocean experiment is similar to what is seen under RCP8.5 forcing, but smaller in magnitude – thus, the authors refer to it as a "mini" global warming. This warming, according to the authors, is caused by a decrease in poleward heat transport in the ocean that is amplified by the water vapour feedback in the atmosphere. The warming in the Arctic also penetrates higher into the atmosphere in the dynamical ocean experiments, even though the warming at the Arctic surface is similar. This is attributed to increased poleward heat transport from the tropics. Chapter 4 will investigate this topic in more detail.

Deser et al. (2015, 2016) show that coupling to the ocean also changes the atmospheric circulation response. In the prescribed sea ice and SST experiments, the zonal winds decrease in strength on the poleward side of the jet and slightly increase in strength on the equatorward side. The zonal wind response in the dynamical ocean experiment is similar, but it has a stronger magnitude as a result of the stronger temperature response in the Arctic mid-troposphere. Similar amplifications of the response in the coupled model experiments are also seen in the SLP responses. The slab ocean experiments, however, show a weakening of the zonal winds on both the poleward and equatorward sides of the jet. This occurs because in the slab ocean model, the heat is able to build up in the ocean, but it cannot be redistributed by the ocean circulation. This leads to a relatively large buildup of heat and strong temperature gradients in the mid latitudes, which does not reproduce the dynamical ocean model results. The authors conclude that the slab

ocean model might provide limited insight into atmosphere-ocean feedbacks. Additional insights into the response to sea ice loss in the coupled climate system will be explored in this thesis in sea ice loss experiments using two versions of a coupled climate model and an AGCM. In the next section, a detailed description of these models and their differences will be described.

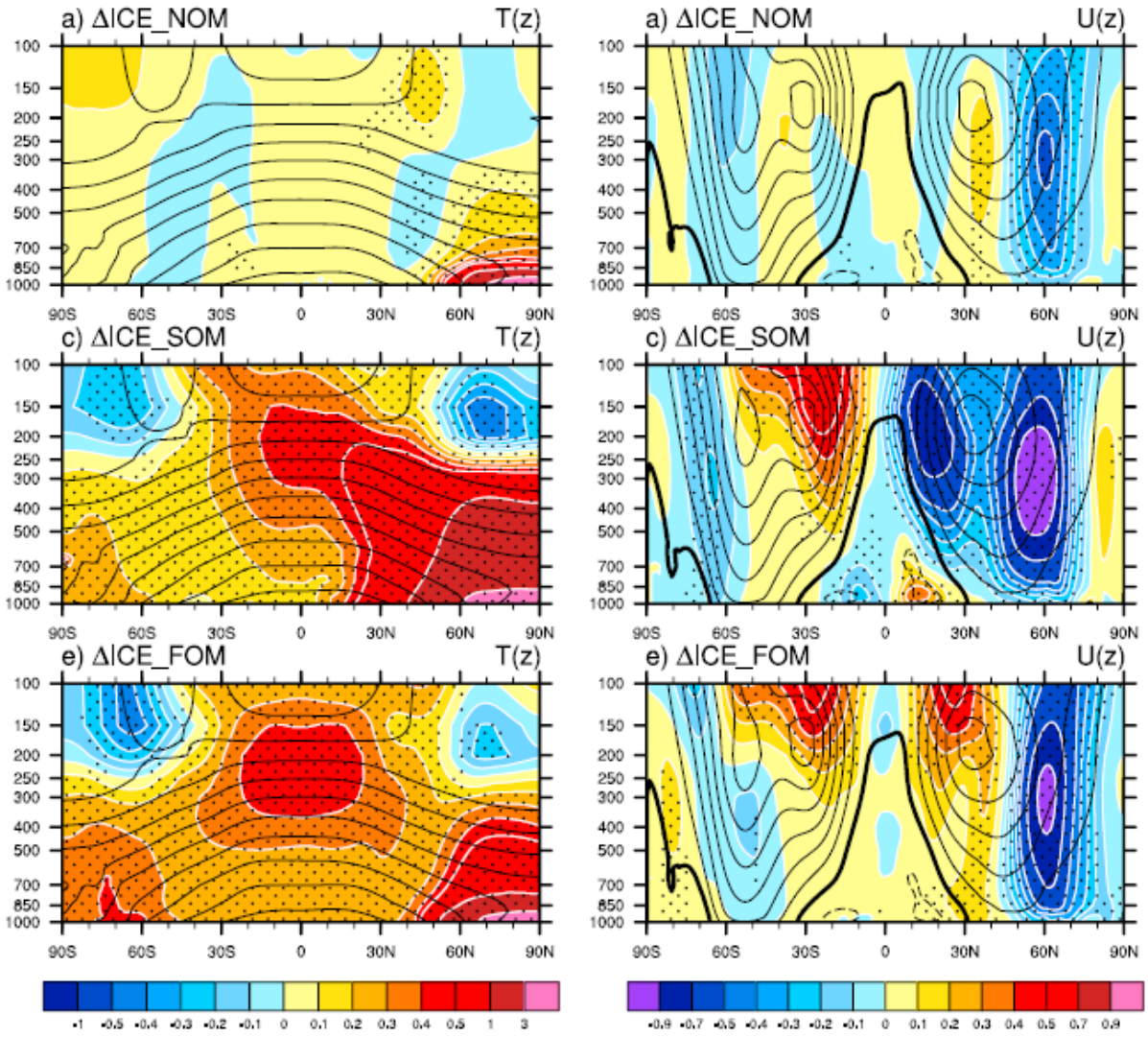

Figure 1.5: Annual zonal mean (a, c, e) temperature (°C) and (b, d, f) zonal wind (m s^{-1}) responses to Arctic sea ice loss in the in ΔICE_NOM (a and b), ΔICE_SOM (c and d), and ΔICE_FOM (e and f) model configurations (color shading: color bars at the bottom of each column; note the nonlinear color scales). Stippling indicates where the response is statistically significant at the 95% confidence level. Contours indicate the twentieth century climatology (contour interval of 10°C for temperature and 5ms-1 for zonal wind with the zero contour thickened) (from Deser et al. 2016).

1.5 Description of the Models

Simulations using different versions of the National Center of Atmospheric Research's (NCAR) climate models are used throughout this thesis. In Chapters 2 and 3, simulations using the Community Climate System Model version 4 (CCSM4; Gent et al. 2011) are used. The atmospheric component of the model is the Community Atmospheric Model version 4 (CAM4; Neale et al. 2013), which has 26 vertical levels up to 3 hPa and uses a finite volume dynamical core on a 1.25° x 0.9° grid. The ocean model is the Parallel Ocean Program version 2 (POP2; Smith et al. 2010) which has 60 vertical levels and uses an approximately 1° grid. The land model is the Community Land Model version 4 (CLM4; Oleson et al. 2010) and is on the same grid as the atmosphere, while the sea ice model is CICE4 (Hunke and Lipscomb 2008) and is run on the same grid as the ocean model.

In Chapters 3 and 4, the Community Earth System Model version 1 (CESM1) (Hurrell et al. 2013) are used. This version of the model uses the same ocean, land and sea ice model as CCSM4, but it uses the Community Atmosphere Model version 5 (CAM5) instead of CAM4. CAM5 and CAM4 have the same finite volume dynamical core and a deep convection scheme, but the remaining physical parameterizations underwent significant changes. These include changes to the shallow convection, radiation, aerosols, planetary boundary layer, turbulence, cloud microphysics and cloud macrophysics. In particular, the cloud microphysics was updated in CAM5 to include prognostic double moment microphysics (Morrison and Gettelman 2008) instead of the single moment microphysics that was used in CAM4. CAM5 also has 30 vertical levels, with the four additional levels being located in the lower parts of the atmosphere to better resolve boundary level processes.

The differences between CAM4 and CAM5 under the climate response to a doubling in CO_2 were examined in Kay et al. (2012). The authors found that the differences in the physical parameterizations between CAM5 and CAM4 is far more important than ocean differences or atmospheric resolution in determining the climate response. CAM5 shows more global warming than CAM4, with climate sensitivities of 4.0 and 3.1. While this amplification of the warming is seen at all latitudes, levels and seasons, the greatest differences are at the Arctic surface in the late fall and winter. This is associated with more sea ice loss in CAM5 than in CAM4. Feedback

analysis was performed to show that these differences are a result of more positive shortwave surface feedbacks and less negative Arctic shortwave cloud feedbacks in CAM5. These results are consistent with differences in the mean states between the two models. Most importantly, due to differences in the cloud parameterizations, the Arctic clouds have a significantly smaller liquid cloud paths in CAM5 compared to CAM4, despite having similar cloud fractions in summer (Fig. 1.6a, b). These optically thinner clouds allow more sunlight to reach the surface increasing the strength of the surface albedo feedback. The response in cloud water path and fraction are also smaller in CAM5 (Fig. 1.6c, d), consistent with smaller negative cloud feedbacks. Surface properties likely also play a role in the in the larger Arctic climate response in CAM5 as it has less extensive and thinner sea ice compared to CAM4.

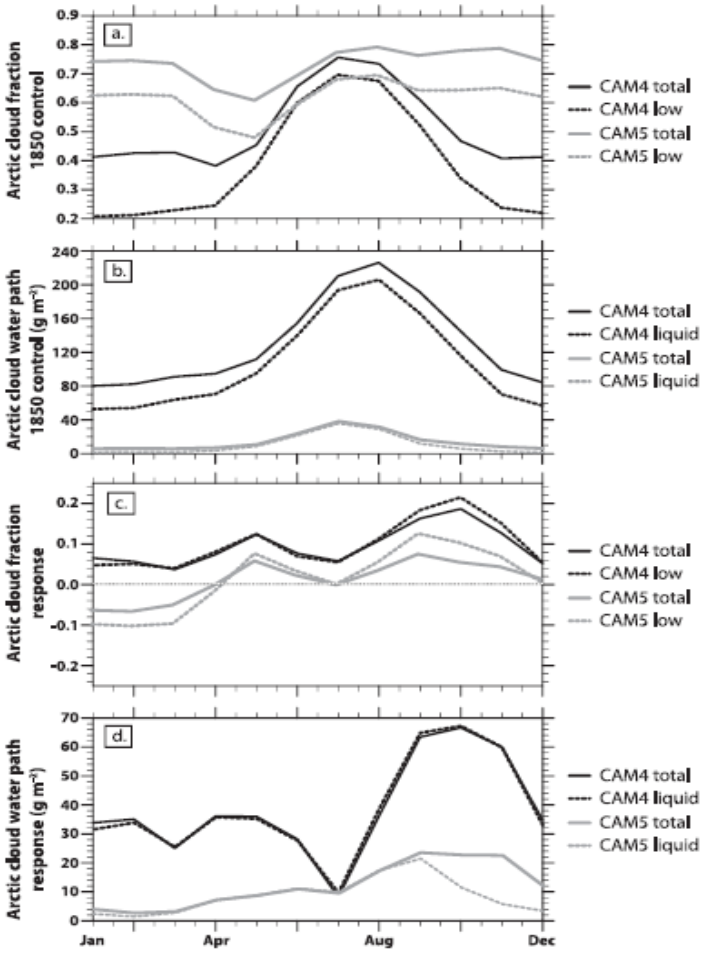

Figure 1.6: Monthly evolution of Arctic clouds in CAM4 and CAM5: (a) total and low cloud fraction, b) gridbox total and liquid cloud water path, (c) total and low cloud fraction, and (d) gridbox total and liquid cloud water path response (from Kay et al. 2012).

1.6 Conclusions

This chapter has reviewed the literature on the atmospheric response to sea ice loss, setting the stage to address a number of new questions. In Chapter 2, coupled model simulations using CCSM4, with reduced sea ice albedo will be used to examine the atmospheric response to sea ice loss. Very long simulations are used in order to get statistically robust responses motivated by Screen et al. (2014) who has shown that many previous studies have used simulations that were too short to adequately sample internal variability, which could lead to spurious disagreement between studies. As discussed in Section 1.2, a number of studies have looked at the change in atmospheric variability in observations, in models forced with greenhouse gas projections, and in idealized models, but there has been little analysis on the change in atmospheric variability in response to sea ice loss in isolation in an AGCM or coupled climate model. This is looked at in Chapter 2, which includes an analysis of variability in temperature, SLP, and 500 hPa geopotential height at different timescales and seasons. It is found that there is a decrease in variability in near surface temperature which spreads out over the mid-latitudes and into the mid-troposphere, and this decrease occurs on nearly all timescales. Similar to what is seen in observations, changes in wave amplitude depend on the metric used and changes are generally small. In addition, a number of shorter simulations are used in order to determine if there is a difference between the initial "transient" response in the first 50 years and the long time scale equilibrium response. It is shown that the response is highly variable between each realization, indicating that internal variability dominates over the signal on these short timescales.

In Chapter 2, it is shown that in response to sea ice loss there is some tropical warming that is part of the "mini" global warming response, consistent with Deser et al. (2015,2016). In Chapter 3, simulations of CESM1 forced with reduced sea ice albedo and the RCP8.5 projections are used together with a pattern scaling technique in order to separate the parts of the response that scale with sea ice loss while keeping low-latitude temperatures constant and vice versa. It is found that that the circulation responses that are seen in the sea ice albedo forcing experiments (that are typical responses seen in other studies) are cancelled out by the response due to low-latitude warming, resulting in very weak responses under global warming. One field where the effects of sea ice loss are seen in the RCP8.5 projections is the reduction in subseasonal temperature variability. In addition, a comparison of the CCSM4 and CESM1 response to sea ice

loss is shown in this chapter as it has been shown by Kay et al. (2012) and discussed in Section 1.5 that the Arctic climate response in the two models is very different.

One of the conclusions of Chapter 3 is that the circulation response to sea ice loss in the coupled model is partially cancelled out by the warming at low-latitudes, so it might be expected that due to the warming at low-latitudes, the response is weaker in the coupled model compared to AGCM studies. However, Deser et al. (2015, 2016) find that the circulation response to sea ice loss is stronger in the coupled model. In Chapter 4, it is hypothesized that the extratropical ocean warming that is induced by sea ice loss causes the amplified response. New AGCM experiments that prescribe sea ice loss with and without these SST changes are performed to show what impact this ocean warming has on the response. It is shown that this additional warming does have a large impact on the circulation response and suggests that this mechanism contributes to the enhanced response seen in Deser et al. (2015,2016).

This thesis includes research that has been published, is under review or is in preparation to be submitted to peer review journals. Chapter 2 has been published in the Journal of Climate (Blackport and Kushner, 2016). Chapter 3 is currently under review in the Journal of Climate. Chapter 4 is in preparation for submission.

Chapter 2
The Transient and Equilibrium Climate Response to Rapid Summertime Sea Ice Loss in CCSM4

2.1 Introduction

To isolate the role that observed and projected anthropogenic Arctic sea ice loss (Stroeve et al 2012; Overland and Wang 2013; Liu et al. 2013; Snape and Forster 2014) has on global climate and circulation, several studies have carried out forced climate simulations that capture the surface perturbations associated with ice melt, sea ice extremes, or observed trends (e.g. Honda et al. 2009; Magnusdottir et al. 2004; Deser et al. 2004, 2010; Screen et al. 2013; Screen et al. 2014; Peings and Magnusdottir 2014; Kim et al. 2014). As discussed in Chapter 1, in these studies, there is considerable disagreement about how the atmospheric circulation responds to sea ice loss. These inconsistencies could be caused by model differences or by differences in the magnitude and spatial extent of the sea ice and related SST forcing. These can lead to differences in the circulation response, since several dynamical processes might be simultaneously involved in linking sea ice loss and the associated warming with atmospheric circulation, including wave-mean flow interactions, changes to the stationary and quasi-stationary waves, and couplings of the waves with stratospheric conditions. In addition, internal climate variability combined with a relatively weak circulation response may lead to relationships that are not statistically significant if too few years are used in model experiments (Screen et al. 2014). This lack of agreement, and a relatively short observational record, mean that proposed impacts of Arctic change, including impacts on storm track variability, the jet stream and weather extremes (e.g. Francis and Vavrus 2012, 2015; Barnes 2013; Screen and Simmonds 2013; Cohen et al. 2014; Screen 2014; Coumou et al. 2014, 2015; Schneider et al. 2015) are challenging to assess theoretically.

In this chapter we examine robust aspects of the climate system's adjustment to rapid sea ice loss in a relatively simple perturbation framework. We use a coupled ocean-atmosphere-sea ice-land model that allows all components of the physical climate system to adjust to sea ice perturbations in an energetically self-consistent way. In our experiment, rapid sea ice loss is forced by suddenly reducing sea ice albedo. This method is similar to that of Scinocca et al. (2009), whose focus was on the stratospheric ozone response to sea ice melt. As in Deser et al. (2015), in this coupled model setup, the direct radiative response first drives sea ice loss and

Arctic surface warming which then spreads through adjustment of ocean temperatures, in the presence of water vapour and other feedbacks, into the midlatitudes and tropics. Deser et al 's approach complements ours: they study the coupled response to longwave-forced sea ice loss associated with greenhouse forcing. Besides driving sea ice loss in summer, this maintains the projected anthropogenic global warming effect over the Arctic, leading to strong sea ice losses from longwave forcing all year. Our study attempts to isolate the forcing more precisely, to answer the climate dynamical question of what might happen to the climate system if summertime sea ice were lost in the Arctic in isolation from anthropogenic forcing. Because our forcing is relatively weak compared to Deser et al. (2015), we need multi-century simulations and sampling to obtain statistically robust results. We also perform a number of shorter perturbation simulations to examine the initial adjustment due to sea ice loss, which allows us to analyze the climate response to rapid sea ice loss in the presence of internal variability. Another similar study is that of Cvijanovic and Caldeira (2015) who compared the CO_2 induced response with active and suppressed sea ice. Our simulations use a simpler approach, as we are looking at only the sea ice response without CO_2 induced warming. We also use a full dynamical ocean model instead of a slab ocean model. We describe the response, the robustness and variability of the response, and the response of atmospheric variability itself, to a sea ice perturbation.

We organize the chapter as follows: in Section 2.2, we describe the experiment design. In Section 2.3, we present an overview of the equilibrium response to sea ice loss, the response of atmospheric variability, and the transient adjustment to equilibrium. We summarize and discuss our results in Section 2.4.

2.2 Experiment Design

We carry out a control simulation of CCSM4 (see Section 1.5 for details) that uses constant, Year 2000 levels of greenhouse gases and aerosol forcing. To obtain this simulation, we branch off of a CMIP5 "historical" simulation at Year 2000, allow the resulting simulation to drift to a new equilibrium over the subsequent 270 years, and integrate the model for another 680 years to use as an analysis period. To drive sea ice loss for our perturbation experiments, we instantaneously alter 3 parameters in the sea ice model code (r_ice = -6.0, r_snw = -6.0 and r_pnd = -6.0); these changes reduce the albedo of the sea ice, snow on top of the sea ice, and the melt ponds. The exact amount that the albedo is reduced depends on the time of year and

location, but on average there is a reduction of approximately 20%-50% throughout the year (not shown). These changes increase the amount of shortwave radiation absorbed, thus directly driving ice and snow-on-ice melt (see Fig. 2.3 for change of shortwave flux into the ocean). This change is applied globally and thus impacts both Antarctic and Arctic sea ice; the focus of this study will be on the Northern Hemisphere extratropical response which presumably is dominated by the Arctic sea ice loss perturbation; the Southern Hemisphere response will be the subject of a separate study. We note that in Deser et al. (2015) the Southern Hemisphere mid-to-high latitude response to Arctic sea ice loss was relatively weak even though the Arctic forcing was generally stronger than ours; thus we expect that the Northern Hemisphere mid-to-high latitude response discussed here will be fairly independent of Antarctic forcing.

We perform several perturbation realizations that are branched off the control. They are initialized 50 years apart to ensure statistical independence, but are otherwise identical. The first perturbation experiment is extended to 800 years to examine the equilibrium response. This length allows long-term oceanic adjustment to the change in sea ice (Section 2.3) to take place. We also examine the transient adjustment of the first 50 years of 7 additional realizations, for a total of an 8-member 50-year ensemble, to the instantaneous change in sea ice albedo. To compare the sea ice albedo response to a standard greenhouse warming scenario, we also include in this study a brief comparison of these results with the ensemble mean of a five-member ensemble of the RCP8.5 scenario of CCSM4 (Meehl et al. 2012;Vavrus et al. 2012), which is available at the NCAR website (http://www.cesm.ucar.edu/experiments/).

2.3 Results

2.3.1 Overview of the response to sea ice loss

Figure 2.1a shows the time series of September Arctic sea ice area (SIA) for the control and the 800-year sea ice perturbation simulation. We use the SIA, which is the total area covered by sea ice (i.e. the area of the grid cells weighted by the SIC), instead of the sea ice extent (SIE), which is the total area with greater than 15% SIC. The SIA in the Year 2000 forced control simulation averages just under 4 million km^2, which is lower than observed in every year up to and including 2006, and is greater than observed every year since 2007.There is less sea ice in our control simulation than in Year 2000 observations, which can in part be attributed to the adjustment to radiative equilibrium under constant Year 2000 forcing in the simulation

(adjustment not shown). For comparison, in the projected greenhouse warming of the CCSM4 RCP 8.5 ensemble mean (see Section 2.2), annual and September-October-November (SON) mean SIA is closest to our equilibrated control simulation in the 10 year period 2032-2041. The September SIA of the low albedo simulation equilibrates at just under 0.5 million km^2, which CMIP5 model projections suggest will happen sometime in the middle of this century (e.g. Snape and Forster 2014). In the case of the CCSM4 RCP8.5 scenario ensemble, ice free conditions occur later than the multi-model mean with SIA reaching below 0.5 million km^2 in the 10 year period 2072-2081, while comparable SIA in SON and the annual mean occurs in the 10 year period 2067-2076. Thus our albedo perturbation simulations drives the approximate equivalent of three to four decades of summertime sea ice loss under ongoing projected anthropogenic greenhouse warming.

The time series of the September SIA for the first 50 years of the 8 perturbation simulations, along with the ensemble average and a sample of 50 years from the control simulation are shown in Fig. 2.1b. In each of the 8 perturbation simulations, most of the ice melts within the first few years after the change in albedo is made, with the ensemble mean SIA dropping below 1 million km^2 by Year 3. But not all aspects of the adjustment are as rapid: the Atlantic meridional overturning circulation (AMOC) (Fig. 2.1c) undergoes several centennial scale oscillations before recovering to a strength approaching that of the control simulation strength after 400 years. For this reason, Years 400-800 years of the perturbation simulation will be defined as an equilibrium period and Years 1-50 of the eight perturbation simulations will be taken to represent the sea ice loss onset period.

Figure 2.2a shows the seasonal cycle of the Arctic SIA for the control simulation and the equilibrium and transient periods in the perturbation simulations. The largest changes occur during late summer and early fall due to the ice-albedo feedback, with only small changes occurring throughout the rest of the year. Unlike the changes in SIA, the sea ice thickness (SIT) (which in the case of the perturbation simulation corresponds to the smaller area of ice that has not melted) shows less seasonality with a relatively constant reduction in thickness throughout most of the year (Fig. 2.2b). The increase in thickness in September occurs as a result of all the thin ice melting leaving only the thickest ice along the Northern coast of Greenland. Thus SIT appears to respond strongly to the ocean-atmosphere warming throughout the year. Most of the response in SIA and SIT occurs within the first 50 years of the albedo change (compare dashed

black to solid black curves), although there is ongoing reduction in both quantities in the adjustment to equilibrium. Sea ice albedo perturbations, which act most strongly in the summer season, do not capture the year-round reductions in SIA expected under long-term greenhouse warming (Deser et al. 2015). Nevertheless, SIT is reduced throughout the entire year, suggesting that summertime sea ice loss can potentially strongly influence the atmosphere outside the summer season.

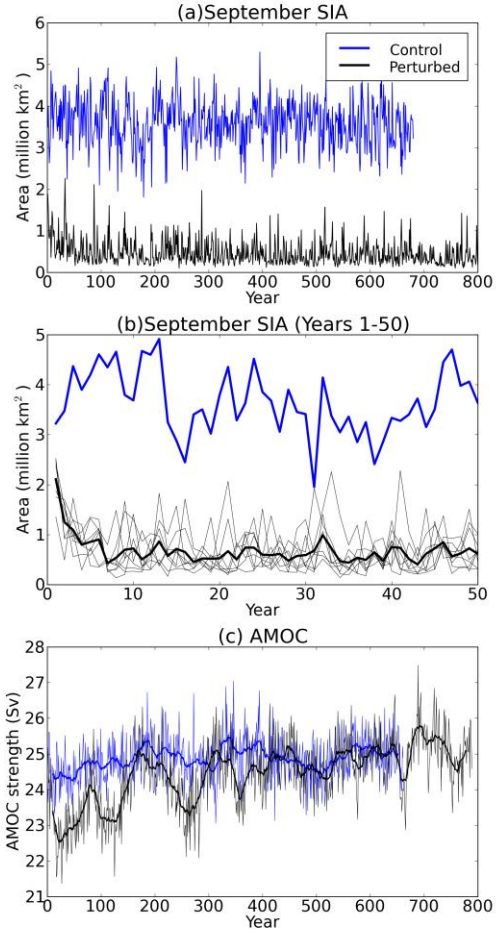

Figure 2.1: (a) September Arctic sea ice area (million km^2) for the control simulation (blue) and the 800-year perturbation simulation. (b) As in (a), but for the first 50 years of the 8 realizations of the transient perturbation ensemble (thin black), the transient perturbation ensemble average (thick black) and a representative 50 year segment (Years 101-150 of the analysis period) for the control simulation (blue). (c) As in (a), but for the AMOC, defined as the maximum in Sv of the North Atlantic meridional stream function between depths 500m and 1800m, for the control (blue) and perturbed (black) simulations.

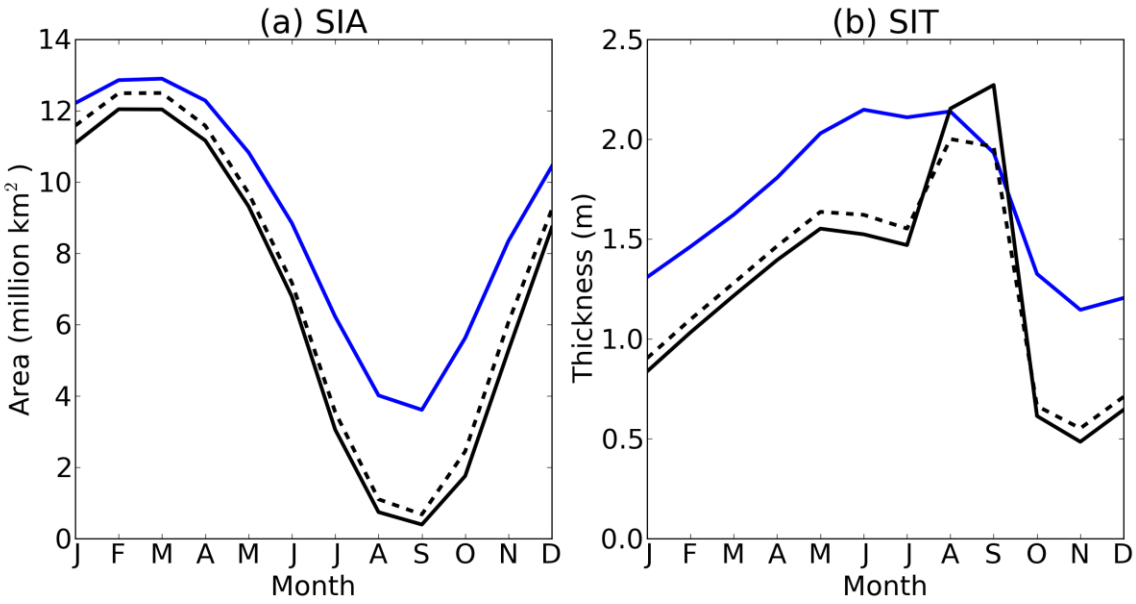

Figure 2.2: (a) The climatological seasonal cycle of the control simulation (blue) and the perturbation simulation during the equilibrium period (solid black) and transient period (dashed black) for Arctic sea ice area (million km^2). (b) As in (a), for Arctic-averaged thickness of sea ice that is present (m).

The atmospheric response to sea ice loss is communicated through a response in surface temperature and surface energy flux. The seasonal cycle of the surface sensible heat, latent heat, and longwave and shortwave radiative flux response for the Arctic Ocean (averaged over grid points from 65°-90°N and less than 50% land) are shown in Fig. 2.3a. A positive response corresponds to an increase in upward heat flux into the atmosphere while a negative response corresponds to a net increased heat flux into the ocean/ice. The response is dominated by the negative shortwave response (note that the line for the shortwave response in Fig. 2.3a is multiplied by 0.1), which peaks in spring and summer, and is a direct result of the albedo perturbation made in the sea ice model. The largest sensible and latent heat flux response, however, occurs in late fall and winter when the temperature difference between the ocean and the atmosphere above it is large. This is qualitatively similar to Fig. 3 in Screen et al. (2013), who forced two different atmospheric models with prescribed, observed sea ice losses. Thus important aspects of the energy budget response are consistent between prescribed sea ice integrations with observed sea ice loss and our forced albedo-driven response. The principal difference between the prescribed simulations and the forced albedo-driven response in the coupled simulations is that in the latter the increased heat flux continues longer into spring. This

could be linked to reductions in SIT captured in the coupled model response: thinned ice allows heat to be conducted more easily between the ocean and atmosphere, even with little to no change in SIC. It also reflects the additional warming of the ocean (not shown) through a general warming response to sea ice loss.

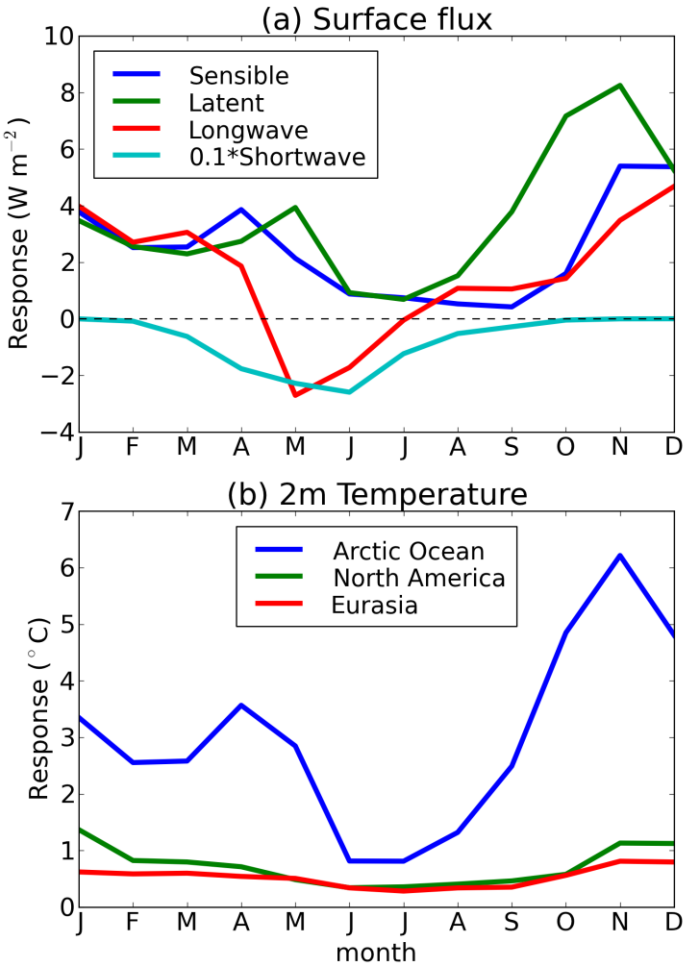

Figure 2.3: (a) The climatological seasonal cycle of the equilibrium response for the net surface sensible, latent longwave and shortwave heatflux multiplied by 0.1 (W m^{-2}) averaged over the Arctic Ocean (65°N-90°N and less than 50% land). (b) As in (a) for temperature response averaged over the Arctic Ocean, North America and Eurasia (°C). Only latitudes between 30°N and 60°N were used for the spatial averages over North America and Eurasia.

The seasonal cycle of the 2-meter temperature response averaged over the Arctic Ocean, North America and Eurasia is shown in Fig. 2.3b. The Arctic Ocean temperature is averaged over the same region as Fig. 2.3a and for the North America and Eurasia temperatures only the

land area between 30°N and 60°N is used. The Arctic ocean temperature warming follows the sensible and latent heat flux response in Fig 2.3a, with a peak in November of over 5°C along with an approximately 3°C response during spring. Over North America and Eurasia there are small increases in temperature throughout the whole year, with the largest changes occurring during November, December and January over North America, which sees an increase of 1.0-1.5°C averaged over the continent.

By construction, our experiment yields a highly Arctic amplified response with a weak global warming: the Arctic warms 2.4°C and the Northern Hemisphere 0.6°C in the annual mean in the Northern Hemisphere. Arctic amplification expressed as the ratio of Arctic to Northern Hemisphere warming is 2.4/0.6=4.0. (For SON the values are 3.5°C for the Arctic, 0.7°C for the Northern Hemisphere, and 3.5/0.7=5.0 for the Arctic amplification.). The Arctic and Northern Hemisphere annual mean warming between the RCP8.5 periods 2067-2078 and 2032-2041 mentioned above are respectively 3.4°C and 1.6°C, with Arctic amplification 3.4/1.6~2.1 (For SON, the values are 4.4°C for the Arctic, 1.8°C for the Northern Hemisphere, and 4.4/1.8~2.4 for the Arctic amplification). Thus the sea ice albedo perturbation and resulting summertime sea ice loss drives approximately three quarters of projected Arctic anthropogenic greenhouse warming over a 30-40 year period. This warming is much more strongly confined to the Arctic, with stronger Arctic amplification than expected under greenhouse warming.

The zonal mean equilibrium temperature response for SON is shown as a latitude-pressure cross section in Fig. 2.4a. The largest temperature response is, as expected from the Arctic amplification ratio, confined to the Arctic. It is also confined to the lowest levels in the atmosphere, below 850 hPa, consistent with Screen et al. (2012). The lack of penetration of the response above 850 hPa leads to a relatively weak wind response described next. The global warming effect of the sea ice loss is linked to a warming of the tropical upper troposphere of about 0.5°C, which is part of a tropospheric global warming response of 0.2°C–0.6°C.

The equilibrium zonal mean wind response (Fig. 2.4b) is very weak with only a small (less than 0.3 m s^{-1}) decrease in the westerly winds between 60°N and 80°N and a positive (westerly) response in the tropical upper troposphere and stratosphere. These changes are consistent with thermal wind balance, with the slight weakening of the westerlies reflecting very modest reductions in baroclinicity above 850 hPa. The zonal mean response in the ensemble

mean of the transient phase (averaged up to Year 50) is similar (not shown), that is, there is no pronounced difference in the zonal winds during the transient adjustment phase. Shorter segments of the integrations exhibit stronger zonal wind changes, especially in the Arctic stratosphere (not shown), but these average out as the length of the averaging period is increased to several centuries. The increase in the meridional temperature gradient in the upper troposphere at lower latitudes (10°N-30°N) coincides with a positive anomaly in the zonal wind which reflects the moderate global warming simultaneously induced by Arctic and Antarctic sea ice loss in these integrations.

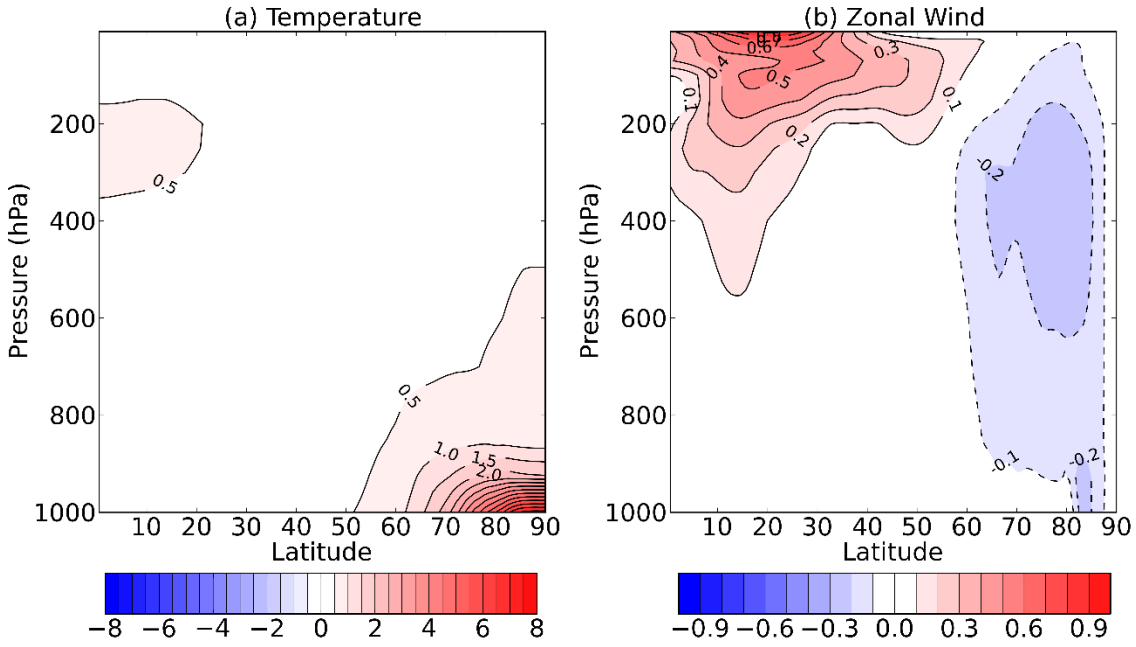

Figure 2.4: (a) The zonal average equilibrium response during SON for temperature (°C). (b) As in (a), for zonal wind (m s^{-1}).

The zonal mean wind and temperature for winter (DJF) are similar to SON, with a smaller temperature response that is still confined to below 850 hPa, and a very small decrease in the zonally averaged westerly wind speeds (not shown). The size of the response in winter compared to fall that we see in our simulations is smaller than what it would be for future projections of anthropogenic greenhouse warming (Deser et al. 2015). Nevertheless, it is striking that the notable wintertime surface warming driven by our sea ice albedo perturbation is not accompanied by a stronger midlatitude circulation response.

It has been proposed that Arctic warming may lead to a weakened and more meandering jet stream which in turn might be associated with increases in extreme weather events (e.g. Francis and Vavrus 2012). In this experiment, we have tried to isolate that part of Arctic warming associated with summertime sea ice loss and found a relatively weak jet stream response. Specifically, in this model, an almost complete induced loss of summer sea ice induces 3-4°C of SON Arctic warming, which is comparable to several decades of global warming, and a reduction in midlatitude westerly strength of less than 0.3 m/s in SON. The sensitivity of the winds in the extratropical zonal mean jet stream is thus less than 0.1 m/s per degree Celsius of summertime Arctic surface warming. In other seasons, the response is of similar magnitude. In the next subsection, we investigate in more detail the character of the response of geopotential height meandering and other aspects of variability to sea ice loss. We at this point caution that the results found here may very well be model dependent, and will return to this point in the Discussion (Section 2.4).

2.3.2 Response of atmospheric variability to sea ice loss

We now investigate how the melting of sea ice in the Arctic affects variability and measures of jet meandering. We use 200 years of daily averaged data from the control integration and the equilibrium portion of the perturbation integration to examine the response of atmospheric variability. Beginning with 2-meter temperature, we calculate a daily climatology based on 200 years of data, then remove this from each day of the 200-year period to create a 200-year anomaly time series. In this way we remove the mean warming response. Figure 2.5 shows a probability density function of daily anomalous 2-meter temperatures during SON for individual grid points over a) the Arctic Ocean (75°N,185°E), b) the Arctic coast in Northern Canada (69°N, 226°E) and c) the North American continental interior in Saskatchewan (50°N, 250°E). These points are representative of these regions as nearby grid points show similar temperature distributions (not shown, but see Fig. 2.6 maps of the change in standard deviation). There is a very pronounced narrowing of the temperature distribution in the perturbation simulation for the point over the Arctic Ocean. The standard deviation decreases by over 60% from 5.1 °C in the control simulation to 2.0°C in the perturbation simulation. The temperature extremes are not nearly as large in the perturbation simulation, because the wide tail of the control distribution disappears. The reduction in the standard deviation for the Canadian Arctic coastal point (reduced 11%, from 5.4°C to 4.8°C) and the Saskatchewan point (reduced 8%,

from 5.4°C to 5.0°C) are more modest than the Arctic Ocean point, but are, given our large sample, statistically significant using a Levene test for equal variance.

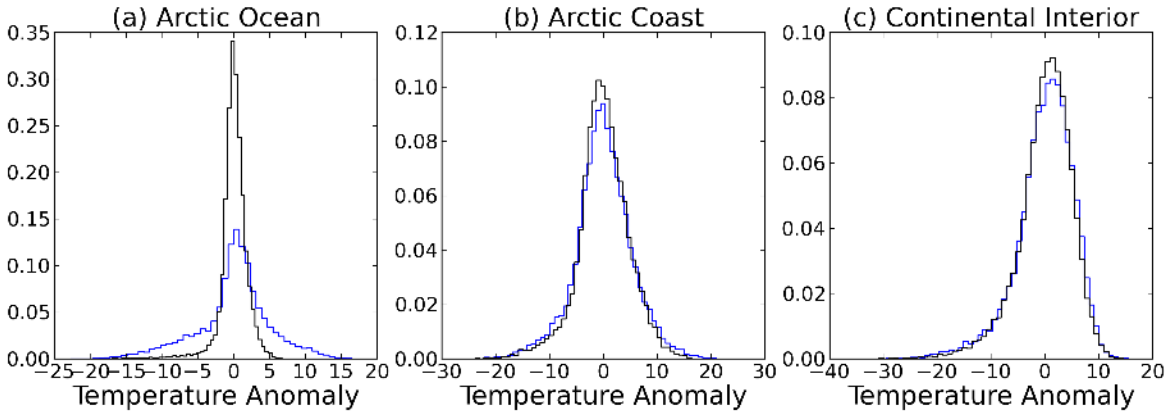

Figure 2.5: Probability density functions for the control (blue) and equilibrium perturbation (black) simulations of daily averaged SON 2-meter temperature anomalies (°C) for a single grid cell over (a) the Arctic Ocean (75°N,185°E), (b) Arctic coast (69°N, 226°E), (c) continental interior (50°N, 250°E). The climatological temperature was subtracted from each day to remove the mean warming response.

To separately map changes to interannual and subseasonal variability, we decompose the 2-meter temperature anomalies on a given day represented in Fig. 2.5 (i.e. the SON daily 2m temperature values with the climatology removed) into that year's seasonal SON mean plus that day's departure from that year's seasonal SON mean. It can be shown that by construction the total SON variance similarly decomposes into the interannual variance of the 200 SON seasonal means plus the subseasonal variance for SON. This is done at each grid point and the difference in the standard deviation (the square root of the variance) between the two simulations measures the responses of the variability at that point. A map of the response of interannual (Fig. 2.6a) and subseasonal (Fig. 2.6b) standard deviation shows that the reduced variability shown at the grid points in Fig. 5 extends throughout the middle and high latitudes. Both the interannual and subseasonal timescales contribute to the reduction in temperature variability. The reduction in the interannual temperature variability is largest in the southern parts of the Arctic Ocean, while there is actually a small increase near the North Pole. There is little change over land with the exception of over northern Russia. The spatial structure of the subseasonal response in the 2m temperature standard deviation is different, with a large reduction over the whole Arctic Ocean as well as smaller changes over the middle and high latitudes over Russia and North America.

There are a number of mechanisms that potentially contribute to the decrease in temperature variability seen in Figs. 2.5 and 2.6. One idea that has been explored by Screen (2014) and Schneider et al. (2015) is that Arctic amplification will weaken surface temperature gradients in the mid and high latitudes and even without any change in the atmosphere dynamics this will reduce the temperature variability on synoptic time scales. The meridional temperature gradient response (Fig. 2.7) indicates that this likely contributes to the reduction in variability in some regions, as the temperature gradients do weaken, particularly in the regions between 70°N and 80°N. However, there are regions where the temperature gradient does not change, yet there is still a reduction of temperature variability. For example, north of 80°N there is little change in temperature gradient, yet on subseasonal timescales, there are still large reductions in variability.

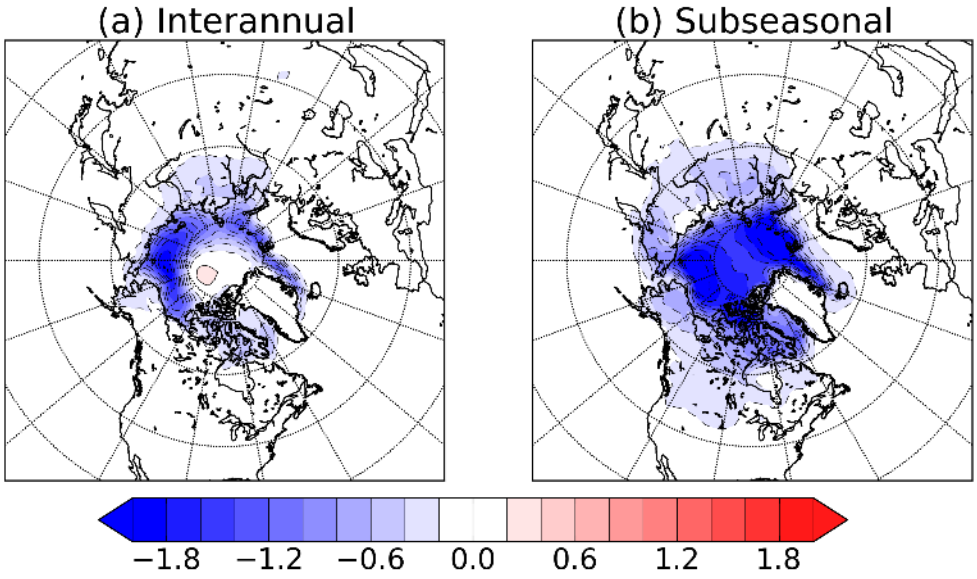

Figure 2.6: The equilibrium response of SON 2-meter temperature standard deviation (°C) for (a) interannual timescales and (b) subseasonal timescales.

Much of the reduction in temperature variability over the Arctic that we see in our simulations is more simply explained as a direct result of decreasing the SIC and SIT. The ocean has a larger heat capacity than sea ice, which will tend to make the temperature less variable over the ocean than over sea ice. We find strong gradients in 2-meter temperature variability across the ice margin in both the control simulation and in the perturbed (not shown); the contrast in surface properties appears to exert a stronger control on temperature variability than background temperature gradients. This suggests that the temperature variability will decrease over regions that have lost sea ice. Consistently, the reduction of sea ice thickness that occurs throughout the

year in our simulations allows more heat transfer and stronger atmosphere-ocean coupling which also tends to reduce temperature variability.

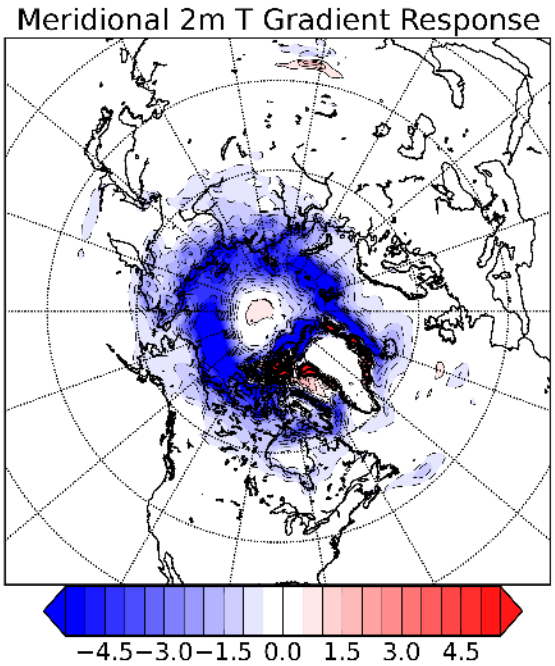

Figure 2.7: The equilibrium response of meridonal SON 2m temperature gradient (°C 1000 km^{-1}).

We note that unlike for the subseasonal response, the patterns of temperature gradient and interannual temperature variability response somewhat resemble each other (Figs 2.6a and 2.7). There is no obvious dynamical reason why interannual temperature variability should be connected to local temperature gradients; this coincidence likely has more to do with both fields being strongly influenced by the spatial redistribution of the melting sea ice and its variability. In particular,

- Regarding variability, regions that go from partially covered ice to ice free see a reduction of SIC variability, while regions that go from completely ice covered to partially ice covered see an increase of SIC variability (not shown). To the extent that these SIC variability changes are coupled to temperature, this might explain the slight increase in interannual variability in temperature poleward of the Canadian Arctic Archipelago in Fig. 2.6a, and might contribute to the reduction in interannual variability

in the Western Arctic Ocean. By contrast, the reduction of subseasonal variability has a wider spatial extent, and reflects a general reduction in temperature variability in an environment that has become more maritime and less continental.

- Regarding temperature gradients, the reduction in temperature gradients reflects enhanced Arctic amplification where sea ice is lost, whereas at the pole the temperature response over the remaining sea ice is quite weak and so is the temperature gradient response.

Other factors contributing to the change in variability over the Arctic Ocean and continents could include dynamical changes in the atmosphere, changes to clouds and precipitation associated with Arctic warming, and the advection of temperature variance. In addition, decreasing the difference in albedo between the ice and the ocean as we have done in these experiments weakens the ice-albedo feedback, which could also reduce the temperature variability, particularly on interannual timescales.

The seasonal cycle of the response of the variability in 2-meter temperature for different regions is shown in Fig. 2.8a. We calculate this by averaging the change in standard deviation over the Arctic Ocean, North America, and Eurasia for each month. The standard deviation here includes both intraseasonal and interannual variability. The season cycle of the change in variability in temperature for each of the three regions resembles the negative of the seasonal cycle of temperature in Fig. 2.3b. Over the Arctic Ocean, the main differences are the timing of peaks of reduction of variability which occur one month early in fall and one month later in spring compared to the temperature. In July, there is a slight increase in 2-meter temperature variability over the Arctic Ocean, which represents an exception to the general tendency of reduced variability. This increase might relate to an increase in the temperature gradient in the perturbation simulation over the Arctic Ocean in July. There are small reductions in temperature variability over land throughout most of the year, with the biggest changes being over North America in the winter. The change in temperature variability over the continents is likely linked to the weakening of temperature gradients as discussed in Screen (2014) and Schneider et al (2015) and possibly advection of the less variable air from higher latitudes.

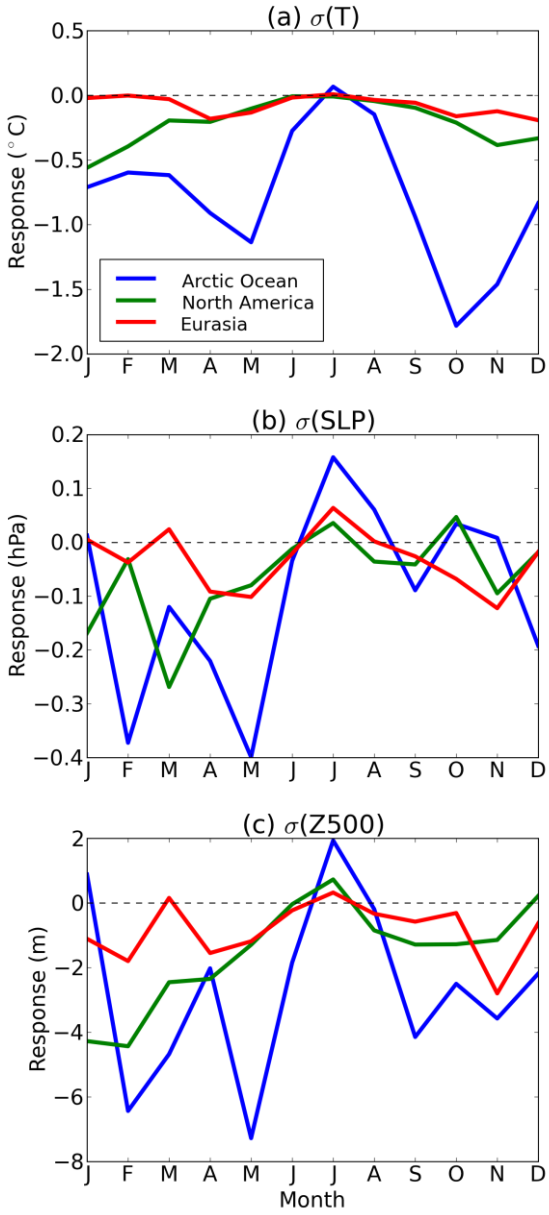

Figure 2.8: Seasonal cycle of the equilibrium response in standard deviation of (a) 2-meter temperature (°C), (b) SLP (hPa) and (c) Z500 (m) over the Arctic Ocean (blue), North America (green) and Eurasia (red). The standard deviation is calculated at each grid point before averaging.

The responses of sea level pressure (SLP) variability (Fig. 2.8b) and 500 hPa geopotential height (Z500) variability (Fig. 2.8c) are relatively small in amplitude compared to the background variability (e.g. changes in springtime Arctic temperature, SLP, and Z500 variability are on the order of 30%, 3%, and 5% respectively of the control simulation variability). The spatial structure of the responses (not shown) is much noisier than that seen in temperature (Fig. 2.6); generally speaking there is a reduction at each point of subseasonal variability of Z500 and a mixture of increases and decreases in interannual variability. As for temperature, for SLP and Z500 there is a decrease in variability in winter and spring particularly over the Arctic Ocean. In July, when the temperature variability increases slightly, there is an increase in SLP and Z500 variability. By the hypsometric equation, Z500 variability is influenced barotropically by surface pressure variability and baroclinically by tropospheric temperature variability (see e.g. Mudryk and Kushner 2011). Features of the change in Z500 variability seem to reflect a combination of changes in SLP and temperature variability.

Next we investigate whether there is any change in the amplitude of planetary waves as has been discussed in observations by Screen and Simmonds (2013), mainly in the context of the discussions about expected changes to midlatitude variability under Arctic amplification (e.g. Francis and Vavrus, 2012; Barnes, 2013). As in in Screen and Simmonds (2013) we use two complementary measures of the amplitude of the waves. The first, meridional amplitude (A_M), measures the meridional amplitude of an individual Z500 isopleth (line of constant geopotential height). As in Screen and Simmonds (2013) we use the 5400, 5500, 5700 and 5600 m isopleths for winter (JFM), spring (AMJ), summer (JAS) and fall (OND), respectively. The second method, zonal amplitude (A_Z), measures the amplitude of the depth and height of the troughs and ridges of the Z500 along the 45°N latitude circle. We use a Fourier decomposition to calculate the amplitude of wavenumbers 1-10 and the total amplitude around the whole northern hemisphere for each day. For a more detailed description of the methods see Screen and Simmonds (2013).

Figure 2.9 shows the percentage change in amplitude between the perturbed and control simulations for A_M (left) and A_Z (right) for wavenumber 1-10 and the total for seasons defined in Screen and Simmonds (2013). A black dot indicates 95% statistical significance using a Student t-test on the monthly means of the daily averaged amplitudes. Figure 2.9 is similar to Figure 2 in Screen and Simmonds (2013), except that they calculate a normalized trend instead of a response

based on equilibrated epochs of our simulations. There is generally an increase in A_M and a decrease in A_Z in response to sea ice loss. The largest changes in A_M are in AMJ when all wavenumbers show a significant increase in amplitude and the total amplitude increases by 6% in Fig. 2.9 or 0.2-0.3 standard deviations of the control run variability (not shown). This is relatively small compared to the 0.3-0.4 standard deviation per decade trend in the recent reanalysis record from Screen and Simmonds (2013). JAS and OND also show smaller but statistically significant increases in the total amplitude of 2-3%. A significant increase is also found in JFM wavenumber 1, but the JFM total response is not significant. The only season that has a statistically significant total response in A_Z is JFM with a decrease in amplitude of 1.5%. The other seasons all have a decrease in amplitude of varying degrees in intensity. The only season and wavenumber in which both methods show a statistically significant response of the same sign is JFM wavenumber one which shows an increase of 5-6% in A_M and A_Z.

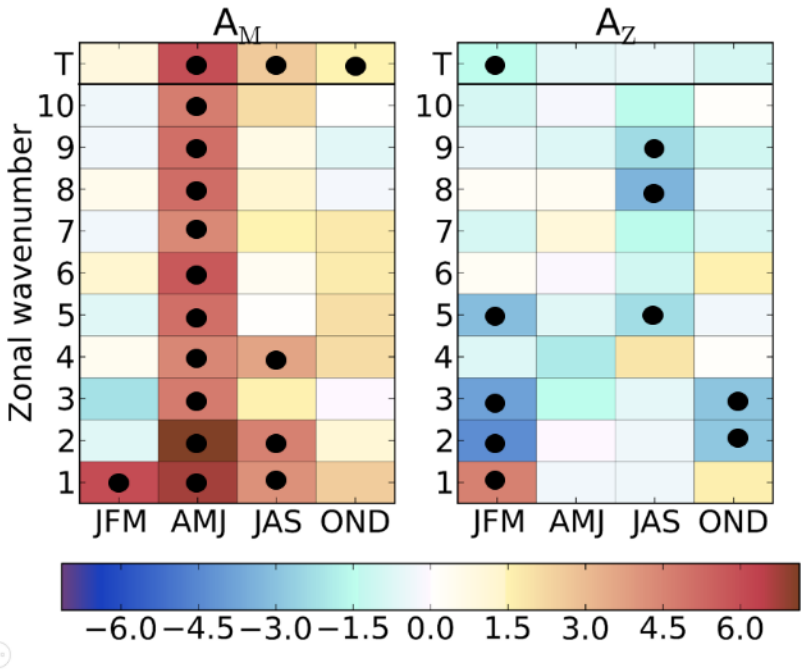

Figure 2.9: The equilibrium response in planetary wave amplitude (% change between perturbed and control simulations) in all four seasons and the first 10 wavenumbers, as well as the total (T) amplitude for A_M (left) and A_Z (right). The isopleths used for A_M are 5400, 5500, 5700 and 5600 m for winter (JFM), spring (AMJ), summer (JAS) and fall (OND), respectively. The black dots indicate a 95% statistical significance using a Student's t-test on the seasonal averages of the daily amplitudes.

Qualitatively, the general increase in A_M and decrease in A_Z was also seen by Screen and Simmonds (2013) in their analysis of the observed trends. Screen and Simmonds (2013) argue that this behaviour is in part expected: since more warming is observed at high latitudes, Z500 isopleths shift more poleward at high latitudes than at lower latitudes, increasing A_M. This same Arctic amplification effect is pronounced in our integrations. On the other hand, A_Z is measured at only one latitude, so it is not directly affected in a predictable way by Arctic amplification. Our results are consistent with this explanation as well. We see a larger contrast between the two methods than found by Screen and Simmonds (2013), and the seasonal and scale dependence of the results are also quite different. Apart from model inaccuracies, such differences are to be expected because observations do not reflect the idealized sea ice loss perturbation being imposed here and because we have the luxury of a multicentury sampling period versus the approximately 30 years of observations used by Screen and Simmonds (2013). The decrease in A_Z seen in our study may in part be due to the decrease in temperature variability and its associated impact on the Z500 variability (Fig. 2.8).

A number of studies have suggested that sea ice loss and associated Arctic amplification would lead to a slower circulation and more persistent weather in the mid latitudes, which could decrease temperature variability on short time scales, but increase it on longer time scales (Francis and Vavrus 2012; Coumou et al. 2015). To investigate the temporal dependence of the change in variability seen in Figs. 2.5,2.6 and 2.8 in more detail we calculate the temporal power spectra (displayed as the variance as a function of period) for SON 2-meter temperature over the Arctic Ocean (Fig. 2.10a), land temperature (Fig. 2.10c), and Z500 (Fig. 2.10e) for both the control and perturbed simulations. These are calculated by averaging the SON power spectra for each of the 200 years and over all grid points. For the land temperature and Z500 only grid points between 30°N and 60°N are used to capture the midlatudes. Figures 2.10b, e and f show the corresponding percent change in variance between the control and perturbed simulations. Over the Arctic Ocean, the power spectrum of the control simulation is very similar to what is seen over land, but it decreases by more than 50% at all periods in the perturbed simulations. The changes over midlatitude land are much smaller, but there is a decrease in variability across almost all periods, including all periods greater than 10 days. This decrease in temperature variability on all timescales is seen over both North America and Eurasia (not shown). The changes in the Z500 power spectra show a decrease in variability at periods less than 5 days and

longer than 30 days, with periods in between these values showing neither a robust increase nor a robust decrease. Similar results are seen in DJF, but with smaller magnitude changes over the Arctic Ocean and bigger changes over land in both 2-meter temperature and Z500 (not shown).

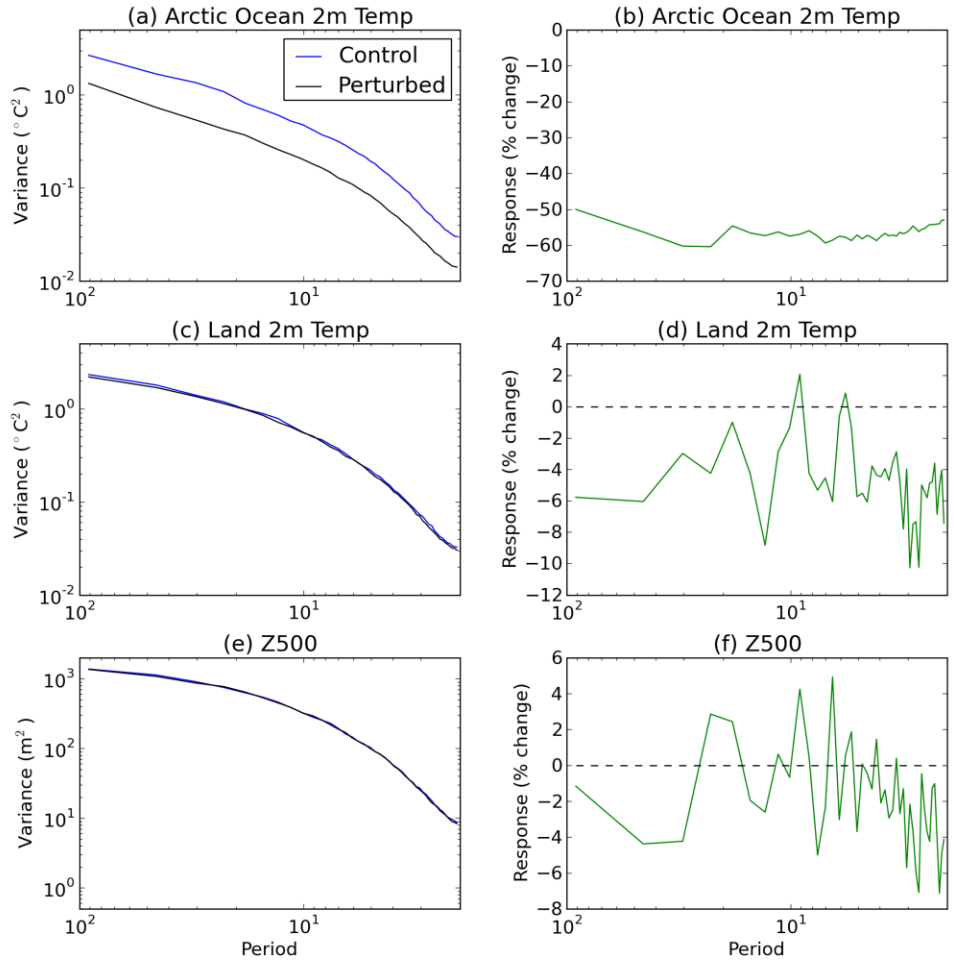

Figure 2.10: The power spectra for SON (a) Arctic Ocean 2-meter temperature (65°N-90°N), (c) land 2-meter temperature (30°N-60°N) and (e) 500 hPa geopotential height (30°N-60°N) for the control simulation (blue) and the perturbed simulation (black). The spectra are displayed as the variance ($°C^2$) as a function of period (days). The corresponding percent change in power spectral variance between the control simulation and perturbed simulations are in (b), (d) and (f).

In summary, for this CCSM4 sea ice perturbation experiment, summertime Arctic sea ice loss in isolation generally drives a reduction of point (spatially local) variability of the surface temperature, surface circulation, and midtropospheric circulation on nearly all times scales. In July, however, summertime Arctic sea ice loss drives a moderate increase in circulation variability. Given that this occurs during the season of maximum observed Arctic cyclone activity (Serreze and Barrett 2008) and there is evidence that Arctic amplification has changed the midlatitude circulation variability during summer in observations (Coumou et al. 2014, 2015), further analysis of this change will be an interesting subject of future study. Summertime sea ice loss drives an increase in the meridional excursion of isopleths, which can be attributed in part to the strong Arctic amplification built into our simulations, but a general decrease in eddy amplitude which is consistent with the point variability changes. This suggests that sea ice loss might be directly responsible for some of the observed trends in these two measures of wave amplitude. One exception is that sea ice loss drives an increase in wave-1 eddy amplitude and meridional excursion in JFM, which also merits future investigation.

2.3.3 Transient response

We now turn our focus to the robustness of the transient response to the sea ice loss during the first 50 years after the change to the sea ice was made. This is of interest because it can qualitatively be related to the global response to rapid sea ice loss that is currently observed. Figure 2.11 shows the December, January, February (DJF) 2-meter temperature difference between the perturbation and control integrations for all eight realizations over the first 50 years. The ensemble mean of this is shown in Fig. 2.13a. All realizations in Fig. 2.11 show an Arctic warming as well as warming over Hudson Bay and North America. Over Eurasia, the changes are more variable: the sign, magnitude, location and spatial extent of the change vary considerably between each realization. For example, relatively strong Eurasian cooling is seen in Realization 3, peaking around 1.5°C in the central part of Southern Russia. Realizations 1, 2 and 8 also have a cooling in eastern Asia of less than 1°C, while Realizations 5 and 6 have a cooling further to the west, north of the Black and Caspian Seas. Realization 4, however, shows a 0.5°-1°C warming over much of the northern part of Eurasia where many of the other realizations saw a cooling. The 2-meter temperature warming over North America is more consistent between realizations, however the amount of warming and the spatial pattern is

variable. For example the warming in Realizations 4, 5 and 6 is more confined to Eastern North America while the other realizations have warming over the western part of the continent as well.

The SLP difference between the perturbation and control integrations for all eight realizations over the first 50 years is shown in Fig. 2.12. Similar to the 2-meter temperature, there is significant variability between realizations. For example, the largest difference is in Realization 3 which has a strong positive SLP anomaly of about 4 hPa over the northern coast of Eurasia and a low pressure anomaly over the northern Pacific Ocean. Realization 4 has an opposite low pressure anomaly of about 2 hPa over the Arctic Ocean and a smaller high pressure anomaly over the northern Pacific Ocean. The other realizations all have a high pressure anomaly somewhere near the Eurasia Arctic coast and a low pressure anomaly over the Pacific, however the size and location varies between them.

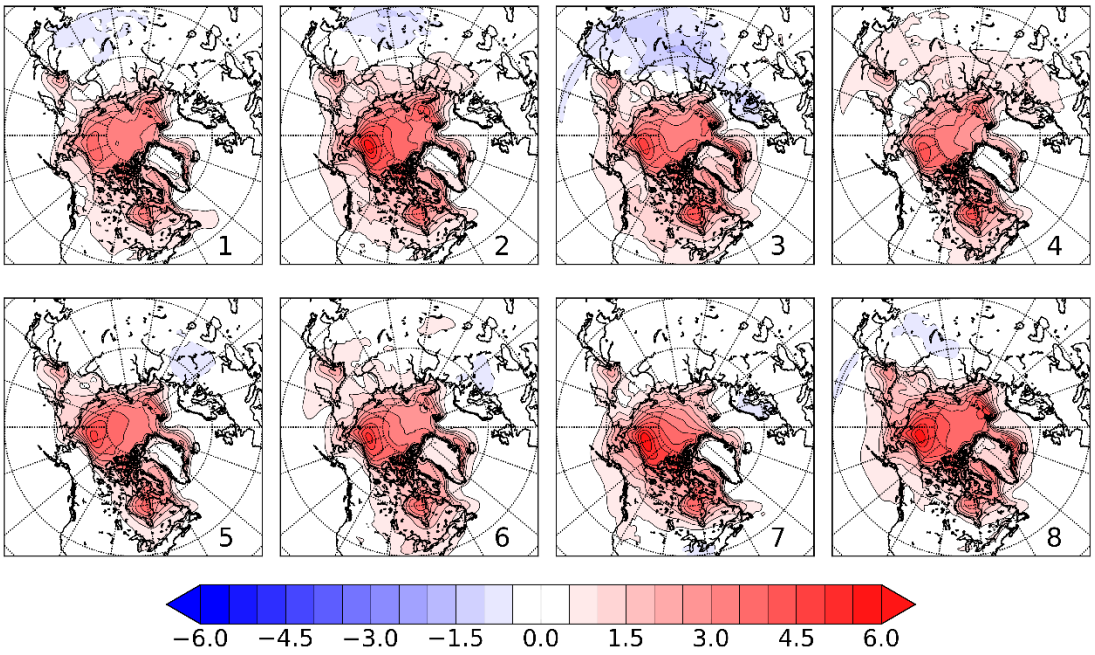

Figure 2.11: The DJF 2-meter temperature difference (°C) between Years 1-50 of each of the 8 perturbation simulations and the control integration.

Many of the differences in the 2-meter temperature changes in Fig. 2.11 can be understood in the context of the SLP changes in Fig. 2.12. For example, the strong high pressure anomaly in Realization 3 is associated with anomalous anticyclonic winds that advect the colder air from the Arctic Ocean and Siberia, creating a large cold anomaly. This can be applied to Realizations 1, 2 and 8; however, in these realizations, the anomalous SLP gradients are weaker

resulting in a smaller cold anomaly. Realization 4 has a low anomaly over the Arctic Ocean, so the cyclonic winds advect warmer air from the west to east resulting in warmer temperatures. Similar reasoning can be applied to explain the different temperature anomalies in the other realizations and over North America.

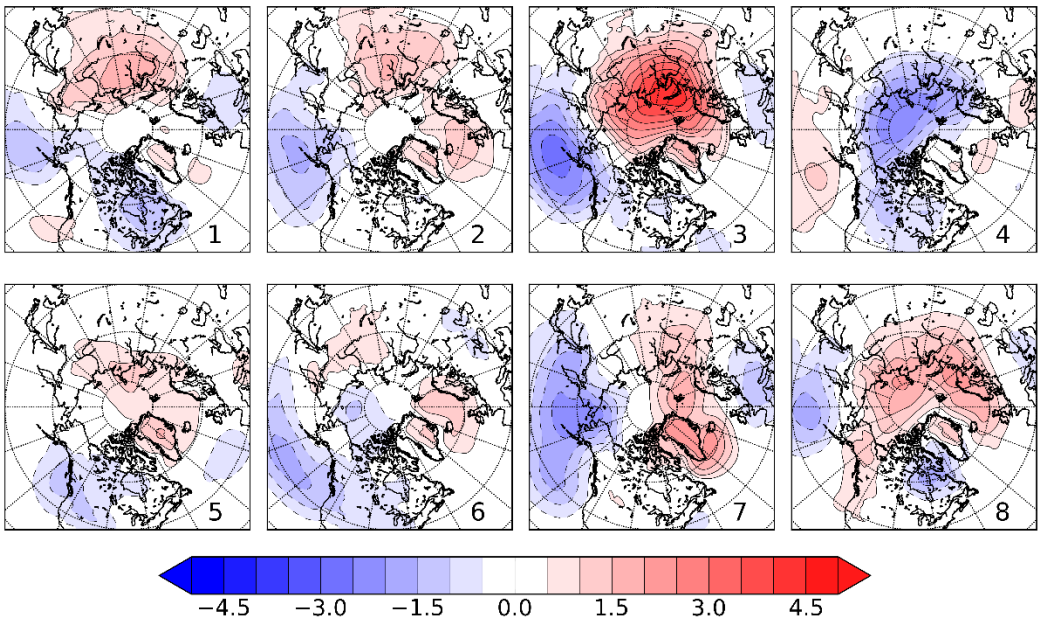

Figure 2.12: Same as in 2.11, but for SLP (hPa).

Figure 2.13 shows the DJF 2-meter temperature and SLP transient response averaged over all 8 realizations compared to the equilibrium response. The biggest difference in the temperature is that there is more warming over Eurasia in the equilibrium response that reflects a general warming of the ocean temperatures in response to sea ice loss (not shown). There is a slight cooling (0.3°C) over Eurasia in the transient response that is below the smallest contour level. It was not possible to find any 50-year periods during the equilibrium perturbation simulation period for which Eurasia was as cold as was found in any of the transient responses in any of the simulations. This suggests that although the difference between the transient and equilibrium responses in 2-meter temperature over Eurasia is small and there is a considerable amount of internal variability, the initial reduction in warming over Eurasia is a robust part of the response. The differences between the transient and equilibrium response in SLP are consistent

with the 2-meter temperature fields, as the only difference is the high pressure anomaly located over the coast of Northern Europe and Russia that advectively cools Eurasia during the transient period. In both the time periods, once sufficient averaging is done, the SLP response is very weak, especially in the equilibrium response where the only place that has a sizeable response is the 1-2 hPa SLP reduction in the North Pacific.

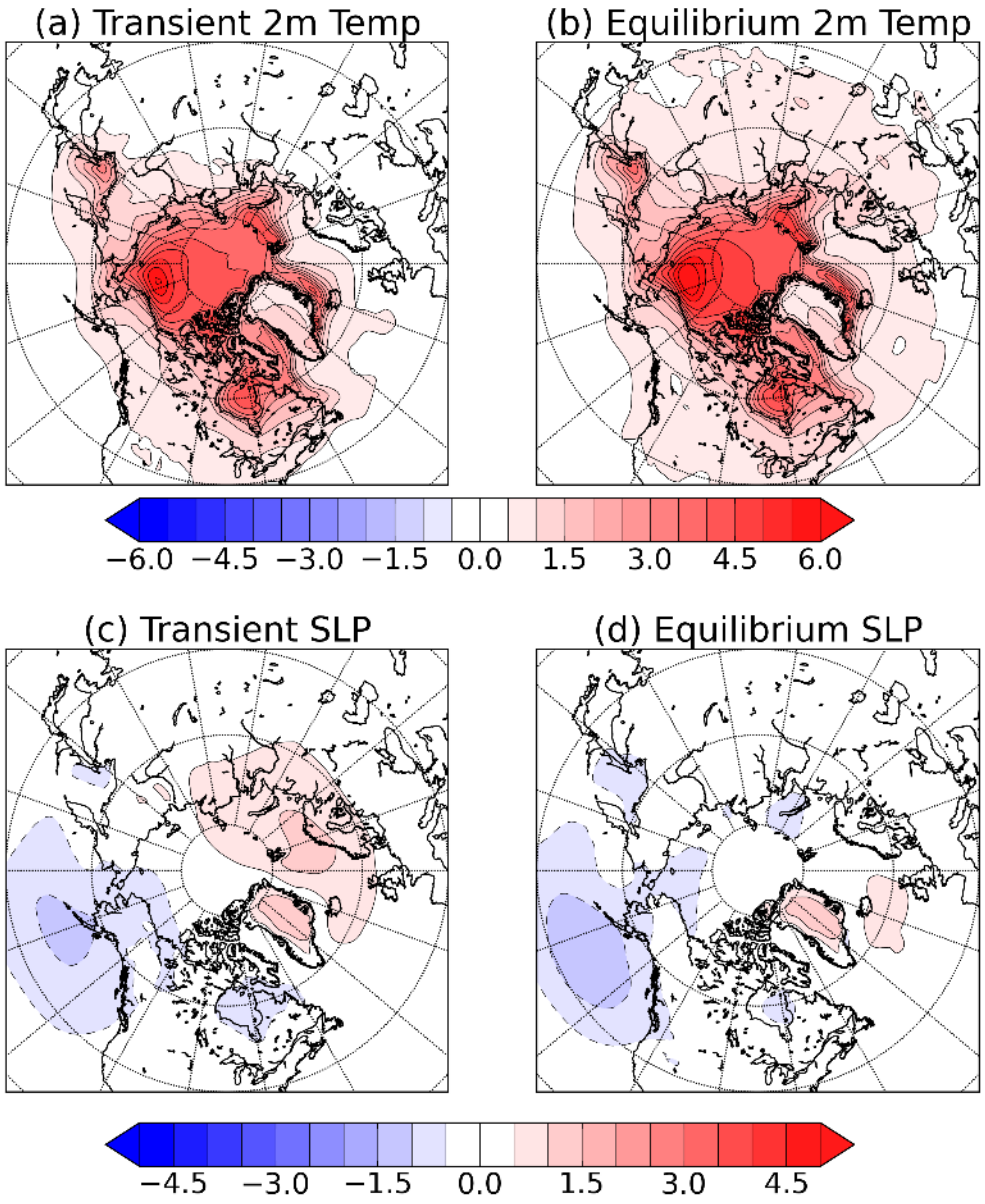

Figure 2.13: The transient (left) and equilibrium (right) response for DJF (a)-(b) 2-meter temperature (°C) and (c)-(d) SLP (hPa).

In this experiment neither of the robust features of the DJF SLP response — the cyclonic North Pacific response in both transient and equilibrium periods and the anticyclonic Eastern Arctic Ocean response in the transient period — resemble hemispheric modes of variability such as the North Atlantic Oscillation or the Northern Annular Mode, as has been suggested by the studies mentioned in the Introduction. The connection between reduced sea ice, particularly over the Barents and Kara Seas, SLP and temperatures over Eurasia has been explored in both observations and models in many other studies. The proposed mechanisms range from a thermally generated Rossby wave that enhances cold air advection from the Arctic to East Asia (Honda et al. 2009), changing the cyclone tracks through a reduction in baroclinicity near the Barents Sea (Inoue et al. 2012), a weakening of the zonal winds that bring warm air from the North Atlantic (Petoukhov and Semenov 2010). The transient winter 2-meter temperature response that we find is consistent with these results even though we do not see the same pattern in every realization. Some studies have suggested that sea ice loss in the Barents and Kara Seas generate upward propagating Rossby waves that weaken the stratospheric polar vortex, which can then propagate downward producing a negative NAM response at the surface and cold temperatures over land (Kim et al. 2014; King et al. 2015; Feldstein and Lee 2014). We do not see a robust stratospheric response in our simulations that survives multi-century averaging, so our simulations are not consistent with these explanations.

2.4 Summary and Discussion

We have examined the equilibrium and transient responses to sea ice albedo-induced summertime sea ice loss in a coupled ocean-atmosphere-sea ice-land model. Although the impact of the albedo perturbation is strongest in late summer, sea ice thickness is reduced and Arctic Ocean warming (not shown in our figures) occurs in all seasons. The seasonal cycle of the Arctic heat flux and temperature equilibrium response are similar to those found in prescribed SST experiments (e.g. Deser et al. 2010; Screen et al. 2013) with the largest response being in the fall and winter and lagging the changes in sea ice area. However, the coupling appears to enhance the springtime sensible and latent heat flux response.

The zonal mean warming, apart from a minor global warming response (Deser et al. 2015), is mainly confined to the lowest part of the atmosphere, consistent with Screen et al. (2012). This coincides with very little change in the zonal mean winds: we see an easterly

response per degree of Arctic warming of magnitude less than 0.1 m s^{-1} °C^{-1}. The amount of near surface Arctic warming in our integrations is comparable to several decades of greenhouse warming in the RCP8.5 scenario, and is more strongly Arctic amplified. Therefore, judging from this model, if a large reduction in jet stream strength associated with summertime sea ice loss and associated Arctic amplification is hypothesized, it needs to come from some other source than direct forcing by summertime sea ice loss. For example, the Arctic mid-troposphere is expected to warm for reasons not related to sea ice (Screen et al. 2012, Laliberte and Kushner 2013, 2014), and this will likely have more of an impact on the jetsream.

We find a large reduction in temperature variability throughout the middle and high latitudes in all seasons and at all timescales. The biggest changes are seen over the Arctic Ocean in fall where the standard deviation of the 2-meter temperature is decreased by more than half. This reduction is consistent with Screen (2014) and Schneider et al. (2015) who attribute it to decreased temperature gradients. Although the change in temperature gradients certainly contributes to the decrease in temperature variability, we have proposed that the difference in heat capacity between ice and ocean also plays a large role. This decrease in temperature variability that we see in our experiments implies that cold extremes will become less likely as a result of summertime sea ice loss, in agreement with Screen et al. (2015). Conversely, if an increase in cold extremes is hypothesized under global warming, mechanisms will need to be found that counteract the simple effects of weakened temperature gradients and increased ocean-atmosphere coupling associated with summertime sea ice loss. We also find a decrease in SLP and Z500 variability throughout most of the year and over most regions although the changes were found to be smaller than in temperature. The change in tropospheric planetary wave amplitudes were shown to be dependent on the metric used, with a general increase in A_M and a decrease in A_Z qualitatively similar to what was found in the analysis of observed trends in Screen and Simmonds (2013), apart from a robust increase in Wave-1 amplitude in both A_M and A_Z, which is currently under investigation and is not to our knowledge detected in the observations. The increase in A_M is explained as an impact of Arctic amplification induced by the simulation, and the reduction in A_Z is consistent with the reduction of geopotential variability at each point. The similarity suggests that summertime sea ice loss might have a role in driving changes in variability qualitatively similar to observations. However, the changes are small compared to those observed (0.3 standard deviation reduction in response to sea ice loss in our

simulations versus 0.3-0.4 standard deviation per decade in observations), suggesting a limited role for summertime sea ice loss in driving recent observed changes.

We have investigated the transient adjustment to the sea ice albedo perturbation in the presence of internal variability. We find that the wintertime SLP and 2-meter temperature response to rapid sea ice loss in the first 50 years is different to that equilibrium response, with a high-pressure anomaly response over the Eurasian coast that is not seen after its adjustment to equilibrium. This high-pressure anomaly is associated with a cold temperature response over Eurasia as a result of colder air being advected from the Arctic. Although the ensemble mean transient response was found to be different from the equilibrium response, there is considerable spread in the location, magnitude, and even the sign among realizations. The total amount of sea ice reduction in each of these realizations was very similar and there is no correlation between any regional differences in SIC and the response patterns (not shown), so internal atmospheric variability is likely the main reason why we see such large differences. The large samples required to detect a robust response reinforces the point that attributing observed changes in circulation to sea ice loss will remain an ongoing challenge.

We conclude with a note of caution concerning the robustness of these results. For example, sea ice loss experiments with different models, have shown more significant changes in the strength of the jet stream. As will be shown in Chapter 3, CESM1 has a larger magnitude response to sea ice loss in wintertime even when scaled by the amount of sea ice loss or temperature response (see also Peings and Magnusdottir, 2014). One way that model differences could lead to different responses to sea ice loss is through how the stratosphere is represented. It has been shown that CAM4, the atmosphere model used in CCSM4, produced a weaker tropospheric circulation response compared to a version of the same model with a better resolved stratosphere (Sun et al. 2015) and that, more broadly, intermodel spread in stratospheric wind response contributes to the intermodel spread in Arctic circulation change in CMIP5 climate change experiments (Manzini et al. 2014). In addition, there is some evidence that the climate model response to climate variability is too weak compared to observations, particularly in the North Atlantic (Gastineau et al. 2013; Eade et al. 2014), so it is possible that this could also be the case in our simulations in response to sea ice loss. Multimodel comparisons are required to better assess the extent to which changes in midlatitude winds can be separately attributed to

Arctic sea ice loss and mid-tropospheric Arctic warming from the global warming process (Screen et al. 2012; Laliberte and Kushner 2013, 2014).

Chapter 3
Isolating the Atmospheric Circulation Response to Arctic Sea Ice Loss in the Coupled Climate System

3.1 Introduction

Some of the more recent studies that have investigated the impact of sea ice loss have shown that sea ice loss in models with a full dynamical ocean component contributes to a moderate global warming signal (Chapter 2; Deser et al. 2015, 2016). Some aspects of the signal can be attributed to thermodynamic and dynamical changes in the ocean (Deser et al. 2016; Tomas et al. 2016) through experiments with prescribed sea surface temperatures and a slab ocean model that can be compared to simulations with a full ocean model. These studies show that the global warming signal is directly induced by polar warming, is spread through the climate system by the ocean-atmosphere circulation, and is amplified by water vapour greenhouse feedbacks. Although this global warming signal is small, the associated atmospheric changes outside the polar regions are difficult to disentangle from the direct impact of the sea ice loss.

The purpose of the sea ice loss modelling experiments is to isolate changes associated with sea ice loss in observed and projected climate change. Sea ice loss, under standard forcing scenarios (e.g. from CMIP5), occurs concurrently with global warming, lower tropospheric polar amplification that reduces lower tropospheric temperature gradients, and upper tropospheric tropical amplification that increases upper tropospheric temperature gradients. These different temperature gradient changes have separable influences on storm track responses in the models contributing to CMIP5 (Harvey et al. 2014). Other work reveals a “tug of war” between the warming in the tropics and warming at the poles (Barnes and Polvani 2015): CMIP5 models that have more Arctic amplification tend to have a weaker and more equatorward jet response than models that have less Arctic amplification associated with sea ice loss. This is consistent with results from a simple general circulation model in which upper tropospheric and lower tropospheric temperature gradients can be separately controlled (Butler et al. 2010). These studies show that even though sea ice loss can impact the circulation at lower latitudes, this effect can be masked or counteracted by the effects of lower latitude warming (Barnes and Screen 2015).

In this chapter, we ask whether it is possible to separate the direct influence of sea ice loss from low-latitude ocean warming using information from available coupled greenhouse-dominated radiative forcing simulations and sea ice forcing simulations. We probe this question with two sets of climate model experiments, each performed with two coupled Earth System Models from the National Center for Atmospheric Research (NCAR; Section 3.2). The first set of experiments is forced with historical and then with representative concentration pathway 8.5 (RCP8.5) future projections of forcing, which produces a significant amount of sea ice loss and relatively strong warming at lower latitudes. The second set of experiments is forced with sea ice albedo reduction under constant radiative forcing, as in Chapter 2, which produces significant sea ice loss but relatively weak warming at lower latitudes (Section 3.3).

The classical idea of *pattern scaling* in climate change simulations posits that the response in many variables, including sea ice loss, to climate change is proportional to the amount of global warming (Santer et al. 1990, Tebaldi and Arblaster 2014). But in coupled sea ice loss experiments, the amount of sea ice loss per degree of global warming is much greater than for greenhouse-dominated radiative forcing (Chapter 2; Deser et al. 2015, 2016). We use this information to attempt to isolate the response to sea ice loss on multidecadal mean fields such as the zonal mean circulation and the midtropospheric flow. As indicators of the two processes that vary at least partially independently in response to the different forcings employed, we use the total SIA and the spatial mean of low-latitude SSTs. We hypothesize that we can use information from both types of experiments to separately attribute the pattern of atmospheric circulation response to sea ice loss without low-latitude surface warming and to low-latitude surface warming without sea ice loss (Section 3.4). We demonstrate the consequences of this hypothesis (Section 3.5) by decomposing the response under RCP8.5 forcing separately to the two processes. We show that potentially useful information can be produced when combining information from equilibrated timeslice experiments (as in the sea ice loss simulations) and transient climate forcing experiments (RCP8.5), provided sufficient data is available to average out internal variability. Follow-on ideas for generalizing this approach and more carefully testing the hypotheses are presented in Section 3.6. The Appendix provides additional background on the response in the different Earth system model simulations.

3.2 Models and Experiments

3.2.1 CESM1 experiments

We focus on two sets of experiments using CESM1, a coupled atmosphere/ocean/land/sea ice model (see section 1.5 for more details). To determine the atmospheric response to historical and projected anthropogenic and natural forcing, we use the CESM1 large ensemble (Kay et al. 2015). This is a 30-member initial condition ensemble that simulates the climate from 1920-2100. The 30 realizations are initialized by perturbing the temperature with numerical round-off differences in air temperature on Jan 1st 1920 in a historical forcing simulation. These 30 realizations are then forced with historical greenhouse gas, aerosol, solar and volcanic forcing, as well as prescriptions of land use change, until 2005, where they are then forced with the RCP 8.5 anthropogenic and natural forcings until 2100. Because each realization has the same forcing, any difference between the realizations is due to internal variability, which is averaged out in the ensemble mean provided a sufficiently large ensemble is used.

To isolate the climatic response to sea ice loss we follow the method used in Chapter 2. First, a 725 year long control simulation that has constant Year 2000 radiative forcing is branched off one of the CESM1 large ensemble members at Year 2000. After some adjustment as the planet continues to warm to its equilibrium state (see Section 3.3), a sea ice albedo forcing simulation is branched off the control simulation at year 301 (nominal Year 2300). As in Chapter 2, this is created by instantaneously altering three parameters in the sea ice code that change the albedo of the sea ice, allowing it to absorb more sunlight and rapidly melt. This sea ice albedo forcing simulation is run for a total of 525 years. The albedo change is applied to the whole sea ice field in both hemispheres, causing summertime sea ice loss in both the Arctic and Antarctic and warming in both hemispheres.

3.2.2 CCSM4 experiments

We will also use a similar set of experiments using the CCSM4. Details of the model and the differences between CCSM4 and CESM1 are outlined in Section 1.5. As for CESM1, we use sea ice albedo forcing and an RCP8.5 forcing experiment for CCSM4. The sea ice albedo forcing experiments are the same simulations used in Chapter 2and are set up identically to the CESM1

experiments just described. They consist of a 780 year long Year 2000 radiative forcing control simulation and an 800 year long sea ice albedo forcing simulation. The CCSM4 RCP8.5 forcing simulations are similar to the CESM1 experiments, however only 5 realizations are available compared to 30 realizations for CESM1. This means that internal variability plays a larger role in the CCSM4 RCP8.5 results, as will be noted in Section 3.5b.

For reference, in the Appendix we briefly compare selected aspects of the long-term sea ice albedo forcing experiments for CESM1 and CCSM4, including the seasonal cycle of sea ice loss, warming, and surface energy budget changes. In the plots below, significance of model responses is tested using a student's t-test, assuming that each year is independent. This likely overestimates significance, but is adequate to assess relative significance of the response in different fields. Statistical significance for the variability plots (Fig. 3.10) is calculated using an f-test for equal variance. The number of degrees of freedom used for the f-test is the total number of days divided by 10.

3.3 Sea Ice and Sea Surface Temperature Response

The time series of the annual mean Arctic SIA for the CESM1 simulations are shown in Fig. 3.1a. The blue curve shows the ensemble mean SIA for the 30 realizations of the CESM1 historical and RCP8.5 forcing simulations from 1920 to 2100. Because much of the internal variability is averaged out, the SIA time series is a relatively smooth curve that represents the forced response. The annual mean SIA is relatively constant at about 11 million km^2 until toward the end of the 20^{th} century when it starts to decrease significantly to less than 4 million km^2. At year 2000 in one of the ensemble members, the Year 2000 control simulation (red curve) is branched off and the sea ice continues to slowly melt, with SIA decreasing from about 10 to 9 million km^2 over about two hundred years as the coupled system adjusts to equilibrium. The sea ice albedo forcing simulation (green curve) is branched off at year 301 of the Year 2000 control. In the first year, over 2 million km^2 of sea ice melts; the ice continues to melt as SIA equilibrates at about 6 million km^2. The seasonal cycle of sea ice loss (see Appendix) shows a sea ice free Arctic (< 0.5 million km^2) in August, September and October, reflecting the large shortwave forcing and albedo feedbacks in the polar Arctic. Wintertime sea ice loss is more modest but the sea ice experiences thinning throughout the year.

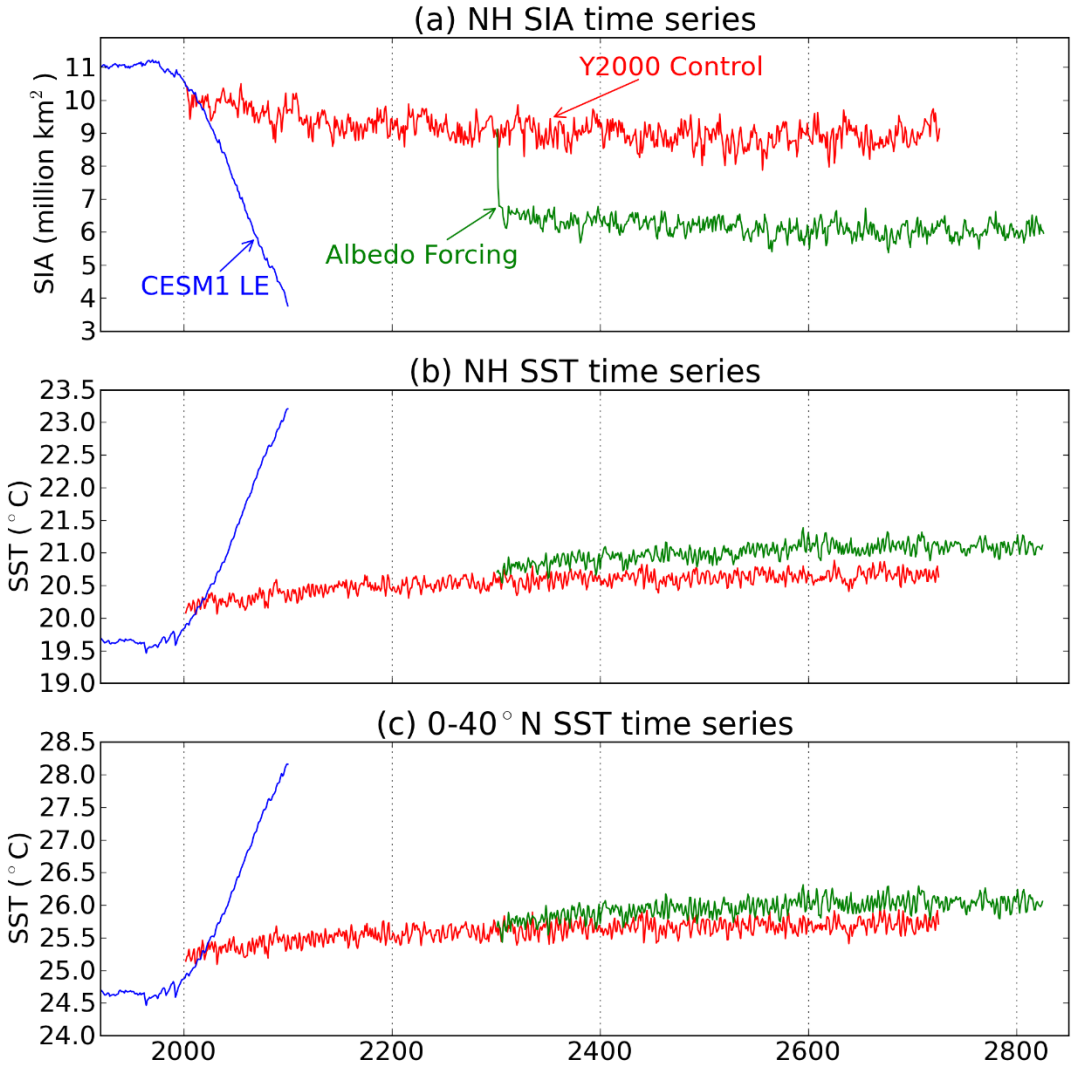

Figure 3.1: (a) The time series for the Northern Hemisphere SIA (10^6 km^2) for the ensemble mean of the CESM1 large ensemble (CESM LE) historical and RCP8.5 simulation (blue), the CESM1 Year 2000 control simulation (red) and the sea ice albedo forcing simulation (green). (b) As in (a) but for the Northern Hemisphere average SST (°C). (c) as in (b), but averaged only between 0° and 40° N.

The annual mean, northern hemisphere mean SST is shown in Fig. 3.1b. As expected, the SSTs warm very strongly in response to greenhouse gas-dominated radiative forcing in the historical and RCP8.5 forcing simulations. In addition, temperatures continue to increase by approximately 0.4°C in the Year 2000 control simulation before equilibrating. In the sea ice albedo forcing simulation, there is about 0.3°C warming immediately after the perturbation is imposed and then a slow warming as the system adjusts to a new equilibrium on a global scale. Figure 3.1c shows the SSTs averaged between 0° and 40°N in these three experiments to

represent low-latitude northern hemisphere warming away from the Arctic. Even at these lower latitudes, albedo forcing drives a small warming of about 0.3°C that reflects the "mini" global warming (Deser et al. 2015) induced by a warmer ocean and greenhouse warming related to water vapour feedback. One task of our analysis is to try to separate out the impact of this additional warming from the sea ice loss response.

Figure 3.2 plots the Arctic SIA response against the low-latitude SSTs (averaged from 0-40°N) in each of the simulations for the annual mean, September-October-November (SON) and December-January-February (DJF). Each blue dot represents the ensemble mean for each year of the 30 transient CESM1 historical and RCP8.5 simulations, and the red and green dots represent the time mean Year 2000 control simulation and sea ice albedo forcing simulations respectively. Only the last 425 years for the control and 275 years for the sea ice albedo forcing simulation were used, because this is when the simulations had reached equilibrium. In the annual mean (Fig. 3.2a), there is a linear relationship between the SIA and lower latitude SSTs: for every 1 million km^2 of sea ice loss there is an increase in SSTs at the lower latitudes of approximately 0.49°C. This linear relationship has also been seen between SIA and global temperatures in most climate models (Winton 2011; Mahlstein and Knutti 2012).The equilibrated Year 2000 control simulation lies very close to the RCP8.5 forcing simulation in the early 2030's. This means that for CESM1 under RCP8.5 forcing, there is the equivalent of just over 30 years of SST warming and sea ice loss in the adjustment to equilibrium in the Year 2000 control simulation. In the sea ice albedo forcing simulation there is less warming compared to the amount of sea ice loss, so it does not lie on the same line as the transient RCP 8.5 simulation. For every million km^2 of sea ice loss, there is approximately 0.12°C warming in the SST at lower latitudes, or about four times less than in the RCP8.5 simulations.

The scatter plots of SIA vs the SSTs averaged from 0-40°N for SON and DJF for the RCP8.5 do not show as straightforward a linear relationship. Towards the end of the 21^{st} century during SON, there is less SIA decrease per increase in SST as result of the Arctic becoming ice free in these months. In DJF, the opposite happens: the sea ice loss per degree of low-latitude warming increases in the middle of the 21^{st} century. This could be the result of the ice edge entering the Arctic Ocean at this time making more ice available to melt, as described by Eisenman (2010) to explain why the rate of Arctic ice loss is faster in summer than in winter. In

other words, the reason for increased rate of sea ice loss in winter could be that the sea ice edge becomes more "summer like" once the ice edge retreats into the Arctic Ocean.

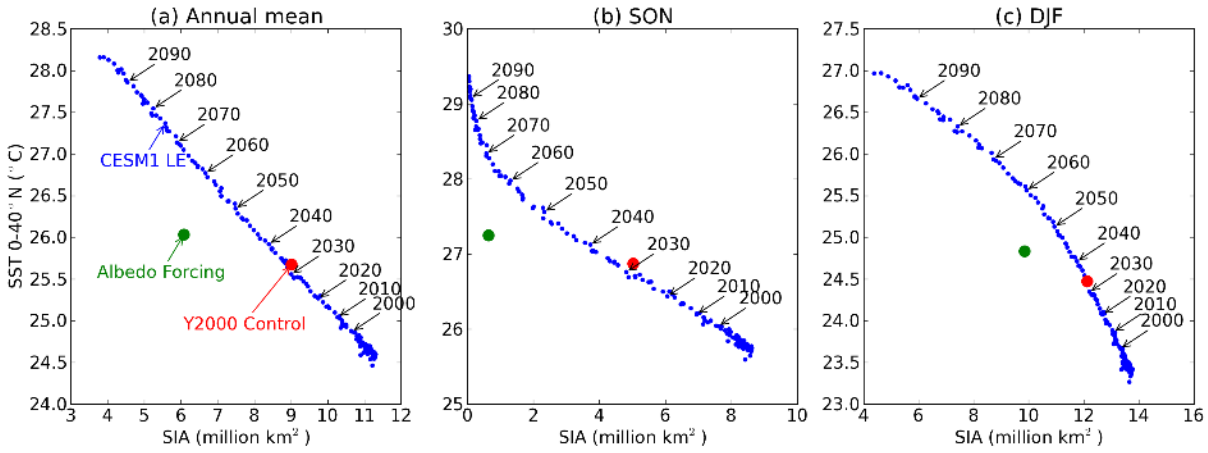

Figure 3.2: Scatter of Northern Hemisphere SIA (10^6 km^2) against SST (°C) averaged from 0° and 40° N for the annual mean (a), the SON mean (b), and the DJF mean (c). Each blue dot represents the ensemble mean from one year of the CESM1 large ensemble historical and RCP8.5 forcing simulations. The red and green dots represent the equilibrium mean year 2000 control simulation and sea ice albedo forcing simulation respectively.

A summary of the change in Arctic SIA and SST from 0-40° N for the annual mean and for DJF for each experiment are presented in Table 3.1. To easily compare the sea ice albedo forcing experiments with the RCP8.5 experiments, we have used 10-year averages of the ensemble mean of epochs when total Arctic SIA matched as closely as possible their amounts in the Year 2000 simulation and the sea ice albedo forcing simulation. These epochs are 2027:2036 and 2063:2072 for the annual mean and 2027:2036 and 2057:2066 for DJF. (For CCSM4, we used 20 year averages to compensate for the relatively small number of transient RCP8.5 realizations. The epochs are 2030:2049 and 2062:2081 for the annual mean and 2032:2051 and 2052:2071 in DJF for CCSM4.) The difference between these two epochs defines the climate response in the RCP8.5 experiments. The reason that the separation between epochs is shorter for DJF than for the annual mean is that sea ice albedo forcing drives less sea ice loss in winter than in summer due to a lack of shortwave forcing in winter (Deser et al 2015). The amount of low-latitude warming in the sea ice albedo forcing experiments in CESM1 is about 25% of that in the RCP8.5 forcing experiments in the annual mean (about 30% in DJF). The CCSM4 results are similar, except that we see less ice loss in response to the same albedo forcing, especially during DJF. We see more low-latitude warming relative to the RCP 8.5 experiments than Deser et al.

(2015) did, possibly a result of the Antarctic sea ice melting, which was not included in Deser et al. (2015), contributing to the global warming response, or a result of the different methods used to melt the sea ice.

Table 3.1: The change in Northern Hemisphere SIA (δI) and SST averaged between 0° and 40°N (δT) and their ratios for the different experiments in either the annual mean or the DJF mean.

	Arctic SIA δI (10^6 km^2)	0-40N SST δT (°C)	$\delta T / \delta I$
Annual CESM1 RCP8.5 forcing (2063:2072-2027:2036)	-2.90	1.44	-0.495
Annual CESM1 sea ice albedo forcing	-2.94	0.358	-0.122
DJF CESM1 RCP8.5 forcing (2057:2066-2027:2036)	-2.36	1.16	-0.494
DJF CESM1 sea ice albedo forcing	-2.28	0.360	-0.157
Annual CCSM4 RCP8.5 forcing (2062:2081-2030:2049)	-2.16	0.927	-0.429
Annual CCSM4 sea ice albedo forcing	-2.12	0.221	-0.104
DJF CCSM4 RCP8.5 forcing (2052:2071-2032:2051)	-1.25	0.558	-0.447
DJF CCSM4 sea ice albedo forcing	-1.17	0.227	-0.194

Figure 3.3 shows the spatial maps of the response of the DJF SIC and SIT in both the RCP8.5 forcing experiments and the sea ice albedo forcing experiment and their differences. The responses in the RCP8.5 experiments are calculated using the epochs in Table 3.1. Despite the different forcing mechanisms, the two experiments show a similar spatial pattern of sea ice loss. For SIC, the region that shows that biggest difference between the two experiments is the Barents-Kara Sea region, where the RCP8.5 experiment has greater losses (about a 20% larger change in SIA averaged from 40°E-80°E and 70°N to 80°N). The RCP8.5 experiment also has a larger decrease in SIC in the Bering Strait region and a smaller decrease in SIC throughout most of the rest of the Arctic Ocean. For SIT, both experiments show similar thinning of the sea ice

throughout the entire Arctic Ocean, but the sea ice albedo forcing experiment generally shows more thinning (the differences are less than 0.15 m).

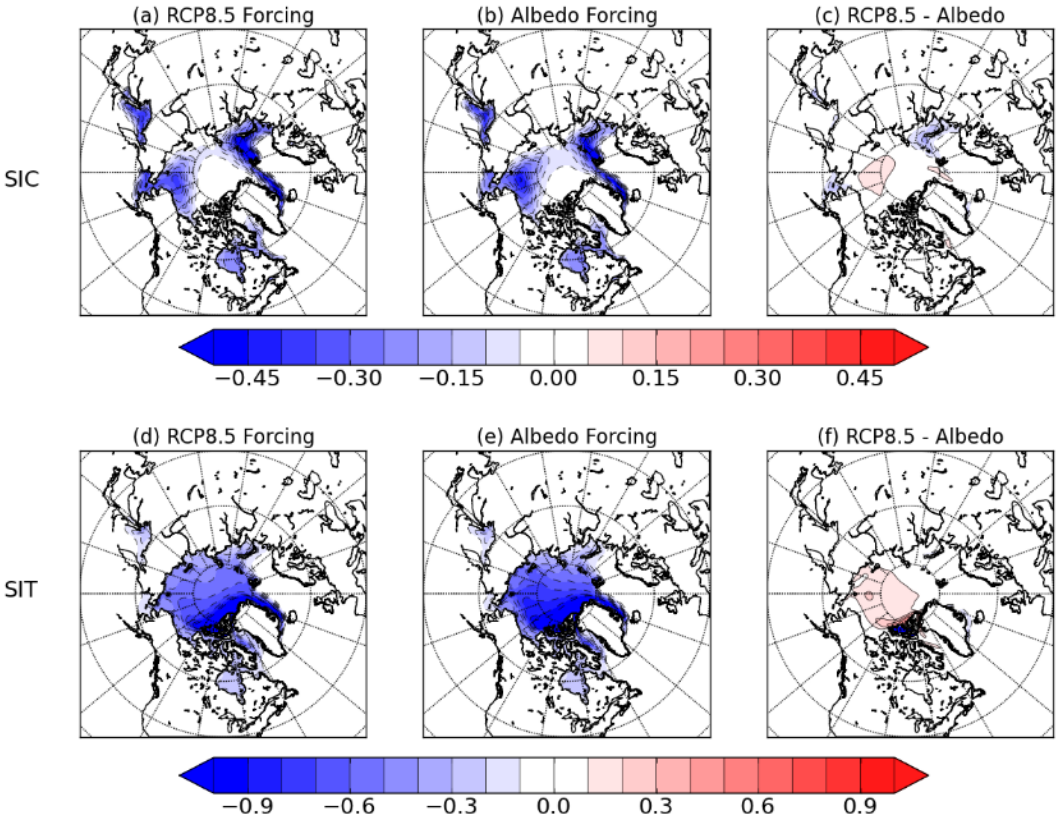

Figure 3.3(a): The DJF SIC response (fraction) for the ensemble mean of the CESM1 RCP8.5 forcing experiment, expressed as the difference between the 2027:2036 epoch and the 2063:2072 epoch. (b) As in (a), but for the CESM1 sea ice albedo forcing experiments, expressed as the difference between the sea ice albedo perturbation experiment and the Year 2000 control experiment. (c) The difference in the SIC responses (RCP8.5 forcing –Albedo forcing). (d)-(e) As in (a)-(c), but for the SIT response (m).

3.4 Using Pattern Scaling to Isolate the Response to Sea Ice loss

Figures 3.4a and b, which will be described in more detail in the next section, show the response of the annual mean and zonal mean temperature for the RCP8.5 and sea ice albedo forcing experiments, respectively. Figure 3.4a shows the temperature response as a difference for the RCP8.5 epochs whose net sea ice loss (i.e. reduction of sea ice area) is quite similar to that found in the sea ice albedo forcing experiment (Section 3.2 and Table 3.1). A key point to notice is that the amplitude and structure of the lower tropospheric warming in the two simulations is

quite similar. This suggests that aspects of the atmospheric response to sea ice loss might be controlled by the total amount of sea ice loss and might be less sensitive to details such as the spatial pattern of the sea ice loss (Fig. 3.3) and the cause of the sea ice perturbation. We also notice that there is moderate tropical upper tropospheric warming in the sea ice albedo forcing experiment, a feature also found more strongly in the RCP8.5 forcing experiment. This is part of the "mini" global warming induced by sea ice loss in the coupled climate system (Deser et al. 2015). This response is described classically as a response to low-latitude surface warming, which is stronger under greenhouse warming, and can be considered separately from the sea ice response. This motivates our approach of decomposing the total response due to the separate controls of sea ice loss and low-latitude ocean surface warming.

We propose a pattern scaling approach in which Arctic sea ice area (*I*) and low-latitude SST (*T*), are the controlling variables. Defining *Z,* which represents a field, such as 500 hPa geopotential height at a given northern hemisphere geographic location, that could be affected by both sea ice loss and low-latitude surface warming, we write *Z=Z(T,I).* We consider how *Z* varies in response to small variations in *T* and *I.* Symbolically we write

$$\delta Z = Z(T+\delta T, I+\delta I) - Z(T,I) \approx \left.\frac{\partial Z}{\partial T}\right|_I \delta T + \left.\frac{\partial Z}{\partial I}\right|_T \delta I \,. \qquad \text{Eq. (3.1)}$$

The first partial derivative on the right hand side of this equation represents the response of *Z* to a change in low-latitude temperature while the sea ice area is held constant and the second partial derivative represents the response of Z to a change in sea ice area while the low-latitude temperature is kept constant. To estimate these derivatives we use the output of the two sets of experiments, according to Eq. (3.1):

$$\delta Z_A = \left.\frac{\partial Z}{\partial T}\right|_I \delta T_A + \left.\frac{\partial Z}{\partial I}\right|_T \delta I_A \qquad \text{Eq. (3.2)}$$

$$\delta Z_R = \left.\frac{\partial Z}{\partial T}\right|_I \delta T_R + \left.\frac{\partial Z}{\partial I}\right|_T \delta I_R \,. \qquad \text{Eq. (3.3)}$$

Here the subscript *A* indicates the response (long-term equilibrium difference from control) in the sea ice albedo forcing experiment and the subscript *R* the response (ensemble mean epochal

difference) in the RCP 8.5 forcing experiment. We can diagnose all quantities in these equations except the two partial derivatives. Since we have two equations and two unknowns we are able to solve for these terms by inversion:

$$\begin{pmatrix} \left.\frac{\partial Z}{\partial T}\right|_I \\ \left.\frac{\partial Z}{\partial I}\right|_T \end{pmatrix} = \frac{1}{\delta I_A \delta T_R - \delta I_R \delta T_A} \begin{pmatrix} -\delta I_R & \delta I_A \\ \delta T_R & -\delta T_A \end{pmatrix} \begin{pmatrix} \delta Z_A \\ \delta Z_R \end{pmatrix} . \qquad \text{Eq. (3.4)}$$

The two terms are simply linear combinations of the responses in each of the two experiments, weighted by the amount of sea ice loss and low-latitude surface warming in each experiment. Note that the partial derivatives on the left-hand side of Eq. (3.4) and the quantities δZ_R and δZ_A on the right-hand side of Eq. (3.4) are spatial fields. The denominator and two-by-two matrix on the right-hand side of Eq. (3.4) are not spatial fields but simply the four numerical values obtained from the sea ice loss and low-latitude warming in the two experiments.

We note that the expressions above are somewhat ambiguous to interpret. For example, although we use the SSTs from 0-40°N as the T to perform this calculation, it does not necessarily mean that any part of the response that appear in this term is directly caused by the low-latitude warming. Instead, it means that that part of the response scales with the SSTs from 0-40°N in these experiments as distinct from the scaling with Arctic sea ice loss. Thus, the first term on the right-hand side of Eq. (3.1) can be thought of as the part of the response due to low-latitude surface warming not related to sea ice loss. Similarly, the second term on the right hand side of Eq. (3.1) can be thought of as the part of the response due to sea ice loss that is not related to low-latitude surface warming. This is distinct from the result of the sea ice forcing experiments because of the warming induced at low latitudes in the coupled system.

For the CESM1 results, the values for δZ_R, δI_R, and δT_R will be calculated using the epochal difference between two time periods used in Table 1, so that the simulations have similar amounts of sea ice loss with $\delta I_R \approx \delta I_A$. Defining $\varepsilon = \delta T_A / \delta T_R < 1$ as the ratio of the sea ice albedo forcing's warming to the RCP8.5 forcing's warming at this time (ε ranges from 25% to 40% in Table 1), then some algebraic manipulation leads to the following expressions for the low-latitude surface warming and sea ice loss contributions diagnosed for the RCP8.5 response:

$$\frac{\partial Z}{\partial T}\delta T_R = \frac{\delta Z_R - \delta Z_A}{1-\varepsilon},\ \frac{\partial Z}{\partial I}\delta I_R = \frac{\delta Z_A - \varepsilon\delta Z_R}{1-\varepsilon}\ . \qquad \text{Eq. (3.5)}$$

The first equality represents the diagnosed part of the RCP8.5 response associated with low-latitude temperature change and the second equality the response associated with sea ice loss. These expressions provide four useful special cases: if $|\delta Z_R| << |\delta Z_A|$ (i.e. the magnitude of the RCP8.5 response is negligible), then

$$\frac{\partial Z}{\partial T}\delta T_R = \frac{-\delta Z_A}{1-\varepsilon},\quad \frac{\partial Z}{\partial I}\delta I_R = \frac{\delta Z_A}{1-\varepsilon}\ . \qquad \text{Eq. (3.6)}$$

This implies that if the RCP8.5 forcing response is negligible the low-latitude surface warming and sea ice loss parts of the decomposition are approximately equal and opposite and inflated by a factor of $1/(1-\varepsilon)$. If $\delta Z_A = \varepsilon\delta Z_R$ then

$$\frac{\partial Z}{\partial T}\delta T_R = \delta Z_R,\ \frac{\partial Z}{\partial I}\delta I_R = 0\ . \qquad \text{Eq. (3.7)}$$

This implies that if the response in the sea ice albedo forcing experiment is a factor of ε times the response in the RCP8.5 forcing experiment (i.e. matches the relative low-latitude warming scaling of the sea ice albedo forcing to the RCP8.5 forcing), the sea ice loss contributes nothing to the response. If $\delta Z_R = \delta Z_A$,

$$\frac{\partial Z}{\partial T}\delta T_R = 0,\ \frac{\partial Z}{\partial I}\delta I_R = \delta Z_A \qquad \text{Eq. (3.8)}$$

all the RCP8.5 response can be attributed to sea ice loss, leaving nothing to explain from low-latitude surface warming. Finally, if $\delta Z_R = -\delta Z_A$,

$$\frac{\partial Z}{\partial T}\delta T_R = \frac{-2\delta Z_A}{(1-\varepsilon)},\ \frac{\partial Z}{\partial I}\delta I_A = \frac{(1+\varepsilon)}{(1-\varepsilon)}\delta Z_A \qquad \text{Eq. (3.9)}$$

both the sea ice and low-latitude surface warming parts of the decomposition have opposite sign and are inflated, with low-latitude surface warming part having a greater magnitude.

Throughout this study, we use total SIA change (δI) and low-latitude warming (δT) for a given seasonal mean to diagnose the response in that mean (e.g. DJF mean values for δI and δT,

to diagnose DJF δZ). A process-based approach might introduce lags between the sea ice loss and the atmospheric response and test for regional effects. For example, to test whether it is important to explicitly account for how summertime sea ice loss can influence the wintertime atmosphere (e.g. Laîné et al. 2016), we have tried using June-August or September-November sea ice area to diagnose DJF responses and found that the results of the decomposition are very similar – for most variables and regions, only the magnitude of the calculated terms change (not shown). Similarly, a test the impact of sea ice loss in the Barents-Kara Sea region, which has been identified as being important for the circulation response (e.g. Petoukhov and Semenov 2010) again yielded similar results apart from the change in magnitude for each of the terms in the decomposition (not shown).

While we have emphasized the DJF season, the suggestion that the circulation response to the sea ice loss peaks in late winter (Kim et al. 2014; Sun et al. 2015) motivates us to examine the February-March (FM) response. The results are similar but indeed point to the midlatitude RCP8.5 response being more dominated by sea ice loss to some extent (not shown). For example, the decrease in zonally averaged mid tropospheric wind speed at high latitudes in the RCP8.5 response is about 0.5 m s^{-1} in FM compared to 0.3 m s^{-1} in DJF (Fig. 3.6). This suggests that in late winter, sea ice may play a somewhat larger role than low-latitude warming in CESM1.

We have also considered whether the relationships between δI and δT with δZ might change with time. In the North Atlantic in the RCP8.5 simulations, weakening of the Atlantic Meridional Overturning Circulation (AMOC) results in reduced warming there (not shown). In the sea ice albedo forced simulations, the AMOC first weakens, then recovers to nearly the strength in the control simulation (not shown, but similar behaviour was seen in Fig. 2.1 for CCSM4). For the analysis presented in the next section we use the long-term average after the AMOC has recovered to perform all of the calculations. If we use an earlier time period in the albedo-forced simulation, when the AMOC is still weak (Years 50-200), we get nearly identical results with only small differences in maps over the North Atlantic. The results also do not depend strongly on the epochs chosen in the RCP8.5 experiment, with the exception of using epochs in the latter part of the 21st century for DJF. During these times, ε starts increasing, i.e. the amount of sea ice loss per unit low-latitude surface warming increases and becomes closer to what it is in the sea ice albedo forcing simulations, which makes the calculation less robust. In

addition, the pattern of sea ice loss is quite distinct in the two experiments when epochs in the latter parts of the 21st century are used.

Finally, caution should be used in applying this decomposition to the stratosphere, where projected anthropogenic greenhouse gas increases cool the stratosphere through their direct radiative impacts. This process does not operate in the sea ice albedo forcing experiments with fixed greenhouse gas concentrations, even in the presence of the sea ice induced low-latitude warming. The situation in the RCP8.5 simulations is further complicated by the recovery of stratospheric ozone in the models, which is projected to warm the stratosphere, although to a lesser extent than the greenhouse gas cooling (Forster et al. 2011).

3.5 Results of the Decomposition

3.5.1 CESM1 results

In Figs. 3.4-3.14, we will show the results of the decomposition described in Section 3.4 for a number of different fields related to atmospheric circulation and variability in a standard format. For each field, we will show four panels as follows:

- Panel (a): The response (epochal difference for the epochs in Table 3.1) in the RCP8.5 forcing experiment.
- Panel (b): The response (long-term mean of sea ice albedo forcing minus Year 2000 control) in the sea ice albedo forcing experiment.
- Panel (c): the low-latitude surface warming-related response in the RCP 8.5 experiment (corresponding to the first term on the right hand side of Eq. 3.3).
- Panel (d): the sea ice loss-related response in the RCP8.5 experiment (corresponding to the second term on the right hand side of Eq. 3.3).

By construction Panel (c) plus Panel (d) equals Panel (a). Note that Panels (a) and (b) are determined directly from the model output in the two experiments, while Panels (c) and (d) are calculated using the methods described in Section 3.4 (note that no statistical significance test was developed for these derived quantities).

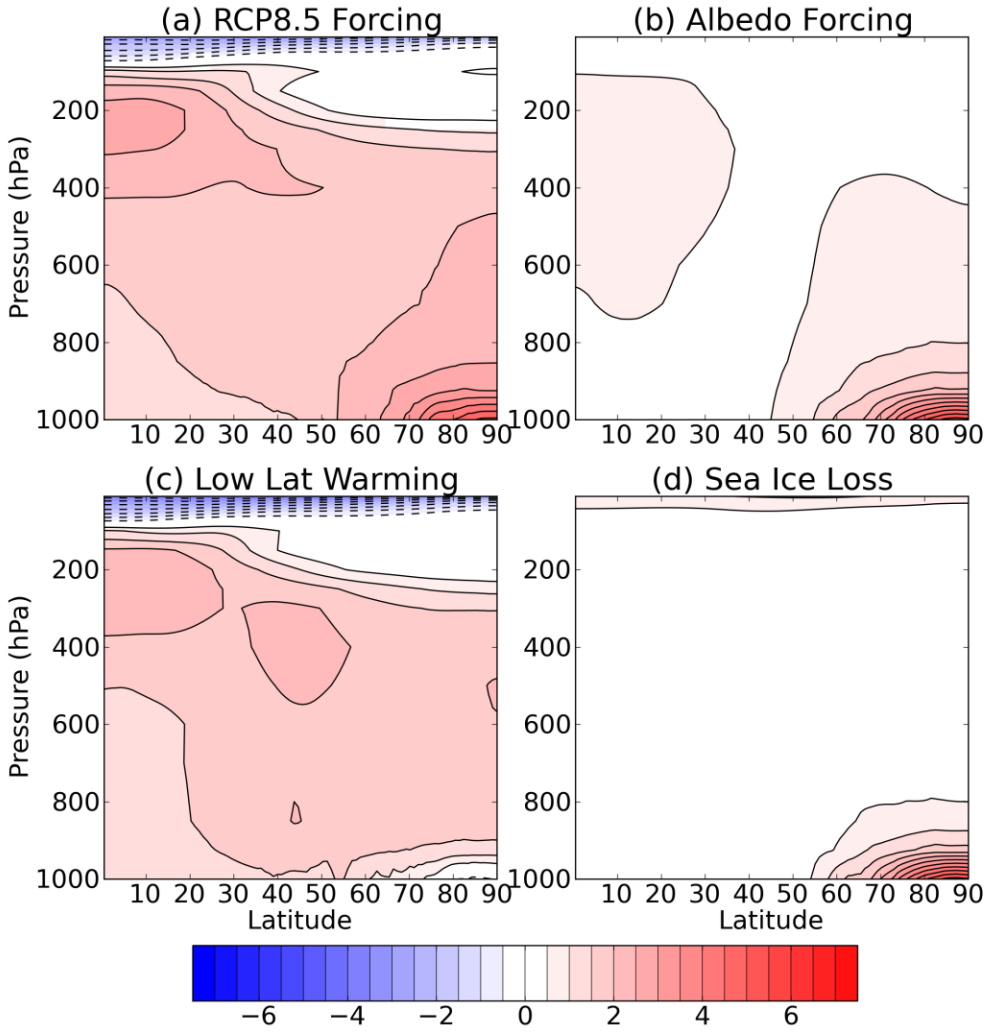

Figure 3.4. (a) The annual mean zonal mean temperature response (°C) for the ensemble mean of the CESM1 RCP8.5 forcing experiment, expressed as the difference between the 2027:2036 epoch and the 2063:2072 epoch. (b) As in (a), but for the CESM1 sea ice albedo forcing experiments, expressed as the difference between the sea ice albedo perturbation experiment and the Year 2000 control experiment. (c) The diagnosed zonal mean temperature response to low latitude surface warming using the decomposition, calculated using Eq. (3.4). (d) As in (c), but for the response to sea ice loss. Note that Panels (c) and (d) sum to Panel (a). In panels (a) and (b) shading is only shown if the response is statistically significant at the 95% confidence level.

Figure 3.4 shows the decomposition for the annual mean, zonal mean temperature, using the annual mean δI and δT. In the RCP 8.5 forcing experiment (Fig. 3.4a), there is warming everywhere in the troposphere, with the largest increases in temperature being in the Arctic lower troposphere and in the tropical upper troposphere. In the sea ice albedo forcing experiment (Fig. 3.4b), there is a similar structure and magnitude of the warming signal in the Arctic

planetary boundary layer, as well as additional warming in the Arctic lower troposphere. Since the epochs in the RCP8.5 were chosen to have similar sea ice loss to the sea ice albedo forcing response, the near-surface warming provides a good match between the two experiments. This is borne out in the decomposition in Figs. 3.4c-d. Figure 3.4c suggests that the low-latitude surface warming part (Fig. 3.4c) is responsible for the warming throughout the troposphere including the tropical warming, while the sea ice loss part (Fig. 3.4d) is responsible for all of the warming in the Arctic lower troposphere, as in the $\delta Z_R=\delta Z_A$ case (see Eq. 3.8), but none of the tropospheric warming outside this region, as in the $\delta Z_A=\varepsilon\delta Z_R$ case (see Eq. 3.7). This clear separation, which is a consequence of annual mean Arctic lower tropospheric warming scaling with annual mean sea ice loss and the remaining signal scaling with low-latitude warming, gives us some confidence that we can use this method to decompose other fields.

The DJF zonal mean temperature (Fig. 3.5) decomposition is similar to the annual mean in the troposphere, with most of the Arctic amplified lower tropospheric warming attributable to sea ice loss. The decomposition in Fig. 3.5 is different from Fig. 3.4 in that the stratospheric responses are distinctive. As mentioned in Section 3.4, the application of this decomposition in the stratosphere should be treated cautiously, but there is potentially useful information in this analysis. In the RCP8.5 simulation (Fig. 3.5a), there is tropical stratospheric cooling (several degrees) and little change in the Arctic stratosphere, while in Fig. 3.5b, there is polar stratospheric warming (about one degree) and little change at lower latitudes. Our tentative interpretation of this is that in RCP8.5 greenhouse gas increases have cooled the stratosphere from the tropics to the high latitudes, and that this is partially offset at the pole by stratospheric warming induced by sea ice loss (which has been seen in other simulations, e.g. Sun et al. 2015). In the decomposition, polar stratospheric warming that scales with sea ice loss (Fig. 3.5d) appears to cancel the polar stratospheric cooling that scales with low-latitude surface warming (Fig. 3.5c). This corresponds to the $\delta Z_R << \delta Z_A$ case (see Eq. 3.6) where the RCP8.5 forcing response is negligible compared to the sea ice albedo forcing response. However, we question the validity of the result from the decomposition that the influence of sea ice loss warms the low-latitude stratosphere (a similar signal with weaker amplitude seen in Figs. 3.4c-d).

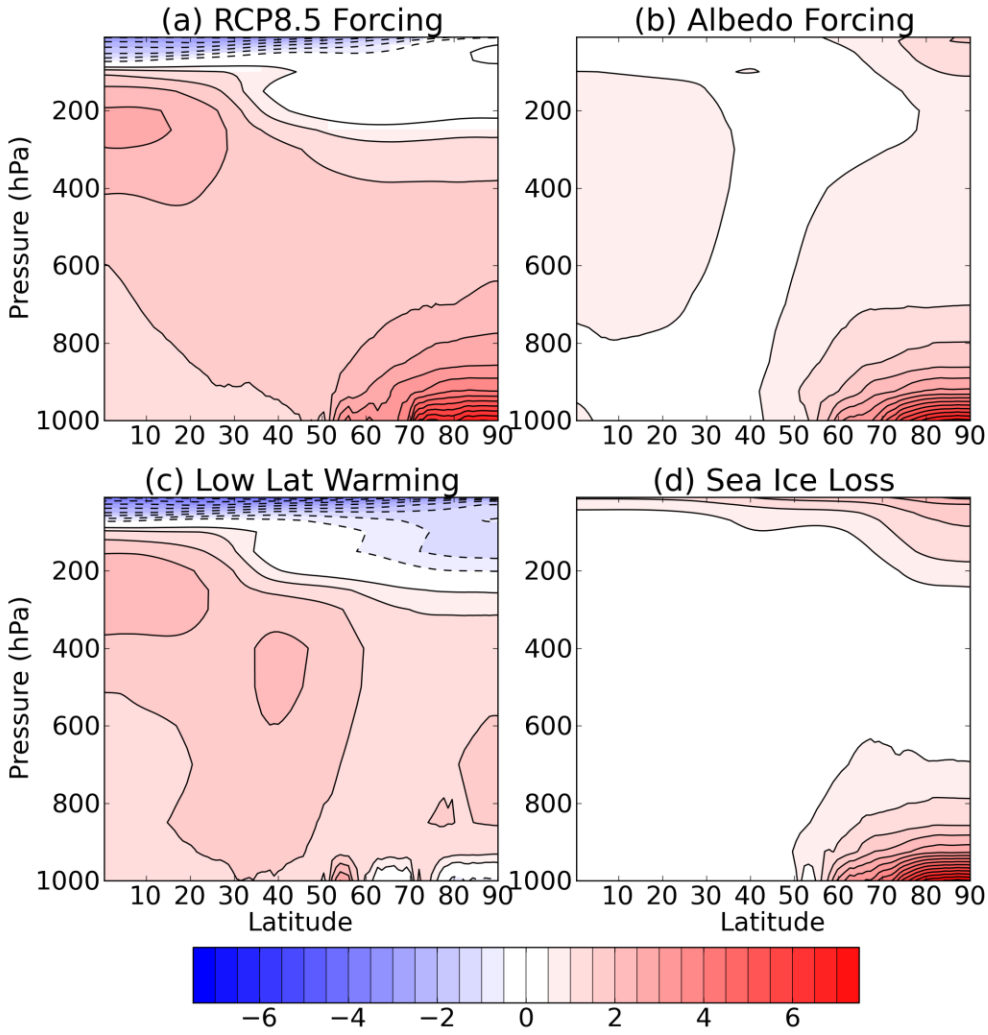

Figure 3.5: As in Fig. 3.4 but for DJF zonal mean temperature (°C). For (a) the response is calculated with respect to the 2027:2036 and 2057:2066 epochs.

The DJF zonal mean wind response in the RCP 8.5 experiment (Fig. 3.6a) is very weak in the troposphere, with only a small (0.3 m s^{-1}) decrease on the poleward side of the eddy driven jet between 60° and 80°N. The sea ice albedo forcing experiment produces a weakening and southward shift in the jet consistent with other sea ice perturbation studies (e.g. Peings and Magnusdottir 2014; Deser et al 2015) but somewhat inconsistent with our own previous study using CCSM4 (Chapter 2); this case will be discussed in the next subsection. Because the RCP8.5 experiment produces very little response and the sea ice albedo forcing experiments produce an equatorward shift of the eddy driven jet, the low-latitude surface warming part of the decomposition consequently corresponds to a roughly equal and opposite poleward shift in the

eddy driven jet as shown in Fig. 3.6c (another case with $|\delta Z_R| << |\delta Z_A|$, see Eq. 3.6). The cancellation is consistent with Barnes and Polvani (2015) who show that the CMIP5 models that have more (less) Arctic amplification tend to have more of a decrease (increase) in the strength of the tropospheric jet and an equatorward (poleward) shift of the jet. Consistent with the stratospheric temperature response in Figure 3.5, we find a decrease in the strength of the stratospheric polar vortex in the sea ice albedo forcing experiments and in the estimated response to sea ice loss. This result is in agreement with Peings and Magnusdottir (2014) who found a similar result forcing CAM5, the atmospheric model used in CESM1, with lower sea ice concentrations.

In summary, wintertime sea ice loss in isolation, with low-latitude surface warming supressed, drives an equatorward shift of the tropospheric jet and a weakening of the stratospheric polar vortex associated with a warming of the polar stratosphere (Figures 3.4d and 3.5d). The latter signal occurs despite the fact that CAM5 is a low top model (Peings and Magnusdottir, 2014; Kim et al. 2014, Sun et al., 2015). Within this framework it is difficult to say more about how this impact can be separated from other impacts of climate change in the polar stratosphere.

The results of the decomposition for midtropospheric extratropical warming and circulation as represented by Z500 in DJF is in Fig. 3.7. In the RCP 8.5 forcing experiment (Fig. 3.7a), there are increases in height throughout the entire Northern Hemisphere accompanying tropospheric greenhouse warming. The smallest increases are over the North Atlantic and North East Pacific Oceans. In the sea ice albedo forcing experiments (Fig. 3.7b), there are large increases over Greenland, no increase over the North Atlantic and Western Europe and small decreases over the North East Pacific. However, there are also small increases over the rest of the Northern Hemisphere as a result of the small amount of global warming. The decomposition in Fig. 3.7d removes the small global warming signal from the sea ice loss signal. What remains is the increase over Greenland, a larger decrease over the North Pacific, and a small decrease over Western Europe. Compared to the total RCP8.5 response (Fig. 3.7a), in the low-latitude surface warming part of the response (Fig. 3.7c) there are larger increase over the North Pacific and over Eurasia, with little change over the North Atlantic. This suggests that the sea ice loss is responsible for the decrease in geopotential heights in the North Pacific, and that the low-latitude surface warming part of the response increases heights in this region, cancelling the response to

sea ice loss. It also suggests that both sea ice loss and the low-latitude surface warming are contributing to the relatively small changes in Z500 over the North Atlantic sector.

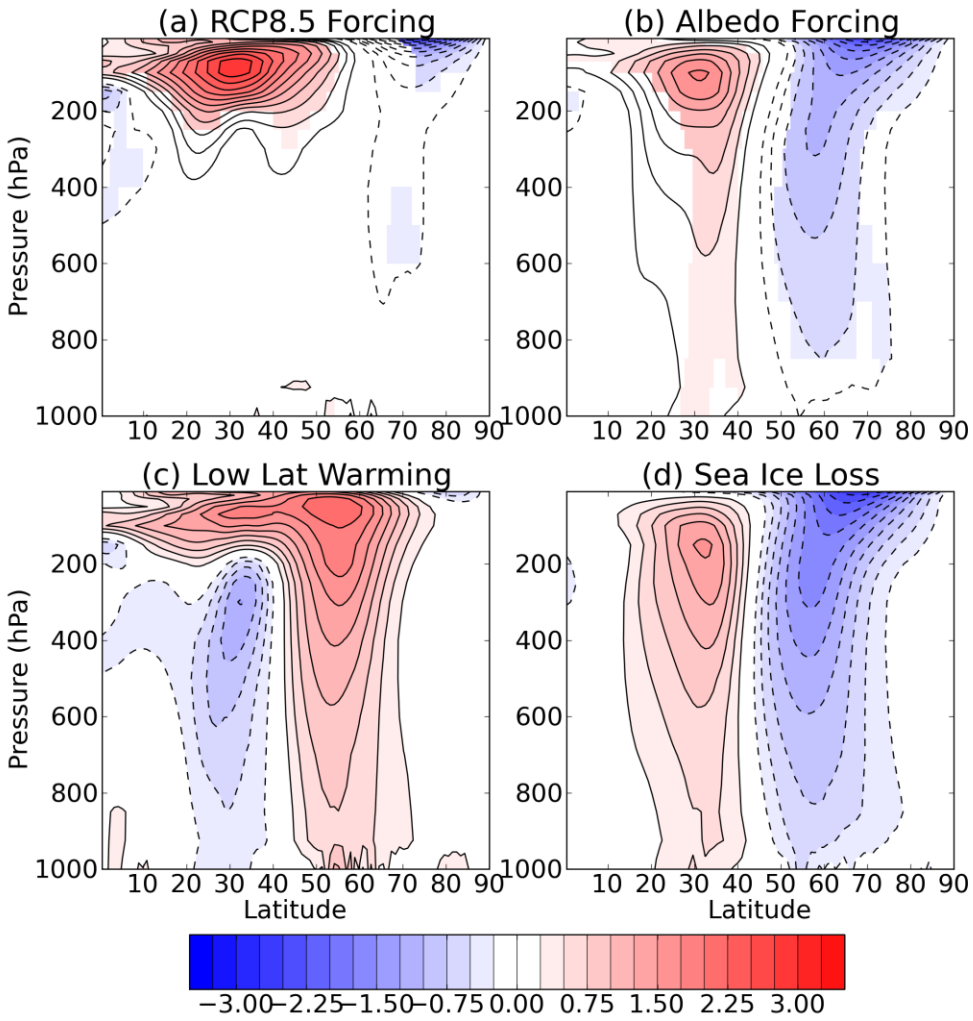

Figure 3.6 :As in Fig. 3.5, but for the zonal mean zonal wind (m s^{-1}**).**

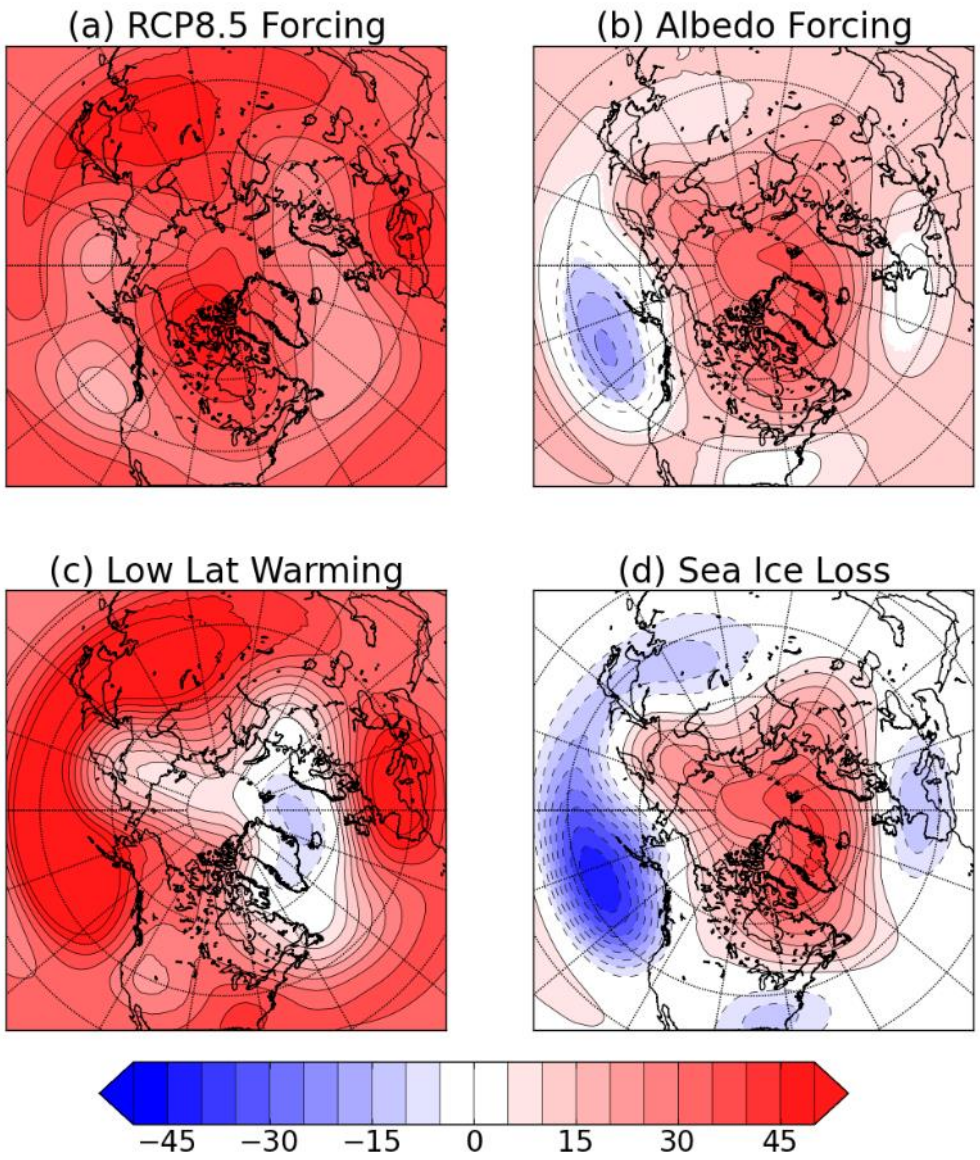

Figure 3.7: As in Fig. 3.5, but for 500 hPa geopotential height (m).

Figure 3.8 shows the sea level pressure (SLP) response in the two experiments and the decomposition into the parts of the response. In the RCP8.5 forcing experiment, there is a decrease in SLP over most of the Arctic Ocean with the largest response over the Barents Sea and the Chukchi Sea, as well as a weak decrease over North America. In the sea ice albedo forcing experiment, however, there is a high-pressure response over Northern Eurasia and a deepening of the Aleutian low. This high pressure response has been seen in many studies (e.g. Honda et al 2009; Mori et al. 2014) in response to sea ice loss in the Barents and Kara seas and can cause a cooling response in East Asia, as a result of cold air advection. Even though both the albedo forcing and RCP8.5 forcing experiments show decreased sea ice loss in this region, the

SLP responses are opposite. Based on this, it no surprise that the decomposition tells us that the low-latitude surface warming and sea ice loss parts of the response, are generally opposite, similar to the $\delta Z_R = - \delta Z_A$ case (see Eq. 3.9). The low-latitude warming and sea ice loss parts both show a reduction in SLP over the Chukchi, Beaufort, and Bering Seas, as well as over parts of the Canadian Arctic. They have opposite signs over a broader hemispheric region including the North Pacific, the rest of the Arctic Ocean and Eurasia, consistent with the zonal mean wind response which also produced an opposite response in the troposphere.

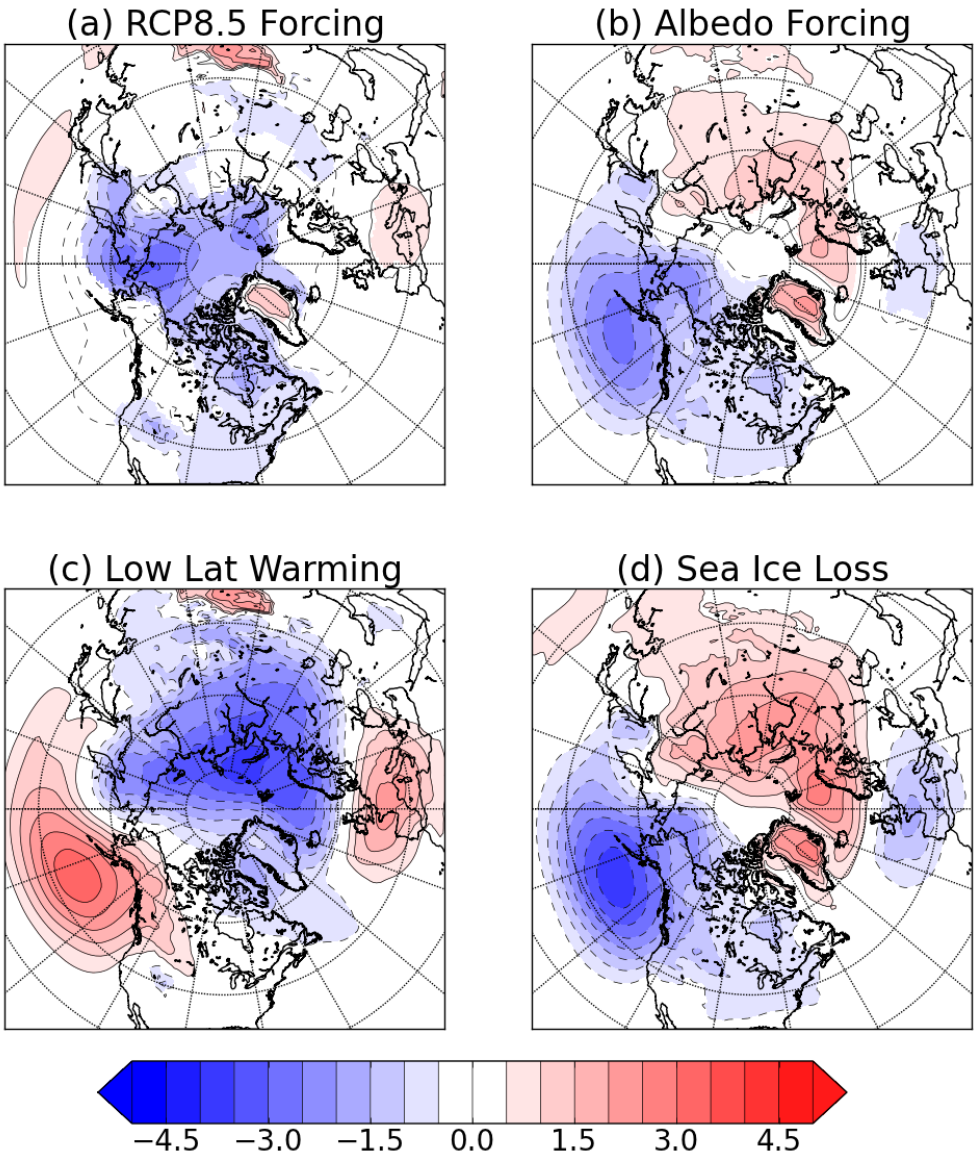

Figure 3.8: As in Fig. 3.5, but for SLP (hPa).

Applying this analysis to 2-meter temperature over land (Fig. 3.9) reveals an advection pattern that can be inferred from the SLP response. The sea ice loss produces a moderate cooling response over East Asia as result of cold air advection from the Arctic consistent with previous studies (e.g. Honda et al 2009; Mori et al. 2014). However, the warming over this same region connected with the low-latitude surface warming is strong, cancelling out any cooling due to sea ice, so there is still significant warming over East Asia in the RCP8.5 experiment. Even in the albedo forcing experiment, the small amount of low-latitude surface warming is enough to cancel any cooling, leaving instead a lack of warming in that region. Over North America, both the sea ice and low-latitude surface warming contribute to the warming at higher latitudes over Canada, but the influence of the sea ice loss does not reach past the northern United States.

Examining Figs. 3.7-3.9 together, we see that much of the sea ice driven changes inferred from our experiments are equivalent barotropic in circulation and project onto planetary wave 1, with a positive center of action over Eurasian and a negative center over the northeast Pacific at the surface (Panel 3.8d) and the midtroposphere (Panel 3.7d). We expect that this pattern reflects regional changes in the regional eddy driven circulation arising from the sea ice perturbation. These equivalent barotropic circulation features are associated with surface temperature advection signals that presumably drive some of the pattern of Eurasian cooling and Western North American warming. However, the response is less vertically coherent over the main sea ice loss regions of the central Arctic and Hudson's Bay. In these regions, the strong regional heating from sea ice loss might directly drive strong changes to the diabatic circulation and lead to less barotropic responses. The combination of direct diabatically driven responses and indirect eddy driven responses are expected to be model dependent, as we will mention in the next subsection.

The analysis applied to winter precipitation (Fig. 3.10) shows that in the RCP8.5 forcing experiment, there are increases in precipitation over most of the mid and high latitudes. In the sea ice albedo forcing simulations, there are more limited increases over the Arctic Ocean where there is sea ice loss, over the west coast of North America and over Western Europe. The increases over the Arctic Ocean and over the west coast of North America are seen in the RCP8.5 experiments as well, meaning the sea ice loss contributes to the increased precipitation over these regions in the projections. The rest of the increases, mainly over the North Pacific and Northern Eurasia, cannot be attributed to sea ice loss but can be attributed to that part of the

global warming response associated with low-latitude surface warming. Some of the precipitation responses can be linked to the equivalent barotropic circulation response in SLP and Z500 in Figs. 3.7 and 3.8. For example, over the Northeast Pacific the increased precipitation over the west coast of North America appears to be connected with the deepening of the Aleutian low.

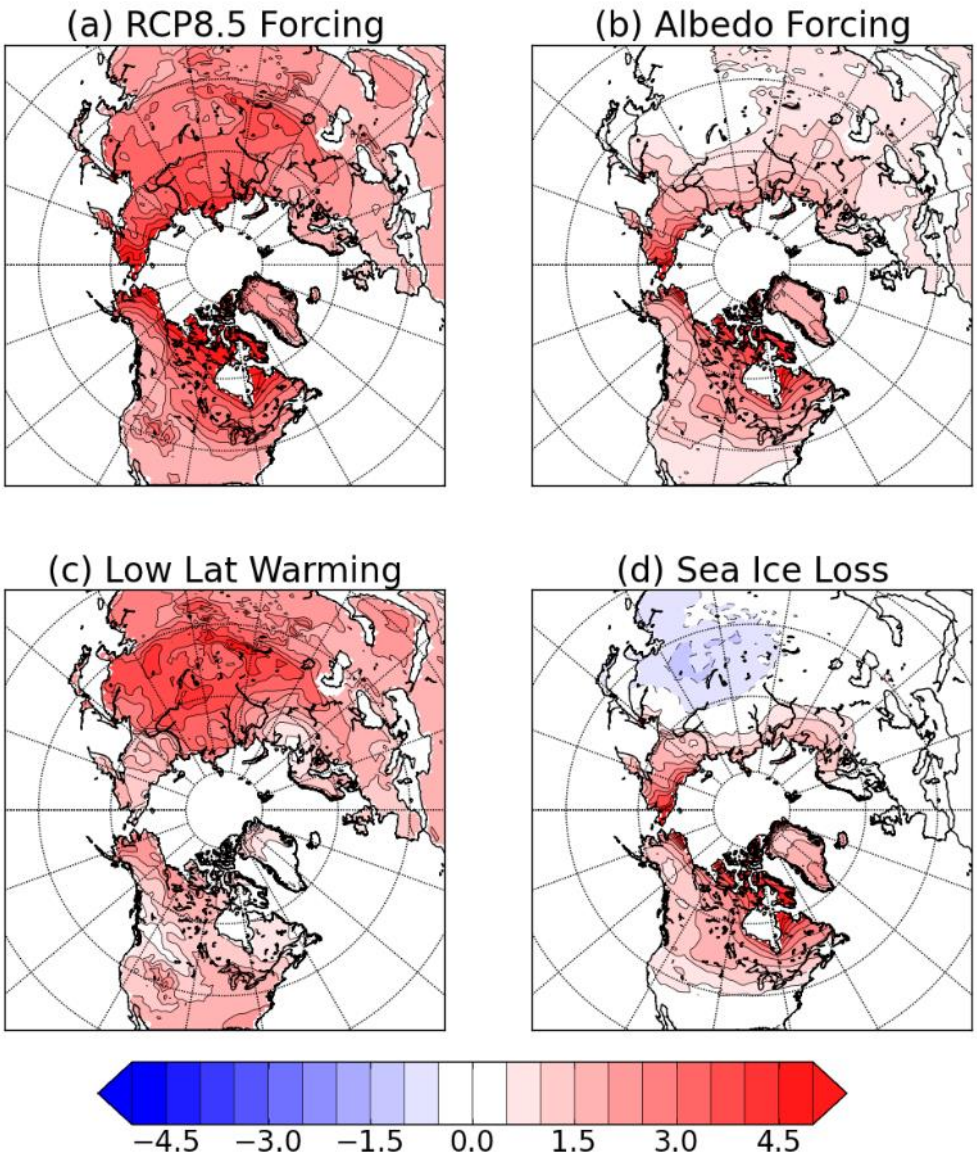

Figure 3.9: As in Fig. 3.5 but for 2 meter temperature (°C).

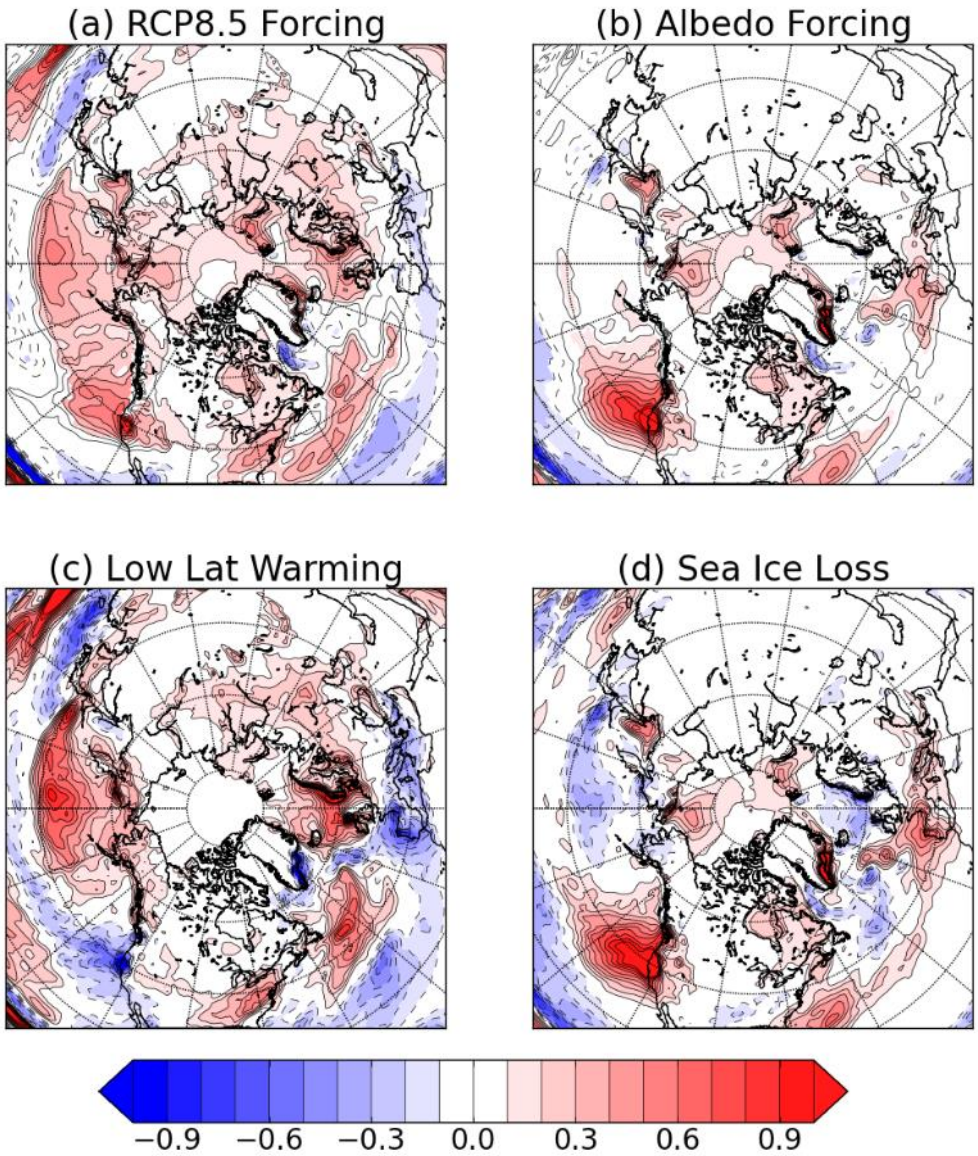

Figure 3.10: As in Fig. 3.5, but for precipitation (mm day^{-1}).

There have been a number of the studies that have investigated how the variability of temperature and other variables is changing in response to greenhouse-dominated radiative forcing and sea ice loss (Chapter 2; Screen 2014; Screen et al. 2015). Here we investigate the role of sea ice loss in the change of temperature variability, by performing the decomposition for the daily averaged 2-meter temperature subseasonal temperature variability in Fig 3.11. In the RCP8.5 simulations, the variability is calculated by taking the daily averaged 2-meter temperature for each of the 30 realizations over the same 10-year epochs used in the previous plots, and subtracting the ensemble mean (this removes the seasonal cycle and the ensemble

mean trend). The DJF seasonal mean of each of the 300 years are subtracted to obtain the subseasonal anomalies from which the standard deviation is calculated at each geographic point. The difference of the standard deviations of subseasonal 2 meter temperature between the two RCP8.5 epochs is plotted in Fig. 3.11a. Similarly, the subseasonal 2 meter temperature standard deviations for the albedo forcing experiments are calculated by subtracting the daily climatological values of the daily temperature and seasonal average DJF temperatures from 200 years of daily data. The difference in this statistic for the sea ice albedo forcing experiments is plotted in Fig. 3.11b, and the decomposition of the responses is plotted in Figs. 3.11c-d.

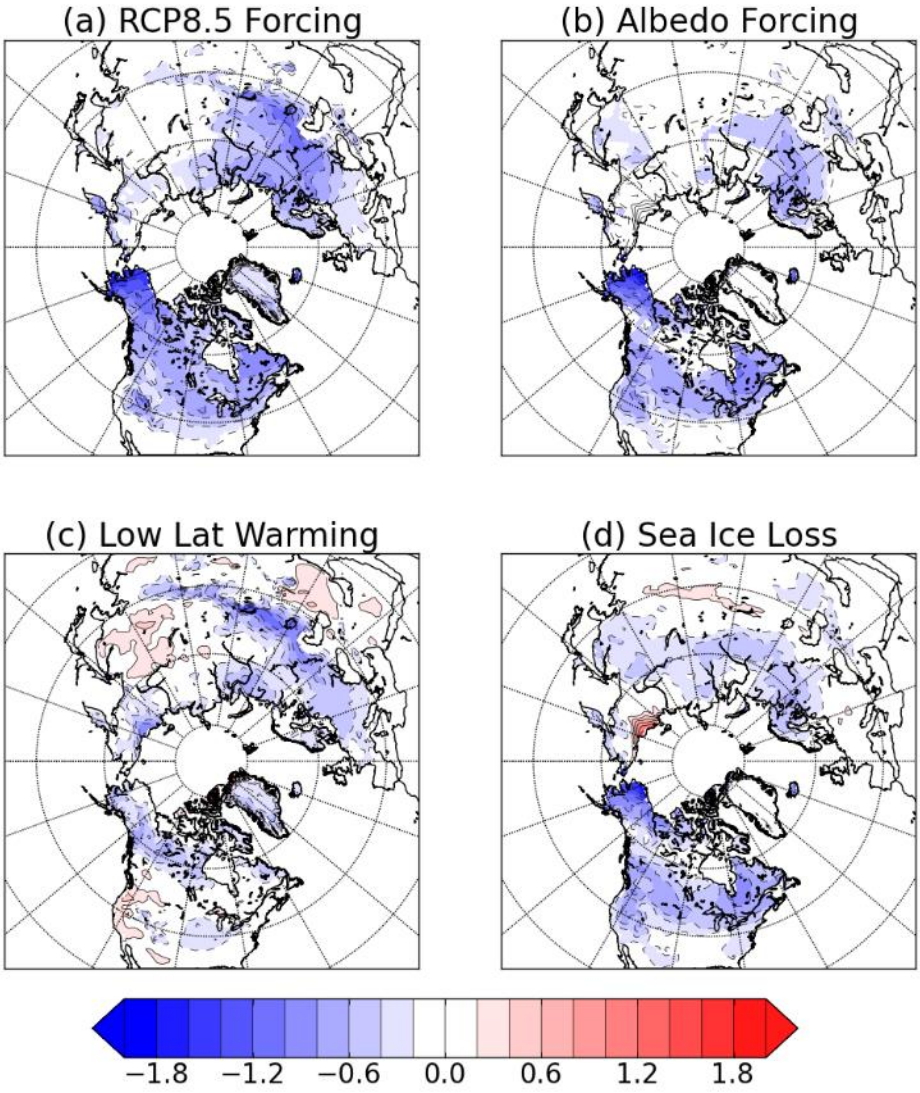

Figure 3.11: As in Fig. 3.5 but for the standard deviation of the subseasonal daily 2 meter land temperatures (°C).

In the RCP 8.5 experiment, there is a decrease in the temperature variability throughout most of the mid and high latitudes, indicating that the Northern hemisphere winters will become less extreme, a result that is robust across all CMIP5 models (Screen 2014). We also see a reduction in variability in the albedo forcing experiment, consistent with other studies that have looked at the temperature variability response to sea ice loss (Chapter 2; Screen et al. 2015). This suggests that sea ice loss plays a large role in the reduction of variability. Once the decomposition is calculated, we find that sea ice loss is responsible for much of reduced variability over southern Canada, Northern United States, Russia and Northern Europe. It is not surprising that sea ice loss is responsible for the reduced temperature variability in the model, as sea ice loss is the primary contributor to Arctic amplification, which causes reduced variability due to a decrease in temperature gradients (Screen 2014; Schneider et al 2015). Also, because sea ice has a lower heat capacity than the ocean, melting ice will cause the regions where the ice was lost to be more maritime, also reducing the variability. Although the sea ice loss contributes to much of the reduced variability, the low-latitude surface warming part of the response also shows reduced variability, especially over Europe and central Asia.

3.5.2 CCSM4 results

We check the robustness of these results with CCSM4, which has weaker Arctic amplification due to shortwave feedbacks associated with optically thicker clouds (Kay et al. 2012). To compensate for having only five realizations of the RCP8.5 experiments (compared to 30 for CESM1) we average two 20-year epochs (2027:2046 and 2047:2066) to calculate the response (compared to 10-year epochs for CESM1). As expected from Kay et al., in the CCSM4 albedo forcing experiment, there is about 50% less sea ice loss in DJF (30% less in the annual mean; see Table 3.1 and Appendix for more details) and less warming. Despite these differences, the amount of low-latitude surface warming per million km sea ice loss is similar to CESM1 (Table1). Because we are using only a third of the number of years to calculate the response in the RCP 8.5 experiment, combined with the weaker forcing, the CCSM4 results are not as robust as the CESM1 results. In particular, changing the epochs used to calculate the response in the RCP 8.5 experiment does change some of the results. Nevertheless, there a few robustly estimated differences between the two models that will be highlighted below.

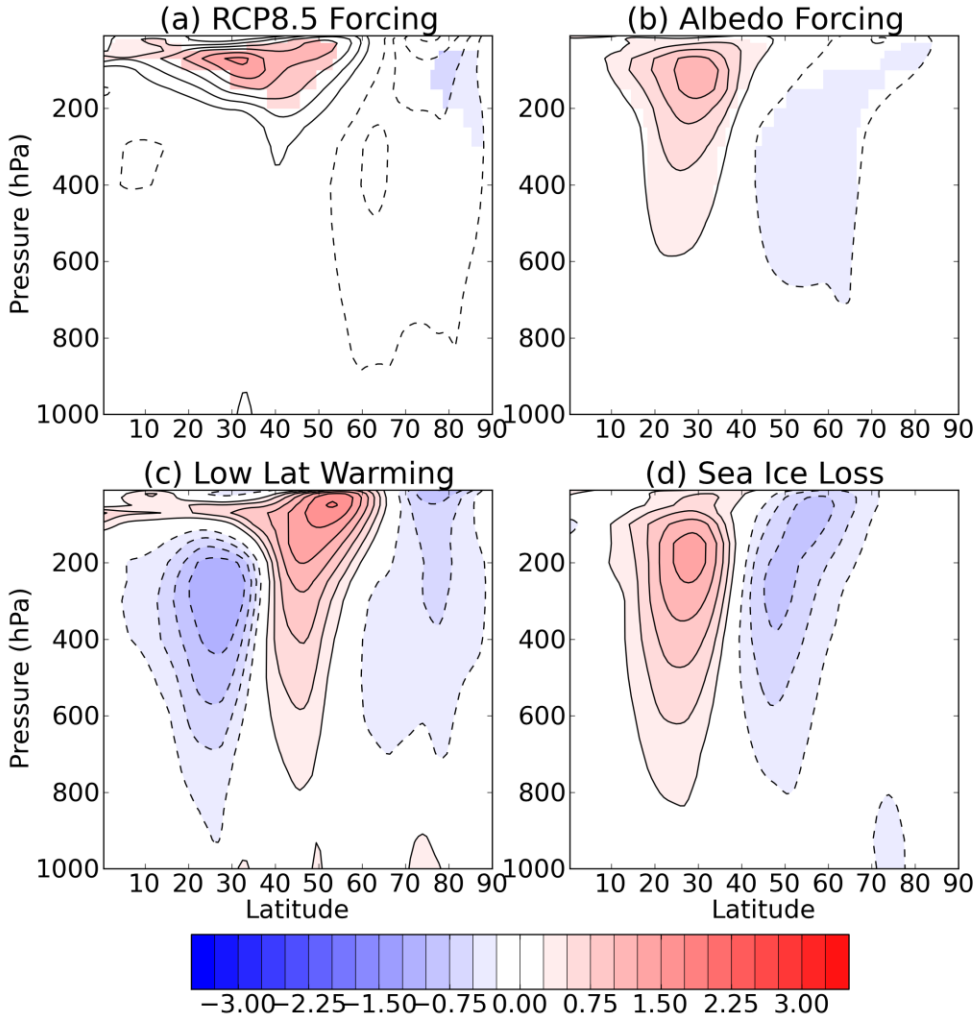

Figure 3.12: As in Fig. 3.6, but for the CCSM4 experiments. For (a) the response is calculated with respect to the 2032:2051 and 2052:2071 epochs.

As in CESM1's RCP8.5 simulation (Fig. 3.6), the extratropical tropospheric DJF zonal mean wind response in the CCSM4 RCP 8.5 simulation (Fig. 3.12) is weak and in the CCSM4 case statistically insignificant. In the sea ice albedo forcing simulation, the response generally has the same sign as in CESM1, but is proportionally weaker, accounting for the weaker forcing from sea ice loss. Unlike in CESM1, the stratospheric wintertime zonal wind response is weak in in the sea ice albedo forcing experiment. This could be associated with the relatively strong CCSM4 control run polar vortex compared to the CESM1 control run (not shown), making it less susceptible to changes associated with altered planetary wave propagation. Likely linked to this is the relatively weak wave-1 circulation response (see for example, Fig. 3.13d). The

decomposition between the two parts of the response in CCSM4 shows the same competing southward and northward jet shifts in the troposphere seen in CESM1. The responses in the troposphere in the RCP8.5 simulations are not statistically significant and changing the epochs used can change the response (not shown). However, the main features of the response decomposition in Figs. 3.12c-d are present for various epochs.

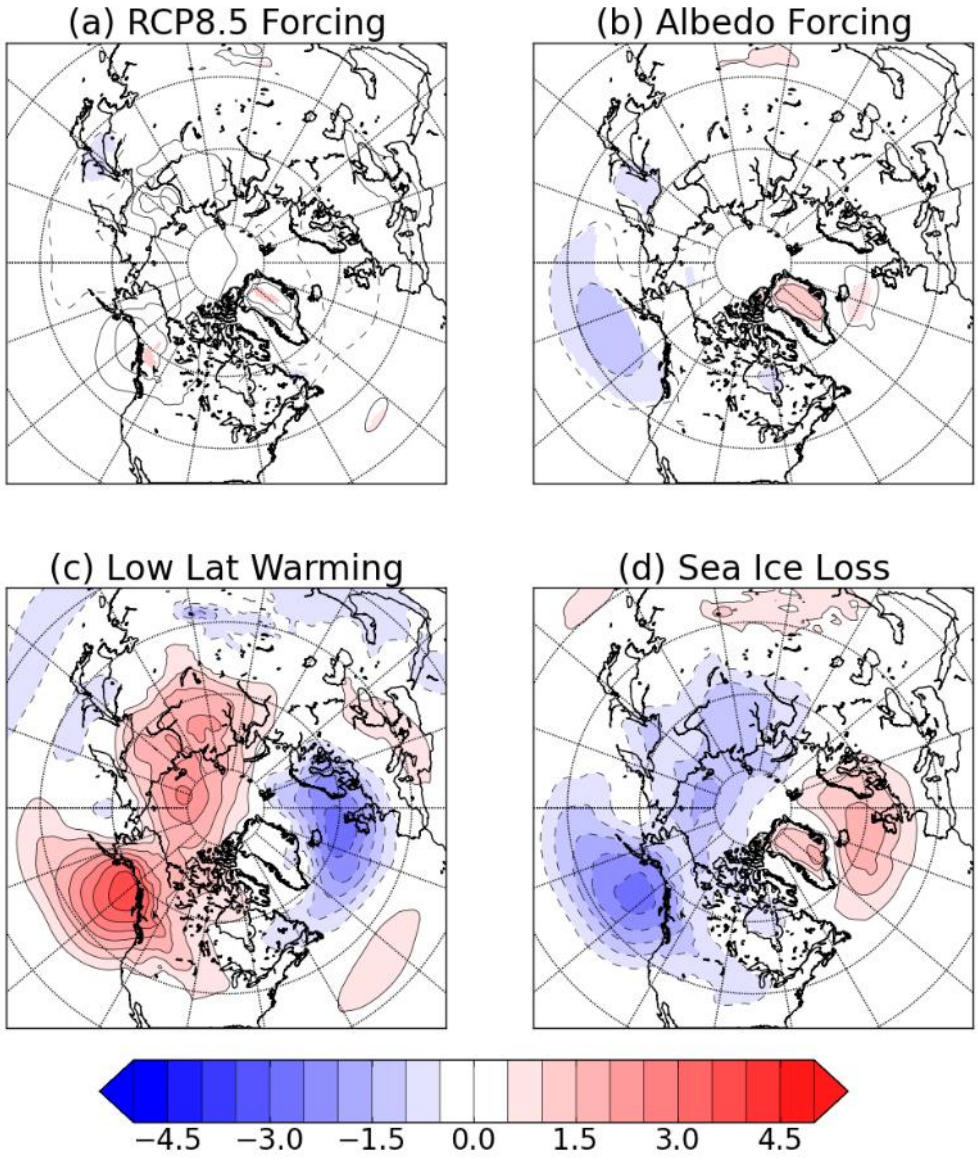

Figure 3.13: As in Fig. 3.12, but for SLP (hPa).

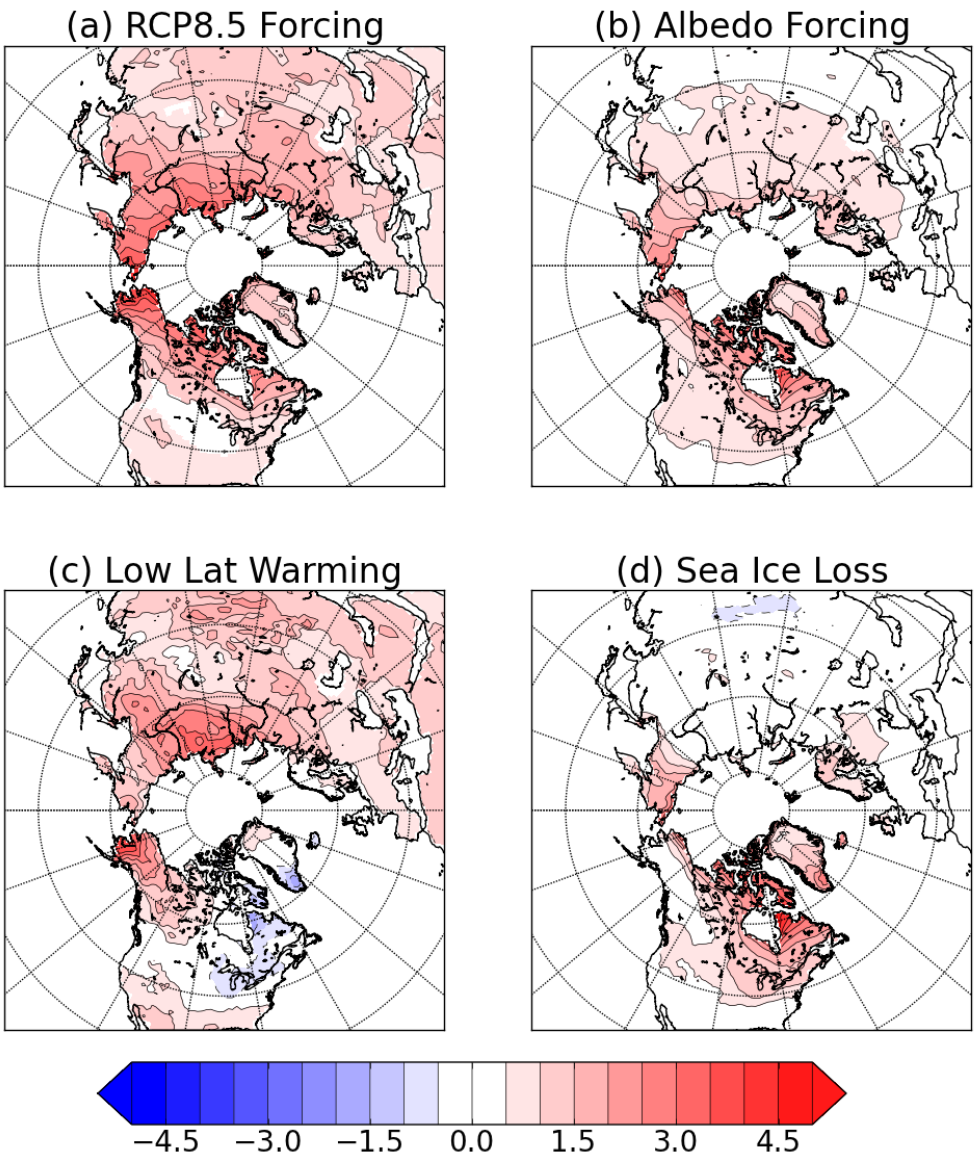

Figure 3.14: As in Fig. 3.12, but for 2 meter land temperature (°C).

The results for the DJF SLP (Fig. 3.13) responses in both the RCP8.5 and the sea ice albedo forcing experiments are generally weaker in CCSM4 than in CESM1. This is at least in part due to the weaker response to sea ice albedo forcing in the CCSM4 experiment. Although the sea ice albedo forcing experiment response is robust, many of the features seen in the RCP8.5 forcing experiment (and therefore in both terms in the decomposition as well) are not, as they are not statistically significant or robust for different epochs analyzed. Notably, for the different epochs analyzed, there is no high sea level pressure response over Northern Eurasia due to sea ice loss (this is also found in Chapter 2). This also results in there being no advective cooling in

the East Asia like there was in CESM1 (compare Fig. 3.14 to Fig. 3.9). A robust feature of CCSM4 and CESM1 is the opposite responses due to sea ice loss and low-latitude surface warming in the SLP response in the North Pacific (compare Fig. 3.13 to Fig. 3.8). This leads to a similar Pacific sector precipitation response in CCSM4 compared to CESM1 (not shown). Many of the remaining features of the SLP response change for different epochs and thus are not robust.

3.6 Summary and Discussion

To isolate the role of sea ice loss in the projected atmospheric response to greenhouse-dominated anthropogenic forcing, we have compared RCP8.5 projections to albedo forcing experiments, which have different amounts of low-latitude surface warming relative to the amount of sea ice loss. We have used a pattern scaling approach in which the projected response to anthropogenic forcing can be decomposed into a part that scales with total sea ice loss and a part that scales with low-latitude ocean surface warming. We have applied this approach to a number of fields to determine how important sea ice loss is in the atmospheric response to greenhouse-dominated radiative forcing in CESM1 and CCSM4. We found the results of our scaling approach were similar for different seasonal lags, for scaling by different regions, and for different epochs.

For zonal temperature, Arctic lower tropospheric warming scales with sea ice loss and the rest of the warming with low-latitude surface warming. The boreal winter Northern Hemisphere extratropical circulation response to sea ice loss was associated with a weakening of the zonal winds, an equatorward shift in the jet stream, a high SLP response over Northern Eurasia and a deepening of the Aleutian low. In addition, the sea ice loss part was associated with a weaker polar vortex, but we pointed out some ambiguity in the interpretation of the stratospheric response in these simulations. For many of these circulation changes, the low-latitude surface warming part was opposite to sea ice loss response, leading to cancellation and a relatively weak projected response in the RCP8.5 simulation.

We have found important examples where sea ice loss and low-latitude warming are more regionally distinct or reinforced rather than cancel each other. For the regional response in precipitation, sea ice loss was responsible for an increase of wintertime precipitation over the west coast of North America, which is also seen in the RCP8.5, while the low-latitude warming

is associated with increases over other sectors such as Eurasia. We also find that sea ice loss and low-latitude warming both act to decrease wintertime subseasonal temperature variability at mid and high latitudes. This response is seen in both the sea ice albedo forcing and the RCP8.5 forcing simulations and both sea ice loss and low-latitude surface warming play a role in it.

The circulation responses in the sea ice albedo forcing experiments and in the sea ice part of the responses have been documented in other studies including those that use prescribed non-interactive SST and sea ice (e.g. Peings and Magnusdottir 2014). The fact that we do not see these same responses in the RCP8.5 experiments, and that such effects are somewhat weaker in the sea ice albedo forcing experiments than in the decomposition, suggests that, in the coupled system, extratropical greenhouse warming responses associated with low-latitude surface warming can be just as, if not more important than, the sea ice loss of Arctic origin. In other words, just because sea ice loss *can* impact the lower latitudes in many ways as seen in previous studies, does not necessarily mean it will be the dominant response to climate change, as discussed in Barnes and Screen (2015). This is in agreement with Barnes and Polvani (2015) who found that many of the proposed impacts of Arctic amplification are not seen in the CMIP5 models under RCP8.5 forcing, though there is a significant amount of spread.

Based on the results of this study, it would be expected that the circulation response to sea ice loss in the coupled model would be weaker than in the experiments that use prescribed SST and sea ice because of the tropical warming partially cancelling out the response. This, however, was not found in Deser et al. (2015, 2016), who found a stronger circulation response in a coupled model sea ice loss experiment compared to one without an interactive ocean under the same amount of sea ice loss, as a result of a larger temperature response that penetrates higher up into the atmosphere. They attribute this to an increase in poleward heat transport associated with a warmer and moister tropical upper troposphere. We do not see evidence of more warming in the Arctic free troposphere in the RCP8.5 response than in the albedo forcing experiments, even though it has much more tropical warming. One factor that may contribute to the stronger response in the coupled sea ice loss experiments, is that the fixed SST and sea ice experiments used in Deser et al. (2015, 2016) only prescribe increased SSTs in the regions where sea ice is lost. In the coupled model experiments, however, there are SST increases well outside these regions that might be attributed to sea ice loss. Indeed, when we perform the decomposition on the SST, we find that there is warming of the high and mid latitude oceans that

can be attributed to sea ice loss (see Fig. 4.1). These could help to produce a stronger temperature response in the coupled model. This will be tested in Chapter 4 by performing AGCM experiments using prescribed SST that are calculated using the decomposition approach described in Section 3.4.

We note that although we do not see many of the impacts of sea ice loss in the RCP 8.5 experiment, this is likely model dependent. Barnes and Polvani (2015) find that there is a significant amount of spread in the jet stream's response to greenhouse-dominated radiative forcing and that some of this spread can be explained by the amount of Arctic amplification. Models that have more Arctic amplification see a response in the jet that looks more like the sea ice part of the response, while models with less Arctic amplification look more like the low-latitude surface warming part of the response. The models analyzed here tend to be in the middle of the range of responses, but in models with more sea ice loss, or in models that have a larger Arctic amplification response, sea ice could play a larger role than in the models analyzed in this study. In addition, even with the same Arctic amplification or low-latitude warming, different models with different parameterizations, resolutions or stratospheric representations, could respond with a different amplitude or even sign. For example, Sun et al. (2015) found a stronger circulation response to sea ice loss using a model with a better representation of the stratosphere, compared to its low-top counterpart.

To reconsider the larger picture, we emphasize that the sea ice albedo forcing Earth System model experiments used here are an artificial means to isolate the part of the sea ice loss process associated with sea ice albedo shortwave feedbacks and summertime sea ice loss (Chapter 2). These experiments show that the tropospheric near-surface warming in the Arctic can be physically attributed to sea ice loss, once the warming is scaled by the sea ice loss (Figs. 3.4 and 3.5). In addition, these experiments, combined with radiative forcing experiments, provide a possible causal chain to explain aspects of the tropospheric circulation response to anthropogenic greenhouse forcing, without the need to run additional experiments. Under greenhouse warming, anthropogenic radiative forcing quickly increases atmospheric water vapour, drives tropical upper troposphere amplified warming, and global stratospheric cooling. In isolation, this will tend to drive the jet stream poleward and strengthen the wintertime Arctic stratospheric vortex (Figures 3.5c-3.6c). However, the greenhouse gas and water vapour enhanced downwelling longwave radiation simultaneously leads to sea ice loss and Arctic

amplification, boosted by positive shortwave sea ice albedo feedbacks (and possibly other positive surface energy budget feedbacks in the Arctic). This additional warming contributes, primarily via oceanic warming in the coupled system (Tomas et al. 2016), to the original global warming effect, and so in terms of the thermal and radiative response provides a positive feedback mechanism for greenhouse forcing circulation change. But the direct dynamical effect of sea ice loss is a negative circulation feedback that pushes the jet equatorward and dynamically warms the polar stratosphere (Figs. 3.5d and 3.6d). Such negative feedbacks associated with the eddy driven response to sea ice forcing have been well documented before in the context of North Atlantic Oscillation trends (e.g. Magnusdottir et al. 2004, Deser et al. 2004) and appear here to be acting in the context of pan-Arctic sea ice loss and the zonal mean circulation. In summary, in this interpretation, greenhouse gas warming induced sea ice loss provides a negative feedback that weakens the impact of the extratropical circulation response to greenhouse warming.

Chapter 4
The Atmospheric Response to Extratropical Ocean Warming Induced by Sea Ice Loss

4.1 Introduction

AGCMs, which have not been used to this point in this thesis, provide useful tools to isolate the impacts of sea ice loss and SST changes on atmospheric circulation within the global warming process. A number of previous studies have prescribed sea ice and SST boundary conditions from coupled ocean atmosphere models with this idea in mind. The boundary conditions can be drawn from coupled models driven by increased greenhouse gas concentrations (e.g. Deser et al. 2010, Peings and Magnusdottir 2014) or by changes to downwelling long wave radiation (Deser et al. 2015,2016) (hereafter D15, D16). Some of the AGCM experiments have included no SST forcing (e.g. Deser et al. 2010) while others have included changes in SSTs in a limited way by forcing where there is significant sea ice loss (Peings and Magnusdottir 2014; D15; D16).

In this chapter, the focus is on an aspect of sea ice loss response that has not been investigated before in the AGCM context. Sea ice loss has the potential to drive changes in the ocean at regions away from region of sea ice loss, through a number of different thermodynamic and dynamic mechanisms. For example, the warming induced by sea ice loss may spread out in the atmosphere and ocean, through advection of the warming response by the atmosphere and ocean circulation, causing ocean warming in these regions. Sea ice loss can also drive changes in ocean circulation directly by altering the salinity and temperature. Finally, changes in atmospheric circulation caused by sea ice loss can also impact the ocean, for example, by changing wind stress or temperature advection.

As introduced in Chapter 1, studies by D15 and D16 using CCSM4 have examined the impact of ocean coupling on the atmospheric response to sea ice loss. They found that the atmospheric circulation response to Arctic sea ice loss in a climate model with a dynamical ocean is similar in overall structure to experiments with prescribed sea ice and SSTs. However, the magnitude of the response is greater; for example, the amount of Arctic warming is magnified by as much as four times in the mid-troposphere and the degree of wind response in the upper-troposphere by as much as two times. In addition, the response in a slab ocean model

which provides the thermodynamic but not the dynamical response to sea ice loss is large in magnitude compared to the prescribed sea ice and SST simulation but also features a strikingly different spatial response pattern. Together, these experiments suggest that coupling to the dynamical ocean and the circulation response in the ocean amplifies the climate system response to sea ice loss.

At this time, the dynamics of this response are only partially understood. D15 attribute the amplification effect to an increase in poleward heat transport into the Arctic mid-troposphere in the coupled system, which reduces the temperature gradient in the free troposphere. In D15, it is posited that the tropical warming that is a part of the "mini" global warming response is what contributes to this extra warming in the Arctic mid-troposphere in the coupled model response to sea ice loss. This suggestion might appear to contradict the results presented in Chapter 3, as there is little evidence of enhanced Arctic mid-tropospheric warming connected to the tropical warming in the low-latitude warming part of the response (Figs. 3.4c and 3.5c). In addition, this tropical warming is associated with a poleward shift in the jet, which should oppose the circulation response to sea ice loss, and weaken the circulation response in the coupled model (Fig. 3.6).

In this chapter, we attempt to reconcile these apparent discrepancies by proposing a two-step process: first, sea ice loss drives ocean warming in the extratropics, and second this oceanic warming causes enhanced warming in the Arctic mid-troposphere and contributes to the stronger circulation response in the coupled model. Previous studies have argued that changes in mid-latitude temperature and moisture can impact the Arctic mid-troposphere through atmospheric transport (e.g. Graversen and Wang 2009; Screen et al. 2012; Laliberté and Kushner 2013,2014; Orbe et al. 2015), however there has been no connection made in the context of the midlatitude warming that itself might result from sea ice loss.

The approach used in this chapter is to estimate what the extratropical SST response to sea ice loss is from coupled model experiments and then to force an AGCM with sea ice loss, both with and without these SST changes, and examine the difference. We begin by using the pattern scaling technique developed in Chapter 3 to estimate the SST response that is connected to sea ice loss without low-latitude warming in the coupled system. This is done by using the coupled model experiments forced with RCP8.5 projections and reduced sea ice albedo (Section

4.2.1). Section 4.2.2 will outline the AGCM experiments used in the chapter. Next, we will show in Section 4.3.1 that including the SST response induced by sea ice loss amplifies the circulation response to sea ice loss similarly to what was found in the coupled model experiments of D15, D16 but in a way that suggests a different forcing mechanism to what those papers proposed. Results of experiments investigating the distinctive roles of changes in SST in the sea ice loss region or away from the sea ice loss region will be discussed in Section 4.3.2. Finally, we present the results of additional experiments that examine the robustness of the response to different background states and a different SST pattern in Section 4.3.3, before finishing with a summary and discussion in Section 4.4

4.2 Experiment Design

4.2.1 Calculation of the extratropical SST response induced by sea ice loss

We wish to isolate the impact that the ocean warming induced by sea ice loss has on the atmospheric response, in the absence of other climate adjustments. To achieve this, we estimate what the SST response would be without the impact of low-latitude warming, using the coupled model experiments and pattern scaling techniques that were presented in Chapter 3. This estimate may not be as well justified for SSTs as it is over land and the atmosphere, but we still expect it to capture the main impacts of sea ice loss on the ocean surface. The wintertime (DJF) SST response in the CESM1 RCP8.5 experiments from the CESM Large Ensemble (Kay et al. 2015) is shown in Fig. 4.1a. As in Chapter 3, we use the ensemble mean epochal difference between years 2057:2066 and 2027:2036 (the epochs that have the same DJF sea ice area as the Year 2000 control and sea ice albedo forcing experiments). In response to greenhouse dominated forcing, there is SST warming everywhere except for a small region in the North Atlantic, which is a common feature seen in climate models (Stocker et al. 2013) and is also seen in observations (Rahmstorf et al. 2015). The strongest warming is in the high latitudes near where the sea ice is lost. The DJF SST response in the CESM1 sea ice albedo forcing experiments is shown in Fig. 4.1b. As in the RCP8.5 response the strongest warming is at high latitudes where the sea ice is lost, but there is also relatively weak warming at low-latitudes (part of the “mini” global warming response also seen in D15, D16). There is some lack of warming in the North Atlantic similar to the RCP8.5 experiment, but within a smaller region. There is also a lack of warming over the Pacific Ocean in the mid-latitudes that is not seen in the RCP8.5 experiments. Overall,

the SST response seen in the sea ice albedo forcing experiments are similar to what was seen in the sea ice perturbations experiments in D16.

To calculate the part of the SST response that scales with sea ice loss in the absence of low-latitude warming, we use the pattern scaling method of Chapter 3. Since a monthly SST dataset is needed to force the AGCM, here we perform the calculation on the monthly data before taking the seasonal average, instead of taking the seasonal average of all fields first. This produces nearly identical, but not exactly the same results as the seasonal mean approach of Chaper 3. The DJF SST response associated with the low-latitude warming and sea ice loss are in Fig. 4.1c and 4.1d (note that these two panels add up to the RCP8.5 response in panel a). In the part of the response that scales with sea ice loss, the pattern is similar to the SST response in the sea ice albedo forcing experiment, but some of the warming, particularly at low-latitudes, is removed. The removal of some of the low-latitude warming introduces some cooling in the mid-latitudes in the Pacific coinciding the lack warming seen in the sea ice albedo forcing experiments. There is also some SST warming in the North Pacific and along the west coast of North America in the sea ice loss part of the response. In the Atlantic, there is strong warming in the Greenland and Barents Seas along with some warming throughout most of the rest of the North Atlantic.

Interpreting the SST patterns in Fig. 4.1d is challenging as there are a number of different mechanism potentially at play. Some insight into what may be causing the changes seen in Fig. 4.1 can be gained by looking at the turbulent heat flux responses (not shown) and the SLP response (see Fig. 3.8). This heat flux response shows that most of the changes in SST seen outside the regions of sea ice, are at least in part forced by the atmosphere (i.e. increases in SSTs are associated with increased turbulent heat flux from the atmosphere to the ocean and vice versa). Warming in the North Pacific along the coast of the Kamchatka Peninsula, in the Bering Sea, and in most of the North Atlantic is associated with heat flux into the ocean from the atmosphere, presumably caused by warm air that occurs as a result of sea ice loss advecting over these regions. Some of the cooling response seen in the Pacific might also be driven by the atmosphere, likely related to the low pressure response causing cold air advection. Two regions where the atmosphere is likely not the primary driver are the dipole in the middle of the North Atlantic, and the warming on the west coast of North America. The former is likely related to ocean circulation changes due to changes in the AMOC, while the latter is not associated with

any change in turbulent heat flux, so may be a result of the low SLP response causing both warm air advection and increased wind stress preventing upwelling. Understanding these SST changes in more detail will be the subject of a future study.

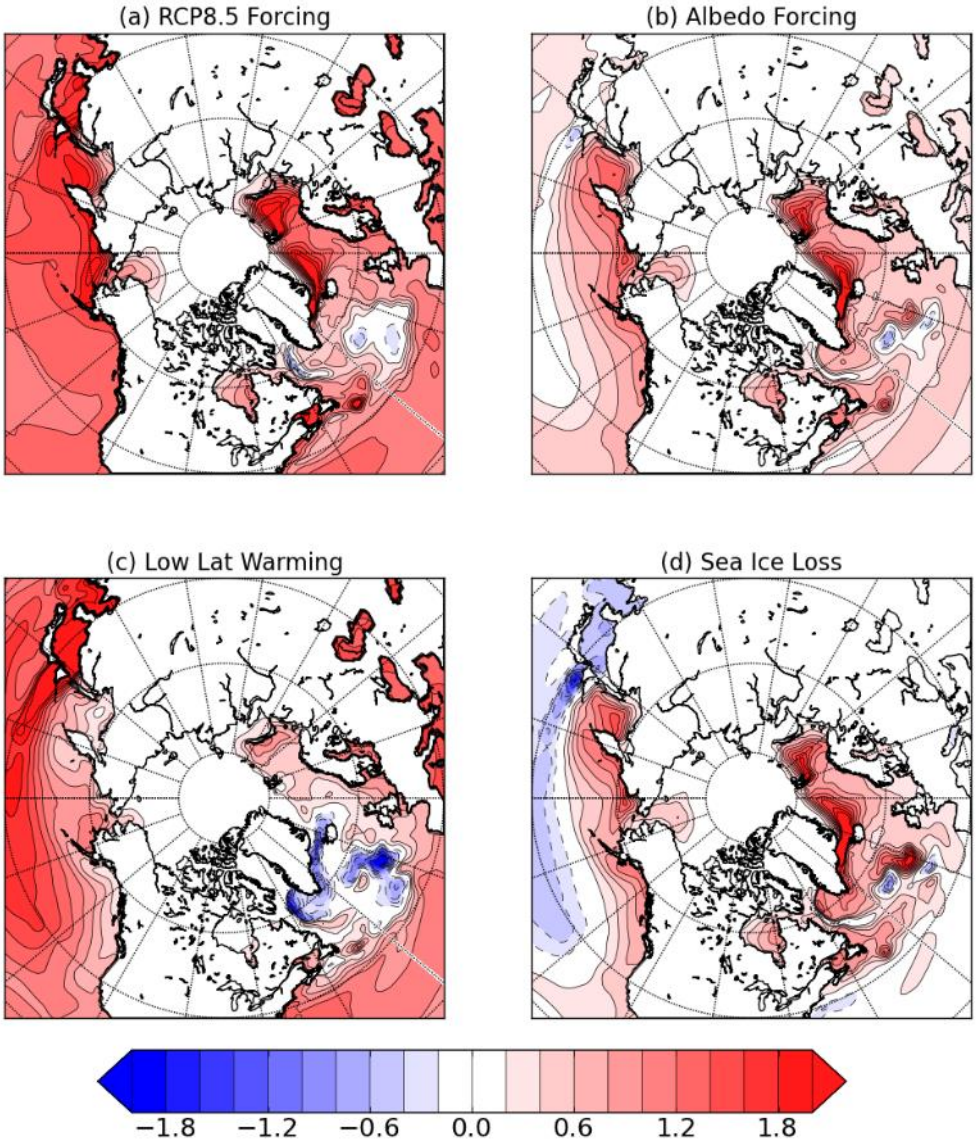

Figure 4.1: (a) The DJF mean SST response (°C) for the ensemble mean of the CESM1 RCP8.5 forcing experiment, expressed as the difference between the 2057:2066 epoch and the 2027:2036 epoch. (b) As in (a), but for the CESM1 sea ice albedo forcing experiments, expressed as the difference between the sea ice albedo perturbation experiment and the Year 2000 control experiment. (c) The diagnosed SST response to low-latitude surface warming using the decomposition, used in Chapter 3. (d) As in (c), but for the response to sea ice loss. Note that Panels (c) and (d) sum to Panel (a).

Despite uncertainty about the origin of the SST patterns that we estimate are associated with the response to sea ice loss, we carry out the AGCM simulations using these patterns as boundary conditions. This is a very common methodology used throughout climate analysis and seasonal climate prediction, and provides an initial sense of driving mechanisms of atmospheric response. Given the uncertainty, our results below should be taken as initial evidence, but not the final word on the ocean's driving role in amplifying the response to sea ice loss.

4.2.2 Description of AGCM modelling experiments

We here describe a new set of AGCM experiments using CAM5 (the atmospheric component of CESM1; see Section 1.5 for details) coupled to the land model CLM4 and forced with a repeating seasonal cycle of prescribed sea ice and SST. Greenhouse gases and aerosols are fixed at Year 2000 levels and all simulations are 100 years in length. A summary of the boundary conditions used in each experiment can be found in Table 4.1. The first set of experiments use the boundary conditions from the RCP8.5 coupled model experiments from the CESM1 Large Ensemble (these will collectively be called the RCP experiments). The control (CTL_RCP) simulation uses the SIC, SIT and SST from a 10 year average of 2027:2036 epoch in the RCP8.5 experiment as boundary conditions. Another simulation called I_RCP, uses the same SST as CTL_RCP, but is forced with the Arctic SIC and SIT averaged over the 2057:2066 epoch of the RCP8.5 experiments. That is, this experiment uses the sea ice loss that results from approximately 30 years of greenhouse-dominated climate change. The differences in DJF SIC and SIT between the I_RCP and CTL_RCP are shown in Fig. 4.2. To examine the impact that the sea ice loss induced warming has on the atmospheric response, a third simulation called I_RCP_T_SIL is used that has the same sea ice as I_RCP, but also includes the Northern Hemisphere SST response that we calculate to be a result of sea ice loss. This pattern is calculated for each month and then is added to the control (2027:2036 epoch) SSTs. The difference between the SST patterns between I_RCP_T_SIL and CTL_RCP averaged over DJF, which is calculated from the coupled simulations, is shown in Fig. 4.1d. This SST pattern will be referred to as the T_SIL pattern throughout the rest of the chapter. The 2027:2036 and 2057:2066 epochs were chosen because they were used to calculate the T_SIL pattern, as this is when the DJF SIA in the RCP8.5 experiments matches the DJF SIA control and sea ice albedo forcing

experiments. In Chapter 3 it was found that these patterns were insensitive to the epochs chosen, with the exception of when two epochs late in the 21st century were chosen.

Some previous studies have included the SST changes in the regions where sea ice is lost (Screen et al. 2013; D15; D16), but such studies have not included SST changes that are associated with sea ice loss, but located away from these regions. We have performed two additional simulations, one that perturbs SSTs with the T_SIL pattern away from the sea ice loss region (called I_RCP_T_SIL_AIL) and one where only the SST in the sea ice loss regions are included (called I_RCP_T_SIL_IL), to examine the importance of the SST changes in each region. In these two simulations, a grid-cell is defined to be in the sea ice loss region if the difference in SIC between the two simulations is greater than 10%.

Previous studies have documented that there is a state dependence to the atmospheric response to sea ice loss (e.g Screen and Francis 2016). To test the robustness of the results to the background state, we also performed a number of simulations that use the boundary conditions from the coupled Year 2000 control and sea ice albedo forcing experiments (collectively called the ALB experiments). The control simulation (CTL_ALB) is forced with the SIC, SIT and SST from the coupled Year 2000 control simulation. Similar to the RCP experiments, we performed a simulation that only includes the SIC and SIT changes from sea ice albedo forcing experiment (called I_ALB) and one that includes both the change in sea ice and the T_SIL pattern of SST warming (called I_ALB_T_SIL). Although the Northern Hemisphere averaged SST and DJF Arctic SIA are very similar in the ALB and the RCP experiments, there are three important differences in the boundary conditions. First, the spatial pattern of the SST, SIC, and SIT in the control simulations are different. Second, the spatial pattern of the SIC and SIT forcing in the perturbed simulations are different (see Fig. 3.3). Finally, although the DJF SIA are nearly the same, the seasonal cycle of the SIA are different, as the ALB experiments have larger changes in the summertime. These differences arise because the boundary conditions are obtained from either equilibrated simulations (ALB) or transient simulations (RCP) and due to differences in forcing mechanisms that used to melt the sea ice in these coupled model simulations. The T_SIL pattern is identical apart from a small (3%) change in magnitude due to the DJF SIA not matching up exactly in the two coupled model experiments.

Table 4.1: List of boundary conditions used in each experiment.

Experiment	Sea ice concentration and thickness	Sea surface temperatures
CTL_RCP	RCP8.5 2027:2036	RCP8.5 2027:2036
I_RCP	RCP8.5 2057:2066	RCP8.5 2027:2036
I_RCP_T_SIL	RCP8.5 2057:2066	RCP8.5 2027:2036+T_SIL
I_RCP_T_SIL_IL	RCP8.5 2057:2066	RCP8.5 2027:2036+T_SIL (ice loss regions only)
I_RCP_T_SIL_AIL	RCP8.5 2057:2066	RCP8.5 2027:2036+T_SIL (away from ice loss regions only)
CTL_ALB	Coupled Year 2000 control	Coupled Year 2000 control
I_ALB	Sea ice albedo forcing	Coupled Year 2000 control
I_ALB_ T_SIL	Sea ice albedo forcing	Coupled Year 2000 control+T_SIL
I_ALB_ T_ALB40	Sea ice albedo forcing	Coupled Year 2000 control (south of 40°N), Sea ice albedo forcing (North of 40°N)

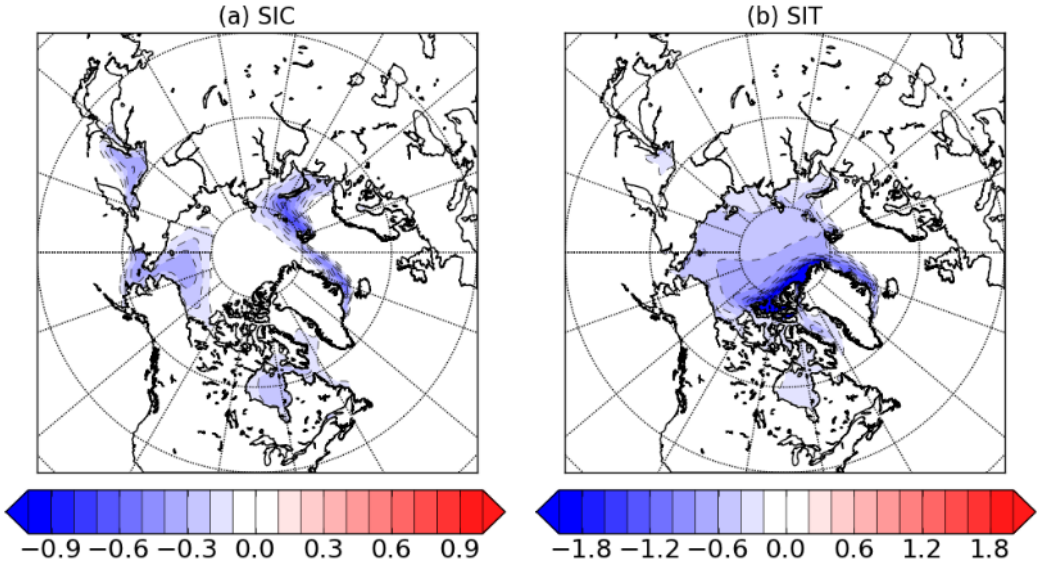

Figure 4.2: (a) The DJF sea ice concentration (fraction) response in the CESM1 RCP8.5 forcing experiment, expressed as the difference between the 2057:2066 epoch and the 2027:2036 epoch (b) As in (a) but for sea ice thickness (m).

Given the uncertainties associated with the estimation of the SSTs induced by sea ice loss using pattern scaling, we performed one last experiment that only includes SSTs and sea ice directly from the coupled model output. This experiment (called I_ALB_T_ALB40) uses the same SIC and SIT as I_ALB, but is also forced with the SSTs north of 40°N directly from the output of the sea ice albedo forcing experiment. South of 40°N, the SSTs remain the same as

CTL_ALB. This captures the extratropical warming that sea ice loss may have caused without any tropical warming, but will also include additional extratropical warming that is part of the "mini" global warming response.

4.3 Results

4.3.1 Impact of SST warming induced by sea ice loss

Figure 4.3 shows the DJF zonal mean temperature response in the I_RCP experiment, the I_RCP_T_SIL experiment and the difference between the two (note the different colour scales). The difference (Fig. 4.3c), represents the impact of the sea ice loss induced ocean warming alone. In the I_RCP experiment, there is strong warming at the Arctic surface, but it is confined to the lowest part of the atmosphere, as there is little warming above 800 hPa. When the induced SST warming is included in the I_RCP_T_SIL experiment, the warming extends further into troposphere in the Arctic. Table 4.3 summarizes the temperature response in the Arctic mid-troposphere (defined as 65°N to 90°N and between 400 hPa and 700 hPa) and the Arctic 2-meter temperature in each experiment. The temperature response in the Arctic mid-troposphere in the I_RCP experiment is 0.13 °C while it is 0.47 °C in the I_RCP_T_SIL experiment. At the near surface, however the relative difference is much smaller as the temperature responses are 4.21°C and 4.61°C respectively. This suggests that the additional warming that occurs in the atmosphere as a result of sea ice induced ocean warming is not confined to the Arctic lower troposphere but extends into the Arctic mid-troposphere. This could be explained by the fact that in the high Arctic during wintertime the air is very stable, so the warming due to sea ice loss gets trapped in the lowest parts of the atmosphere. The additional warming from SSTs, however, extends the forcing to lower latitudes that can influence atmospheric transport pathways that connect the mid-latitude surface to the Arctic mid-troposphere. This transport into the Arctic mid-troposphere from lower latitudes has been shown by Orbe et al. (2015) who used a chemistry climate model to conclude that most of the wintertime air in the Arctic mid-troposphere last touched the surface in the mid-latitudes.

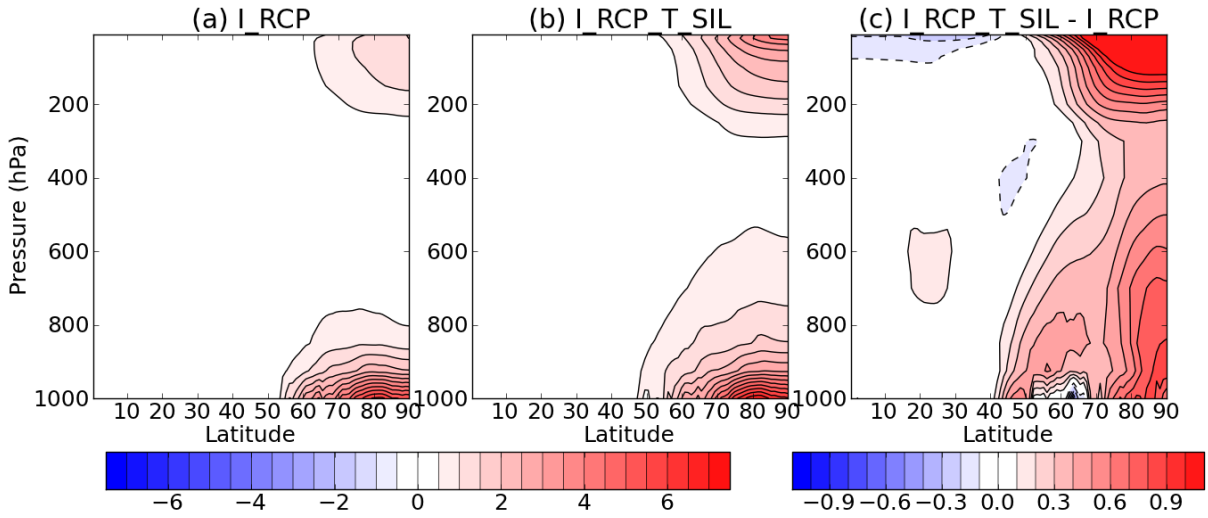

Figure 4.3: (a) The difference in DJF zonal mean temperature (°C) between the I_RCP and the CTL_RCP experiment. (b) As in (a) but for the I_RCP_T_SIL experiment. (c) As in (a) but for the difference between the I_RCP_T_SIL and I_RCP experiments. Note the different colour scale in (c).

Another impact that sea ice induced SST warming has is in the stratosphere where there is greater warming in the I_RCP_T_SIL experiment compared to the I_RCP experiment. This may again be a result of the warming away from the sea ice loss region, which is expected to have a bigger impact on planetary waves that propagate into the stratosphere, although a more detailed analysis of the wave propagation would be needed to confirm this. Also, because this is a low-top model that does not fully resolve the stratosphere, the results should be interpreted with caution, as it has been shown that the stratospheric representation can have an impact on the results of sea ice perturbation experiments (Sun et al. 2015).

Table 4.2: The DJF Arctic mid-troposphere (averaged over 65°-90°N and 400 to 700 hPa) and 2-meter temperature response (averaged over 65°-90°N) for each of the experiments. The response is calculated as the difference between the experiments it's appropriate control simulation.

Experiment	Arctic mid-troposphere temperature response (°C)	Arctic 2-meter temperature response (°C)
I_RCP	0.13	4.21
I_RCP_T_SIL	0.47	4.60
I_RCP_T_SIL_IL	0.14	4.30
I_RCP_T_SIL_AIL	0.32	4.48
I_ALB	-0.02	4.57
I_ALB_ T_SIL	0.23	4.96
I_ALB_ T_ALB40	0.43	5.19

The seasonal cycle of the Arctic cap (averaged from 65°N to 90°N) temperature response is shown in Fig. 4.4. In both the I_RCP and I_RCP_T_SIL experiments, the largest response is at the surface in November-December, but in the I_RCP_T_SIL experiment the response in the mid-troposphere in February is distinctly warmer. Near the surface, the biggest impact of the sea ice loss induced SST warming occurs during late summer and fall, however this does not penetrate into the Arctic mid-troposphere. This is likely a result of these increased SSTs occurring at higher latitudes during this time of year, in contrast to the winter season when the impact at the surface is smaller, but the additional warming is able to be transported into the Arctic mid-troposphere (Fig. 4.4c).

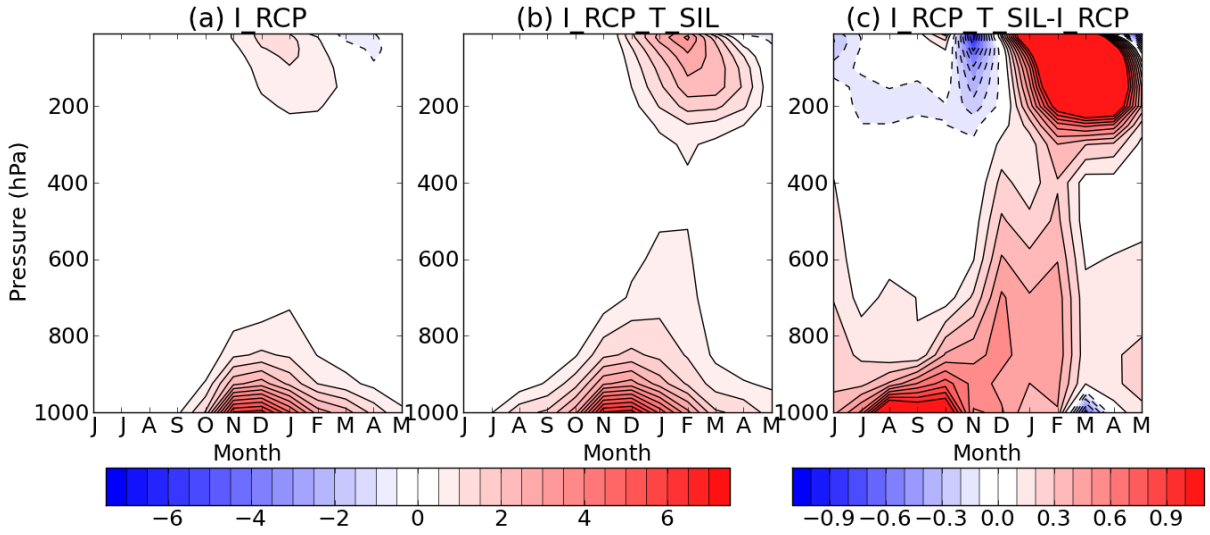

Figure 4.4: As in Fig. 4.3, but for the seasonal cycle of the Arctic cap temperature (°C; averaged from 65°-90°N).

The warming in the Arctic mid-troposphere that occurs as a result of including the ocean warming induced by sea ice loss has a related impact on the DJF zonal wind response (Fig. 4.5). For the sea ice perturbation in isolation, there is an easterly response in zonal wind speeds at mid-latitudes (40°-70°N) and a smaller westerly response at lower latitudes (30°-40°N), consistent with a decrease in strength and equatorward shift in the jet. This is similar to previous studies that performed sea ice loss experiments with prescribed sea ice and SST (e.g. Peings and Magnusdottir 2014; D15; D16). When the SST response is included, there is a similar pattern in the response, however it is about a factor of two stronger: the additional impact of the SST

warming induced by sea ice loss is about the same as the sea ice loss in isolation, and extends to higher latitudes.

The amplification effect from oceanic warming seen in Fig. 4.5 also extends to the DJF SLP response (Fig. 4.6). In the I_RCP experiment, the SLP response is generally weak, with a small decrease in SLP over most of the Arctic Ocean, North Pacific, North America and the Northwest Atlantic and a small increase in pressure over most of Eurasia with a peak over Scandinavia. The typical amplitude of this response is 1.0-1.5 hPa. When the T_SIL pattern is also included in the forcing, the response is amplified by about 1 hPa and presents a clearer wave 1 structure. The amplification is greater over the North Pacific where there is a deepening of the Aleutian Low and a high pressure response centered over the Arctic Ocean and Siberian Coast. The SLP response over the North Pacific is of interest because we expect that in the original simulations with a dynamical ocean it is closely coupled to the SST pattern which is itself prescribed (Section 4.2.1). We conclude that sea ice loss alone causes only a weak reduction in SLP over the North Pacific, however the ocean response to sea ice loss could act to reinforce it, with sea ice loss thus providing a positive feedback via the induced SST warming.

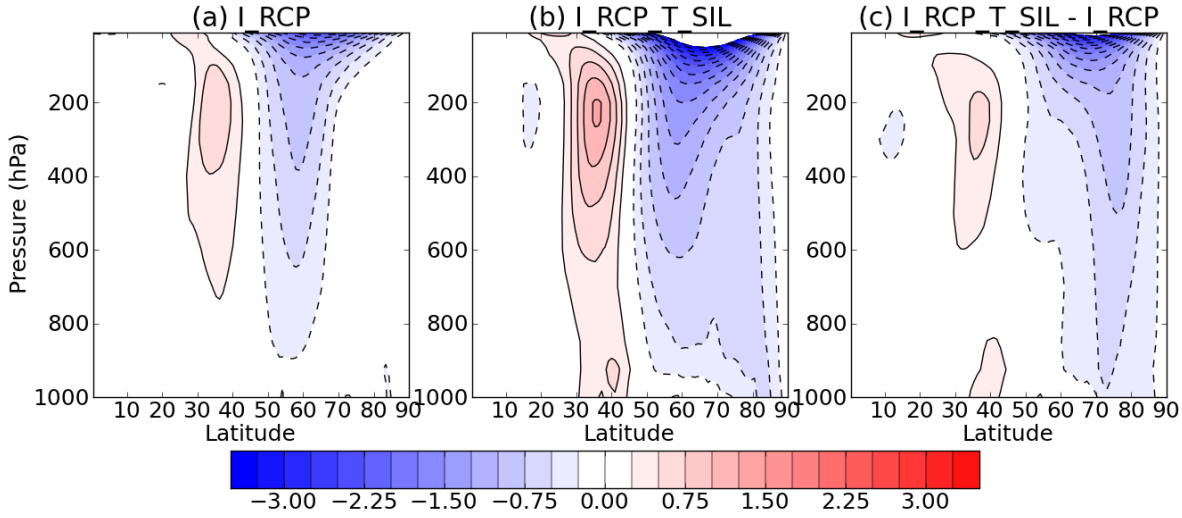

Figure 4.5: As in Fig. 4.3, but for zonally averaged wind speed (m s^{-1}).

The DJF precipitation responses are shown in Fig. 4.7. In response to sea ice loss in isolation, there are increases in precipitation over the regions where there is sea ice loss and over the west coast of the North America. There are also decreases over much of the North Atlantic Ocean. The increased precipitation over the west coast of North America is enhanced and occurs

over a greater area once the effects of the SST response are also included. This is likely related to the deepening of the Aleutian low and the increase in SST that were prescribed along the coast, which increase the latent heat flux into the atmosphere (not shown). The prescribed increase in SST over the North Atlantic also works to increase the amount of precipitation in these regions.

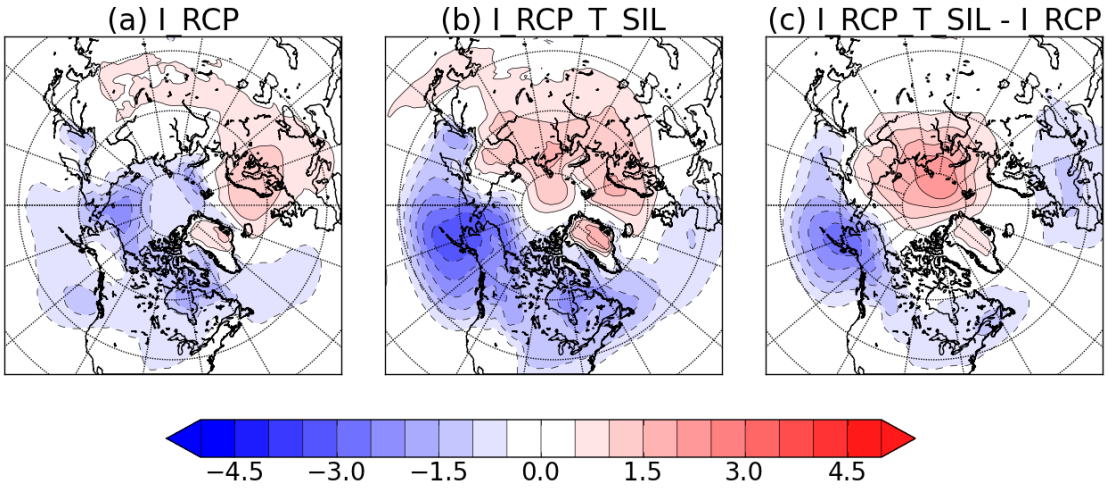

Figure 4.6: As in Figure 4.3, but for sea level pressure (hPa).

Figures 4.3-4.7 taken together show that including the ocean warming when examining the response to sea ice loss in an AGCM experiment increases the temperature response in the Arctic mid-troposphere, as well as the circulation response and some of the precipitation response. In the setting of prescribed SST and sea ice in AGCM experiments, we are able to reproduce many of the features from the coupled ocean-atmosphere experiments described in D15, D16 and in Chapter 3 by including the extratropical ocean warming that we estimated to be induced by sea ice loss, without significantly changing tropical temperatures. This highlights the importance of the coupling to the ocean and indicates that it is the extratropical SSTs that are important for amplifying the response to sea ice loss in the coupled model. This will be discussed further in Section 4.4.

4.3.2 The impact of SST warming in and away from the ice loss region

A number of previous studies that have examined the atmospheric response to sea ice loss in AGCM experiments do account for the SST warming in the regions where sea ice is lost,

either from observations (e.g. Screen et al. 2013) or from model projections (e.g. D15,16). However these studies have not documented the impact of these local SST on the atmospheric response. Because the largest increases in SST that we prescribed are in the regions where there is sea ice loss (compare where the sea ice changes are in Figure 4.2 to the T_SIL pattern in Figure 4.1d), it is reasonable to question if these in isolation have a large impact on the response. In contrast, the SST changes away from ice loss regions could be more important, because although they are smaller in magnitude, they cover a larger area and are at lower latitudes. To test this, we compared experiments that included only SST changes derived from the T_SIL pattern where there was sea ice loss, together with sea ice loss (I_RCP_T_SIL_IL) to experiments that only included SST changes derived from the T_SIL pattern away from the sea ice loss regions (I_RCP_T_SIL_AIL).

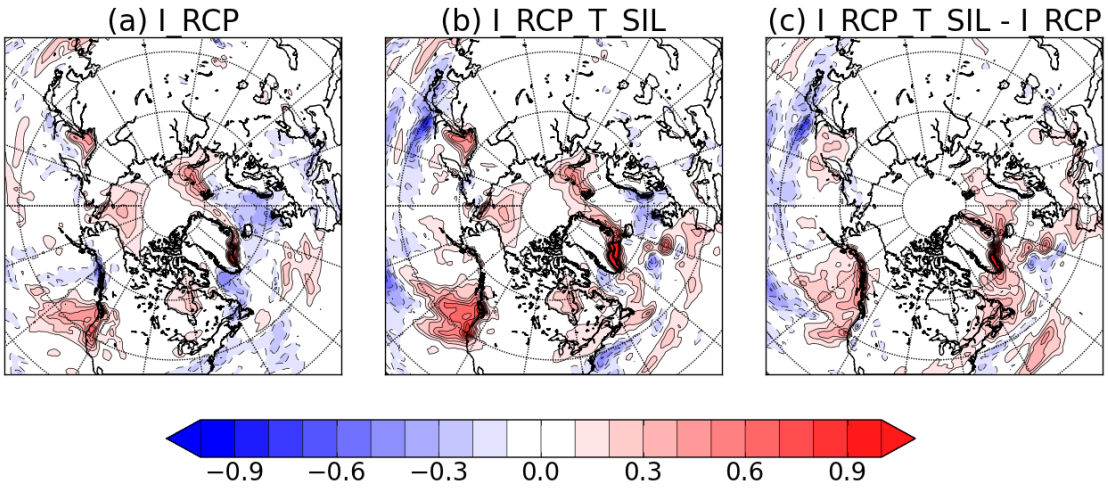

Figure 4.7: As in Fig. 4.3, but for precipitation (mm day^{-1}).

The difference in the zonal mean temperature between I_RCP_T_SIL_IL and I_RCP (i.e. the effect of the SST changes that are in sea ice loss region) (Fig. 4.8a) is small in the Arctic mid-troposphere. In fact, the Arctic mid-troposphere temperature response is nearly identical in the I_RCP_T_SIL_IL and the I_RCP experiments (0.14°C of 0.13°C respectively) and there is only a slight increase in 2m temperature in response to the increases SSTs in the sea ice loss region (4.30°C compared to 4.21°C with no SST changes). Meanwhile, in Fig. 4.8b, the difference in zonal mean temperature between I_RCP_T_SIL_AIL and I_RCP (i.e. the effect of the SST changes that are away from the sea ice loss region) does show greater warming in the

Arctic mid-troposphere and at the surface (the responses are 0.32°C and 4.48°C respectively in the I_RCP_T_SIL_AIL experiments). Thus, SST changes that are prescribed away from the sea ice loss region are responsible for most of the changes seen in Figure 4.3. This is consistent with the idea that lower latitude ocean warming stimulates heat transport to the Arctic mid-troposphere. Not surprisingly, it is the SST changes away from the sea ice that are also responsible for the differences in circulation and precipitation that are seen in Figures 4.5-4.7 (not shown).

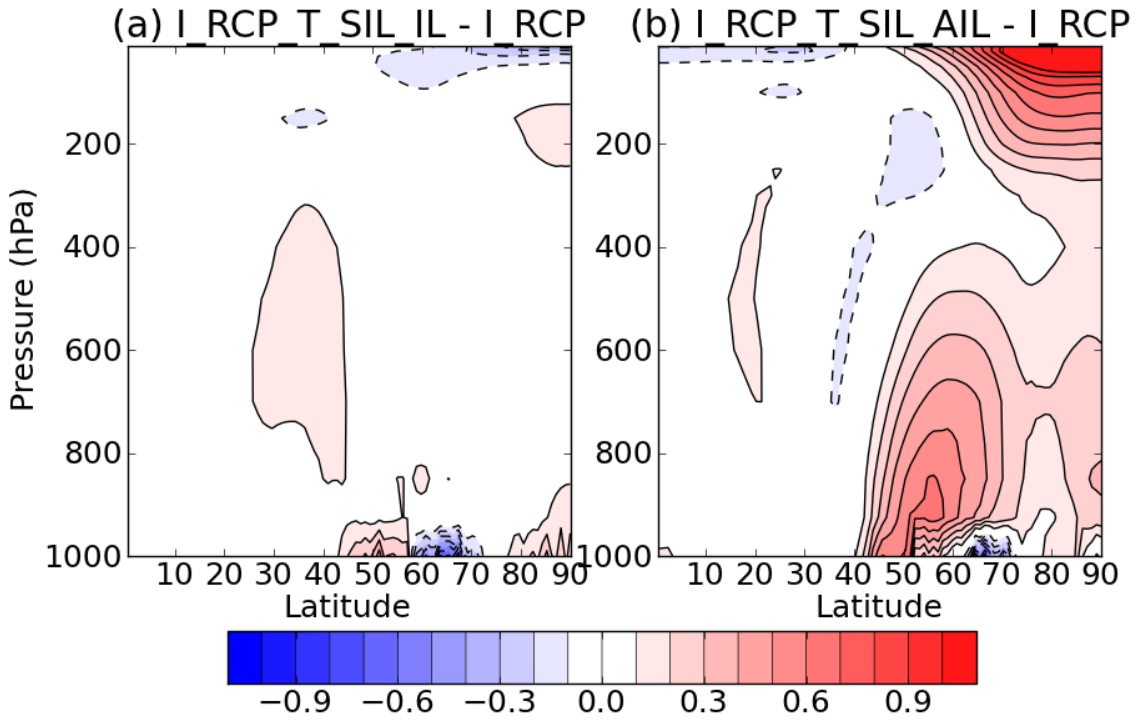

Figure 4.8: (a) As in Fig 4.3c, but for the difference between the I_RCP_T_SIL_IL and I_RCP experiments. (b) As in (a) but for the difference between the I_RCP_T_SIL_AIL and I_RCP experiments

4.3.3 Using additional experiments to examine the robustness of the response

In this section, we describe the results of additional experiments that use slightly different prescribed sea ice and SST (both the forcings and background states) to test the robustness of the results presented in Section 4.3.1. There is evidence that the background SST

can impact the size and structure of the Arctic temperature response to sea ice loss (Screen and Francis 2016), thus we expect that it may impact the response to mid and high latitude SST warming as well. The difference in zonal average temperature and wind speeds between I_ALB_T_SIL and I_ALB are shown in Fig. 4.9. Recall that the difference in forcing between these ALB experiments and the RCP experiments in Figs. 4.3c and 4.5c are nearly identical (to within about 3% in magnitude), but they have different background sea ice and SST states. The zonal mean temperature response to the T_SIL pattern is similar in these experiments compared to the RCP (Figure 4.4c). There is a clear impact in the Arctic mid-troposphere, but the structure is slightly different as there is more warming at lower latitudes (50°-70°N) and less at very high latitudes (80°-90°N) compared to the RCP experiments. This can be seen in Table 4.2, which shows less Arctic mid-tropospheric warming in the in I_ALB_T_SIL experiment (0.23°C) compared to the I_RCP_T_SIL experiment (0.47°C). However, unlike the I_RCP experiment, where there is a small amount of warming in the Arctic mid-troposphere (0.13°C), there is no warming in the I_ALB experiment (-0.02°C), so the impact of the T_SIL SSTs alone are closer between the two sets of experiment, but still weaker in the ALB experiments (0.25°C vs 0.34°C).

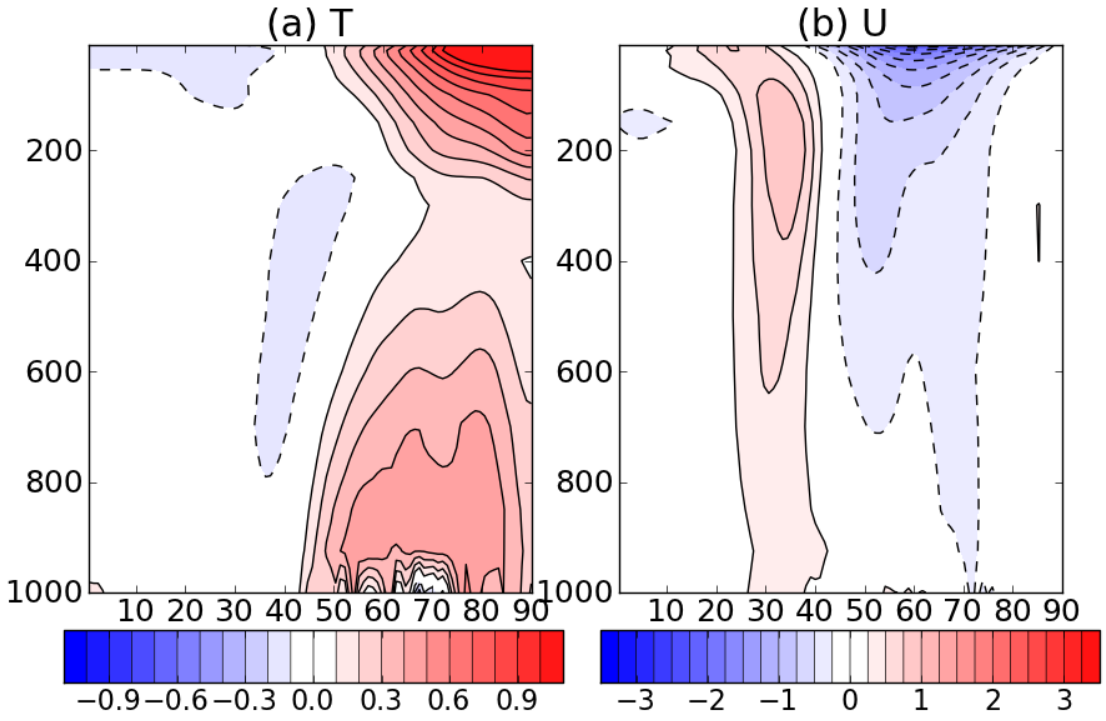

Figure 4.9: (a) As in Fig 4.3c, but for the difference between the I_ALB_T_SIL and I_ALB experiments. (b) As in (a), but for zonal averaged wind speed (m s^{-1}).

The difference in zonal mean zonal wind between I_ALB_T_SIL and the I_ALB (Fig. 4.9b) experiments is also similar to the RCP experiments with an easterly response at higher latitudes and westerly response at lower latitudes. There are however, some structural differences, as the easterly response due to T_SIL in the ALB experiments is slightly weaker and occurs at lower latitudes and the westerly response is stronger compared to the RCP experiments. These differences are likely connected to the differences in magnitude and structure of the zonal temperature responses. It should also be noted that the zonal wind response in the I_ALB and I_ALB_T_SIL experiments are themselves weaker compared to the RCP experiments (not shown), again likely connected with the differences in Arctic mid-troposphere temperature response (Table 4.2). The difference between I_ALB_T_SIL and the I_ALB for SLP (Fig. 4.10) also shows some similarities and some differences. The low pressure response over the North Pacific that was seen in the RCP experiments is also seen the ALB experiments, however, the high pressure response over the Siberian coast is not present, indicating that the background state does matter for this part of the regional response. The precipitation response to T_SIL is similar in the ALB simulations compared to the RCP simulations (not shown).

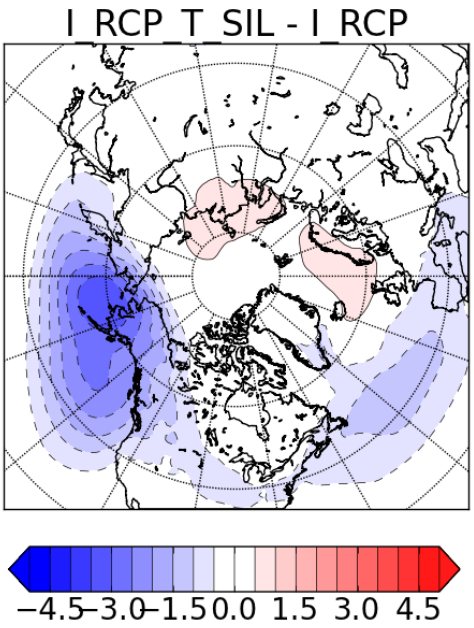

Figure 4.10: As in Fig. 4.9a. but for SLP (hPa).

As discussed in Section 4.2.1, the T_SIL pattern that is calculated can be difficult to interpret and it is possible that the exact magnitude of some of the features my change slightly

depending on the assumptions made. To further test the robustness of the results, we performed an additional experiment where, along with the change in sea ice, the SSTs North of 40°N from the output from the sea ice albedo forcing experiment is also forced (I_ALB_T_ALB40). The goal of calculating the T_SIL pattern was to obtain the SST change that is associated with sea ice loss without warming at lower latitudes. Using the SST north of 40°N is a simpler method to examine the impact of only the mid-latitude SSTs without any tropical SST changes. However, the interpretation is somewhat different in this case because some of the SST warming imposed, particularly in the mid-latitudes, is related to the mini global warming response that was accounted for via pattern scaling in the T_SIL experiments.

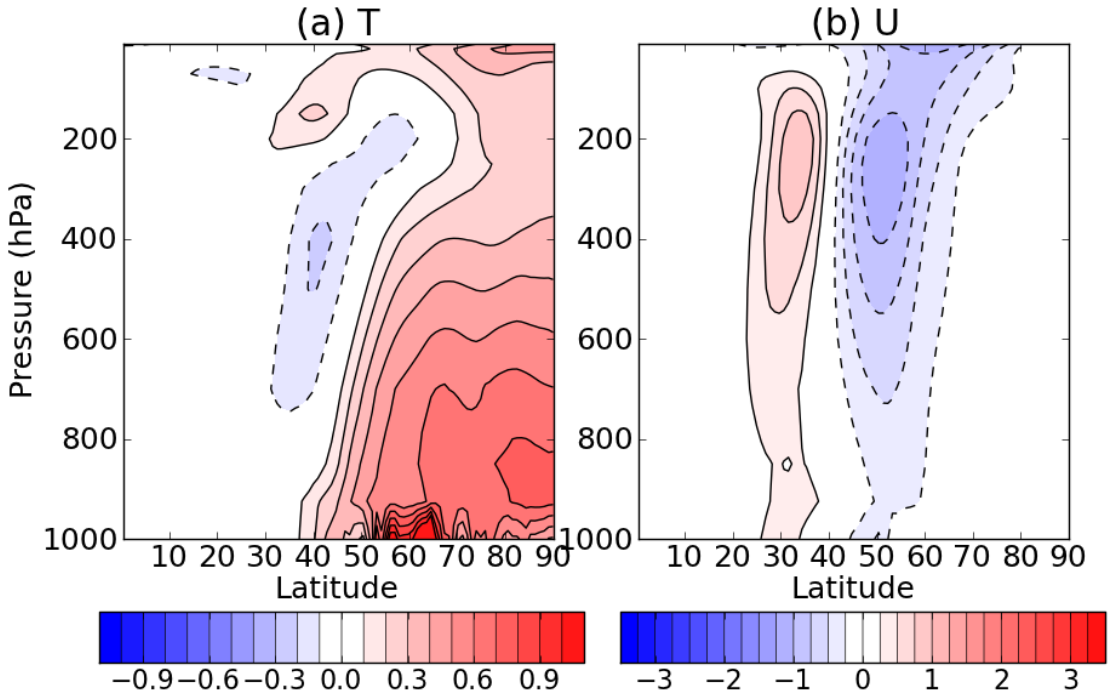

Figure 4.11 As in Fig. 4.9, but for the difference between the I_ALB_T_ALB40 and I_ALB experiments.

Figure 4.11a shows the zonal mean temperature difference between I_ALB+T_ALB40 and I_ALB. Similar to figure 4.9a, and 4.4c, the addition warming from the SST does not get trapped in the lowest part of the atmosphere and is able to make its way to the Arctic mid-troposphere. As the SST forcing is stronger, particularly at mid-latitudes, this results in the temperature response being stronger as well. The Arctic mid-tropospheric temperature response is 0.43°C in the I_ALB_T_ALB40 compared to 0.23°C and -0.02°C in the I_ALB_T_SIL and

I_ALB experiments respectively. The larger zonal mean temperature response to the SST forcing also results in a larger zonal wind response (Figure 4.11b). For SLP, consistent with the other experiments, the low pressure response in the North Pacific is present (not shown) further highlighting, the robustness of this part of the circulation response.

4.4 Summary and Discussion

This chapter investigated the atmospheric response to ocean warming induced by sea ice loss by using a number of AGCM experiments that are based on the coupled model response to sea ice loss and greenhouse gas projections. First, the SST response that is induced by sea ice loss was estimated using the output from these coupled model experiments and a two-parameter pattern scaling technique that was developed in Chapter 3. The SST pattern that was estimated was thus the part of the response that scaled with Arctic sea ice loss, while keeping lower latitude SSTs constant. In other words, this SST pattern can thus by thought of as an estimate of ocean warming from sea ice loss without non-sea ice loss-related global warming processes. Sea ice loss induces SST warming that extends from the region of sea ice loss into the mid-latitudes. This is accompanied by some cooling in the Pacific Ocean from 30°-50°N. Much of the warming likely occurs as result of the sensible heat released into the atmosphere due to sea ice loss being advected equatorward and returning to the ocean. Other changes including the cooling in the Pacific are likely a result of changes in atmosphere and ocean circulation.

In the AGCM experiments, comparisons were made between experiments that prescribed sea ice loss with and without the sea ice loss-related SST changes. It was found that the extra warming that results from prescribing the changes in SSTs that are caused by sea ice loss does not get trapped in the Arctic lower troposphere like the warming directly due to sea ice loss does, but instead is able to make its way into the Arctic mid-troposphere through transport pathways suggested by previous work (Laliberte and Kushner 2013, 2014; Orbe et al. 2015). As this extra warming is able to reduce the temperature gradients in the free troposphere, it also results in a zonal wind response that has a larger magnitude. The impact of the ocean warming due to sea ice loss has a similar impact in magnitude and structure on the zonal mean circulation as the sea ice loss itself. The SLP response is similarly enhanced by the ocean warming, with a deepening of the Aleutian low and high pressure response over the Siberian coast. Additional experiments

show that these impacts were a result of the SST changes away from the sea ice loss regions and not from the changes where the sea ice was lost.

The robustness of the results was tested to a limited extent with different background sea ice/SST states and different SST perturbation patterns. Robust features of these sensitivity tests included more Arctic mid-tropospheric warming, a stronger zonal wind response, a deepening of the Aleutian low, and increased precipitation over the west coast of North America. One response that was less robust across experiments was the SLP response over Eurasia.

In the context of D15, D16, it can be seen that essentially all the impacts that coupling to the ocean have on the extratropical response to sea ice loss can be reproduced in the AGCM experiments when the sea ice loss induced extratropical SST change is imposed in isolation. Because these changes were imposed away from the tropics, this suggests that the tropical response might not play a large role in enhancing the response. This is in contrast to Tomas et al. (2016), who attributed the deepening of the Aleutian low that was seen in D16 to the tropical response. In this study, the Aleutian low deepening was robustly found in all experiments that included the extratropical SSTs and no tropical SST changes.

This chapter further highlights the importance of coupling to the ocean in the atmospheric response to sea ice loss. The majority of the studies that have performed modelling experiments examining the atmospheric response to sea ice loss use an AGCM with prescribed sea ice and SST (e.g. Deser et al. 2010; Screen et al. 2013, 2014; Peings and Magnusdottir 2014). Almost all of these use either no changes to SSTs or confine such changes to where the sea ice is lost. The experiments in Section 4.3.2 show that these latter SST changes have little impact on tropospheric temperature and circulation. The results of this study would suggest that the previous studies underestimate the circulation response that occurs in response to sea ice loss. In fact in one set of experiments we have performed (the ALB experiments), the zonal mean circulation response in the troposphere was nearly zero (not shown), and it was only when the extratropical SST response was included that there was a significant response. It should be noted, however that even though sea ice loss induced ocean warming contributes just as much, or even more than the sea ice loss itself, the circulation response seen here is still small. In response to 30 years of sea ice loss and the associated SST changes, the decrease in the zonal mean wind speeds on the poleward side of the jet at 500 hPa was less than 1 m s^{-1} in all experiments.

While the warming of the extratropical ocean enhances the circulation response to sea ice loss, warming of the tropical ocean might very well have the opposite effect. For example, in response to increased greenhouse gas forcing, there is enhanced warming of the tropical upper troposphere (Stocker et al. 2013), which increases the meridional temperature gradient in the upper troposphere. As discussed in Chapter 3, this tends to have the opposite impact on the circulation response and acts to at least partially cancel out the effects of the Arctic warming. Indeed, global climate models forced with increased greenhouse gases on average see little change in the jet stream, although there is considerable spread in the response (e.g. Barnes and Polvani 2015). This means that despite the ocean acting to enhance the circulation response, we may not actually observe these effects as sea ice melts in the future.

Chapter 5
Conclusions

5.1 Summary

With the rapid retreat of sea ice due to rising global temperatures, it is important to understand what impacts sea ice loss may have on the atmosphere. Sea ice loss causes increased Arctic warming by altering the surface energy budget, which could potentially change the atmospheric circulation through a number of different mechanisms. Observational analysis has suggested that sea ice loss may have already impacted the weather and climate at mid-latitudes by changing the atmospheric circulation (Francis and Vavrus 2012; Cohen et al. 2014). However, understanding the impact of sea ice loss from observations is difficult, due to the short observational record and difficulty in isolating sea ice loss from other processes. To cleanly isolate the role of sea ice loss on the atmospheric circulation, this thesis uses very long coupled climate model simulations and targeted prescribed SST simulations.

Chapter 2 provides an overview of the atmospheric response to sea ice loss in a coupled climate model (CCSM4), with a focus on the atmospheric variability. Some studies have suggested that sea ice loss may lead to increased "waviness" in the jet-stream and an increase in extreme weather (Francis and Vavrus 2012, Cohen et al. 2014), however additional observational analysis and analysis of future projections in comprehensive climate models are inconclusive as to whether this is happening or will happen (Screen and Simmonds 2013; Barnes 2012; Barnes and Screen 2015). In Chapter 2, very long (800 years), adequately sampled simulations that cleanly isolate the impacts of sea ice loss were analyzed. In response to the equivalent of a few decades' worth of sea ice loss under greenhouse gas projections, it is shown that the temperature response is confined to the lowest parts of the atmosphere coinciding with a very weak zonal mean wind response. It is found that there is a large reduction in temperature variability on all timescales over the regions of sea ice loss. This likely occurs as a result of decreased temperature gradients as discussed in Screen (2014) and Schneider et al. (2015) and due to the difference in heat capacity between the sea ice and ocean. A smaller magnitude reduction in variability is also seen in mid-latitude temperatures, SLP and mid-troposphere geopotential height. A spectral analysis showed that the reduction in temperature variability over the mid-latitude land surface occurs at all timescales. The amplitude of waves in the mid-troposphere were also examined in

Chapter 2 using two different measures of amplitude as in Screen and Simmonds (2013), whose focus was on trends in observations. The sign of the response between the two different methods was opposite, in broad agreement with observed trends, however the magnitude of the changes was small. The only season and wave number where the two methods agreed in sign and were statistically significant was for wave-1 in wintertime, where there was an increase in amplitude. This result will be returned to in the following section on future work.

In addition to the 800-year simulations that were allowed to equilibrate in response to the sea ice perturbation, seven additional 50-year simulations were also performed to examine the initial transient adjustment. It was found that there was a significant amount of spread in the SLP and temperature changes between each realization. For example, two realizations had an opposite signed SLP change on the Siberian coast (Fig. 2.12). This led to different near-surface temperature change in each of the realizations as well – some realizations have Eurasian cooling while others do not. Averaged over all realizations, the circulation response is weak and similar to the equilibrium response. The most significant difference is that there is a high-pressure response over Scandinavia in the initial transient response that is not present after it adjusts to equilibrium

One of the impacts of sea ice loss in the coupled model framework is that there is some tropical warming that occurs as a part of a "mini global warming" (Chapter 2 and Deser et al. 2015, 2016). In Chapter 3, CESM1 simulations driven separately by sea ice albedo reduction and projected greenhouse gas increases were used to isolate the response of the atmospheric circulation to sea ice loss. A two-parameter pattern scaling technique was developed that estimates the response to Arctic sea ice loss with low-latitude ocean warming kept constant and vice versa. When this was applied to the zonal mean temperature, the warming in the Arctic lower troposphere was cleanly separated from the warming throughout the rest of the troposphere. It was also shown that many of the wintertime atmospheric circulation responses seen in the sea ice albedo forced simulations (e.g. equatorward shift in the jet, high pressure response over Eurasia, weakening of the stratospheric polar vortex), are not seen in the RCP8.5 forced experiments even with the same amount of sea ice loss, due to cancellation with the impacts associated with low-latitude warming. The calculation also showed that sea ice loss in isolation can cause weak East Asian cooling in wintertime, but it is also opposed by strong warming associated with low-latitude temperatures. Even in the sea ice albedo forced

simulations with only weak low-latitude warming, there was only a weakening of warming in East Asia rather than an actual cooling. Two impacts of sea ice loss, besides the high-latitude warming, that are clearly present in the RCP8.5 forced simulations are the decrease in subseasonal temperature variability and increase in precipitation over the west coast of North America. Simulations of CCSM4 were also analyzed and compared to the CESM1 simulations and similar results were found, however the CCSM4 results were not statistically robust. This was because there were fewer ensemble members of the CCSM4 RCP8.5 simulations available and the responses to the same albedo perturbation in CCSM4 were generally weaker than in CESM1.

Based on the results of Chapter 3, it may be expected that the atmospheric circulation response to sea ice loss in the coupled model should be weaker than in an AGCM experiment with prescribed sea ice and SSTs. This is because the impact of the tropical warming may oppose the impacts of the warming at high latitudes on the circulation response, partially canceling out the response. However, Deser et al. (2015, 2016), found a stronger circulation response to sea ice loss in the coupled climate system. In Chapter 4, it is hypothesized that it is the extratropical ocean warming that is caused by sea ice loss that enhances the response in the coupled model. To test this, the SST response due to sea ice loss was estimated using the pattern scaling techniques developed in Chapter 3. Next, AGCM experiments forced with prescribed sea ice loss with and without the SSTs connected to sea ice loss were performed. Unlike the warming directly due to sea ice loss, the additional warming from the SSTs does not get trapped in the Arctic lower troposphere and instead some of it is transported into the Arctic mid-troposphere. This additional warming causes a stronger zonal mean circulation response, a larger deepening of the Aleutian low, and a high pressure response over the Arctic coast of Eurasia, similar to what was seen in the coupled model in Deser et al. (2015, 2016). The impacts on the atmospheric circulation of the SST response that result from sea ice loss are of similar magnitude and spatial structure to the sea ice loss itself. Additional experiments were performed which confirmed the robustness of most of the responses and that it was the changes of the SSTs away from the sea ice loss that had a larger contribution to the amplification of the response, not the changes of the SSTs in the regions of sea ice loss.

To conclude this summary, there are several key points that are worth emphasizing. First, based on theoretical arguments and trend analysis in observations, previous studies have

suggested that Arctic sea ice melt and the Arctic amplification it causes could increase variability and increase the number of extreme events at mid-latitudes (Francis and Vavrus 2012; Cohen et al. 2014). The analysis presented in Chapter 2 provides evidence of reduction in variability, using a well sampled experiment that cleanly isolates the impacts of sea ice loss. A reduction in temperature variability due to decreased temperature gradients and increased maritime influence is found, implying that cold extremes in the high and mid-latitudes will become less likely in the future. This reduction was seen on all timescales in disagreement with previous studies that have suggested that there will be an increase in variability on weekly to monthly timescales (e.g. Coumou et al. 2015). A reduction was also seen in SLP and Z500 variability, but the magnitude of the change was small, suggesting that the role of sea ice in driving changes in atmospheric variability is small. In Chapter 3, it is shown that the reduction in temperature variability was one of the few impacts of sea ice loss that was also seen in experiments forced with increases in greenhouse gas concentrations.

This thesis also highlights the importance of using very long simulations or a very large ensemble when studying the atmospheric response to sea ice loss. Results from previous studies have shown significant disagreement about the modeled atmospheric circulation response. In Chapter 2, it was shown that 50-year-long simulations that differ only in their initial conditions, exhibit opposite signed SLP patterns in the presence of sea ice loss. Thus studies that have in the past used similar or shorter analysis periods could exhibit disagreements simply because of inadequate sampling. This also emphasizes the difficulty in attributing observed changes in atmospheric circulation to sea ice loss from the approximately 35 years of data from the satellite era. These issues arise because the simulated response is small compared to internal variability. The value of a large number of independent realizations in an ensemble can be seen in the analysis: the five ensemble members of the CCSM4 RCP8.5 simulations were too few to get statistically robust results compared to the 30 ensemble members of the CESM1 RCP8.5 simulations.

In Chapter 3, it was shown that many of the circulation responses due to sea ice loss in isolation are opposed by the impacts of warming at low-latitudes. Some previous studies have shown opposing impacts of Arctic and tropical warming on some aspects of the atmospheric response in idealized models (Butler et al. 2010) or in the spread of many coupled models (Harvey et al. 2014). In Chapter 3, these opposing influences are clearly shown in two

comprehensive climate models. It was also shown that the warming at low-latitudes more broadly opposes nearly all aspects of the atmospheric circulations responses due sea ice loss, including many of the more robust responses seen in many sea ice loss experiments. This suggests that even if sea ice loss is able to alter the atmospheric circulation, this impact may be masked by other aspects of the global warming response to greenhouse forcing.

Finally, Chapter 4 emphasized the importance of dynamical coupling to the ocean in the atmospheric response to sea ice loss. It was shown that extratropical ocean warming caused by sea ice loss acts to amplify the response directly due to sea ice loss. As this warming occurs at lower latitudes compared to the sea ice loss itself, the additional warming is able to be transported into the Arctic mid-troposphere. This causes a decrease in the temperature gradient in the mid-troposphere, which enhances the atmospheric circulation response. It was shown that these extratropical changes in SSTs could account for many of the differences in the extratropical response between the coupled and uncoupled simulations of Deser et al. (2015, 2016). When the ocean cannot respond to the changes in sea ice, as in standard AGCM experiments, they are unable to capture this additional ocean warming and thus will underestimate the response.

5.2 Future Work

The work presented in this thesis has opened up a number of new avenues for future research. The sea ice albedo reduction that was done in the simulations used throughout this thesis was applied to the whole sea ice model, melting the Antarctic sea ice as well, so one obvious area of future work is the study of the atmospheric response to Antarctic sea ice loss. There are important differences between the sea ice in the two hemispheres that could lead to differences in how the atmosphere responds. First, due to difference in the locations of the continents, there is more Antarctic sea ice available to melt in wintertime than there is in the Arctic. In addition this ice is located further from the poles in the Antarctic, which, based on the conclusions of Chapter 4, could lead to a larger mid-latitude circulation response. On the other hand, the forcing due to Antarctic sea ice loss would be relatively symmetric around that pole, meaning that it is less likely to impact planetary waves.

The atmospheric response to Antarctic sea ice loss has received less attention than the response to Arctic sea ice loss, probably because Antarctic sea ice has actually been increasing slightly (Turner et al. 2015) while the Arctic sea ice has been rapidly decreasing. There is no

consensus as to what causes this, but some have suggested it is due to changes in atmospheric circulation (either due to anthropogenic or internal forcing), ocean-sea ice feedbacks, or due to an increase in freshwater from the melting ice sheets (Turner et al. 2015). Despite the current increases in Antarctic sea ice, with rising global temperatures it is still expected to melt eventually, and with this motivation a few studies have investigated the impacts of Antarctic sea ice loss. For example, Kidston et al. (2011) found that while increasing the Antarctic sea ice extent caused a large poleward shift in the mid-latitude jet, a decrease in sea ice extent resulted in very little change to the atmospheric circulation. This non-linearity of the response was suggested to be a result of the increase in sea ice extent altering the meridional temperature gradients closer to the baroclinic zone than a decrease in extent. The authors concluded that a decrease in Antarctic sea ice loss would not result in a substantial change in atmospheric circulation. In contrast, Bader et al. (2013) do find an equatorward shift in the mid-latitude jet and a shift towards the negative phase of the southern annular mode (SAM) in response to projected Antarctic sea ice loss. These previous studies that have investigated the atmospheric circulation response to Antarctic sea ice disagree with each other, reminiscent of the Arctic sea ice loss literature. Besides model differences and differences in the size and spatial extent of the forcing, some of the disagreements could arise due to internal variability, as the simulations performed in these two studies were only 50 and 30 years long. The very long simulations that were used in this thesis are thus ideal for analysing the response to Antarctic sea ice loss.

Preliminary analysis suggest that much like in the Northern Hemisphere, the atmospheric circulation response to Antarctic sea ice loss is weak, with only a small weakening of the wintertime zonal wind speeds on the poleward side of the eddy-driven jet (Fig. 5.1). Also similar to the Northern Hemisphere, the extratropical response to sea ice loss is not evident in the RCP8.5 forced simulations in the zonal winds. In fact, the zonal wind response south of 50°S is the opposite sign in the RCP8.5 forced simulations compared to the sea ice albedo forced simulations. Much of the analysis that has been done for this thesis is being extended to the Southern Hemisphere, including the impact of sea ice loss on the atmospheric variability and wave amplitudes. In addition, it would also be interesting to perform additional AGCM experiments from output from the coupled model experiments to examine the effects of coupling to the ocean in the Southern Hemisphere.

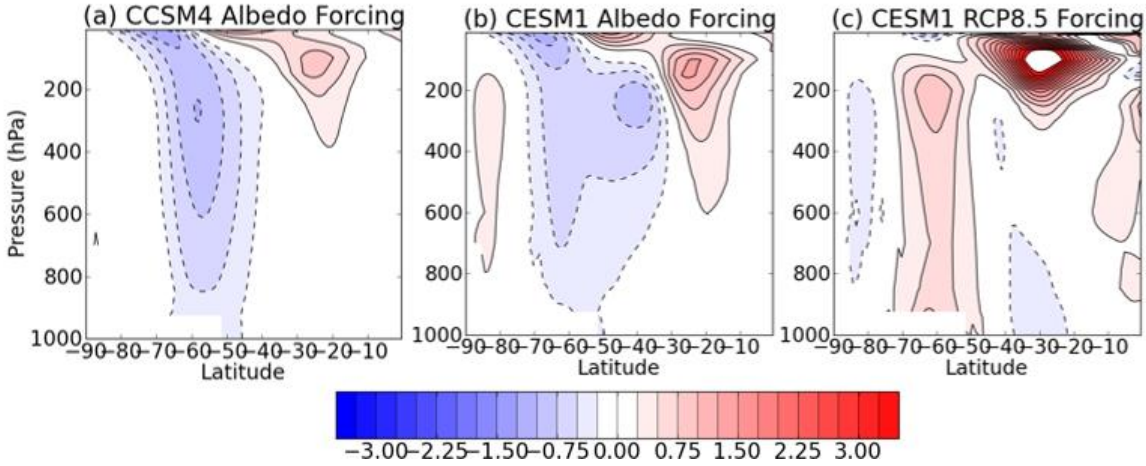

Figure 5.1 : (a) The Southern Hemisphere JJA zonal mean wind response (m s^{-1}) to sea ice albedo forcing in CCSM4. (b) As in (a) but in CESM1. (c) As in (a) but for the ensemble mean of the CESM1 RCP8.5 forcing experiment.

Returning to the Northern Hemisphere response, additional analysis could be done to improve our understanding of the dynamics at work there. For example, in Chapter 2 a simple analysis of eddy amplitude at 500hPa 45°N (Fig. 2.9; right) showed that while the wintertime wave-1 increased in amplitude in response to sea ice loss, the wave-2, 3, 5 and total all show statistically significant decreases in amplitude. Figure 5.2 shows the response of the wintertime wave amplitude at 500 hPa and each latitude, for waves 1-3, divided up into the stationary wave and transient wave for both CCSM4 and CESM1. It can be seen that the increase in wave-1 amplitude arises from an increase in the stationary wave amplitude. The wave-2 and 3 decreases come from a combination of a decrease in stationary and transient wave amplitudes, where the exact contributions depend on the model and latitude. Further analysis into the causes of these change in amplitude is underway using the methodology of Watt-Meyer and Kushner (2015) to separate the amplitude changes into standing and travelling components.

This thesis has focused on the atmospheric response to sea ice loss, but the coupled model simulations used throughout this thesis can also be analyzed to understand the ocean response to sea ice loss. Sea ice loss can impact the ocean either directly or indirectly through changes in temperature, salinity and wind stress. Understanding how these fields change and how they act to change the ocean circulation could help elucidate some the changes to the ocean that were briefly shown in this thesis. For example, in Chapter 2, it was shown that in response to a sudden change in Arctic sea ice, the AMOC decreased in strength, and underwent a number

of centennial timescales oscillations before recovering in strength after 300-400 years (Figure 2.1). The initial decrease in strength of the AMOC is likely caused by the increased fresh water flux into the North Atlantic, but the cause of the oscillations and recovery and the impact it has on the North Atlantic Ocean could be investigated further. Further work could also address the changes seen in the North Pacific seen in Figure 4.1. Specifically, we might ask what causes the lack of warming seen in the in the Western and Central Pacific and the warming along the coast of North America.

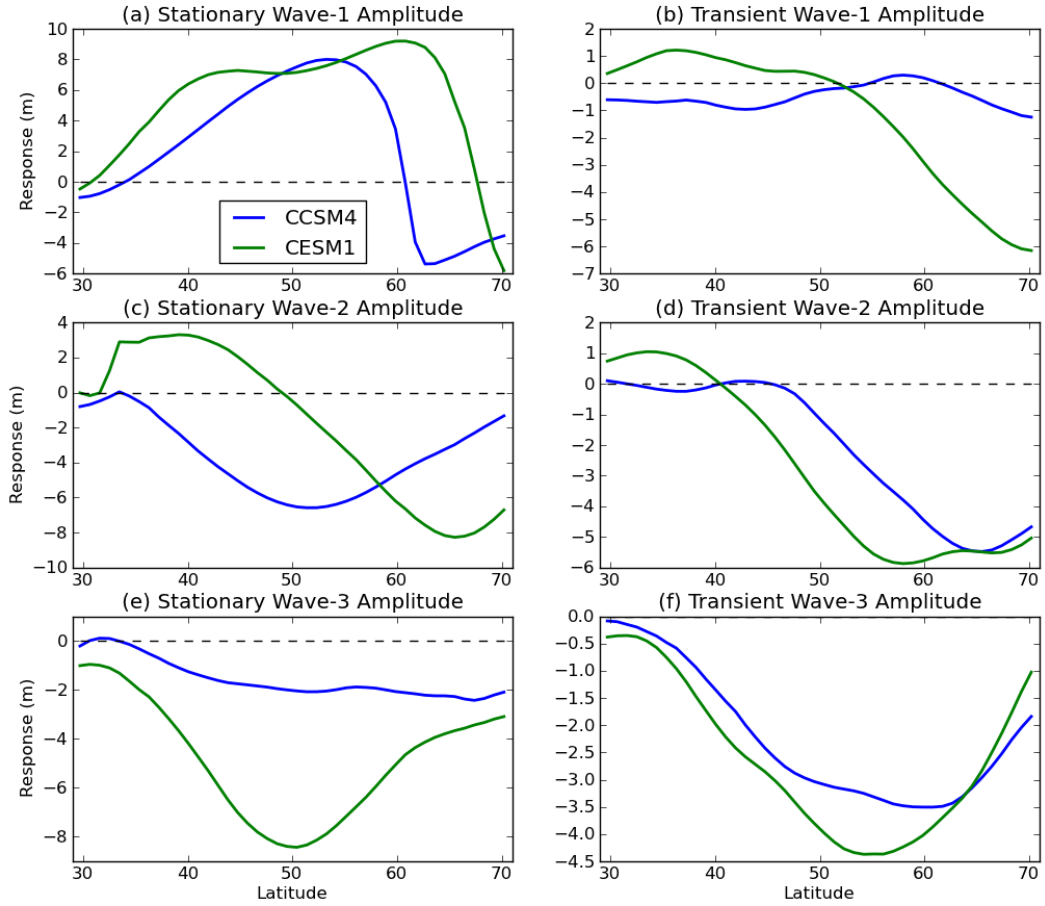

Figure 5.2 : The wave amplitude response (m) to sea ice albedo forcing as a function of latitude in CCSM4 (blue) and CESM1 (green) for (a), (c), (e) stationary waves and (b), (d) (f) transient waves for (a)-(b) wave-1, (c)-(d) wave-2 and (e)-(f) wave-3.

Most of the proposed future work described in this section involves further analysis of the simulations performed for this thesis. However, there are additional coupled model simulations that could be performed to help understand the response to sea ice loss in a coupled model. For example, in Chapters 3 and 4, it was assumed that the equilibrium response to an abrupt sea ice

loss is similar to the response caused by slowly decreasing sea ice in the simulations forced by greenhouse gas increases. This could be tested by running an experiment where the sea ice albedo is reduced slowly over time to better match the sea ice behaviour in climate projections. In addition, previous studies have shown that the ocean may play an important role in a time-lagged response to sea ice loss (e.g Laîné et al. 2016). This could be investigated through targeted experiments by applying the forcing only in certain regions and months or seasons. This could have important implications for the role of sea ice in seasonal prediction.

To conclude, this thesis presents novel results examining the atmospheric response to Arctic sea ice loss in the coupled climate system. It was shown that once sufficient averaging is done, the mean atmospheric circulation response is weak. Apart from a large reduction in temperature variability over the Arctic Ocean, the atmospheric variability response was also found to be weak, but in general was found to decrease. Many aspects of the atmospheric circulation response to sea ice loss were found to be opposed by the response to warming at low-latitudes resulting in very little response to projected greenhouse gas increases. Finally, ocean coupling was found to enhance the circulation response to sea ice loss by allowing the extratropical ocean to warm.

Appendix

Comparison of the response to sea ice albedo forcing between CESM1 and CCSM4

SIA in the control simulations of CESM1 and CCSM4 (Fig. A1a) have similar amounts of sea ice in the annual mean but CESM1 has a larger amplitude seasonal cycle. In most months of the year, the response in SIA is larger in CESM1 than in CCSM4. The only months that do not show this are August and September, but this is only because there is less ice available to melt in the CESM1 control simulations during these months. In DJF, the CESM1 control simulation has slightly more ice, but the sea ice albedo forcing simulation has considerably more ice melt than CCSM4 (2.28 vs 1.17 million km^2 lost). Much of this difference comes in December when there is a 2 million km^2 difference in the amount of ice loss between the two models. All of these differences in the sea ice response between the two models are consistent with there being stronger shortwave feedbacks in CESM1 (Kay et al. 2012).

Arctic sea ice thickness (Fig. A1b) is similar in the two control simulations, but CESM1 has thinner sea ice throughout the summer and fall, consistent with greater downwelling surface shortwave radiation. The responses in both models involves approximately 0.5 m thinning throughout most of the year, but an increase in thickness in late summer when all but the thickest ice near the North coast of Greenland and the Canadian Arctic Archipelago has melted. This peak in ice thickness in the sea ice albedo forcing simulation is shifted a month earlier in CESM1 because the ice melts faster and then by September even the thickest ice has been able to thin to about 0.5 m.

The control simulation's seasonal cycle of Arctic 2-meter temperature (averaged from 65°N-90°N, Fig. A1c) is colder in CESM1 than in CCSM4 in the control simulation, particularly in DJF. Under sea ice albedo forcing simulations, however, the two models show similar Arctic temperatures in DJF. This is associated with approximately 70% more warming in CESM than in CCSM4 (5.8°C vs 3.3°C), which is consistent with the sea ice response. Both models have qualitatively similar seasonal cycles in surface heat flux response (Fig. A2), but CESM1 generally has a larger response, consistent with the sea ice and temperature responses. In June,

when the shortwave response is strongest, CESM1 has about 100% more shortwave absorbed at the surface (note that the shortwave response is multiplied by 0.1).

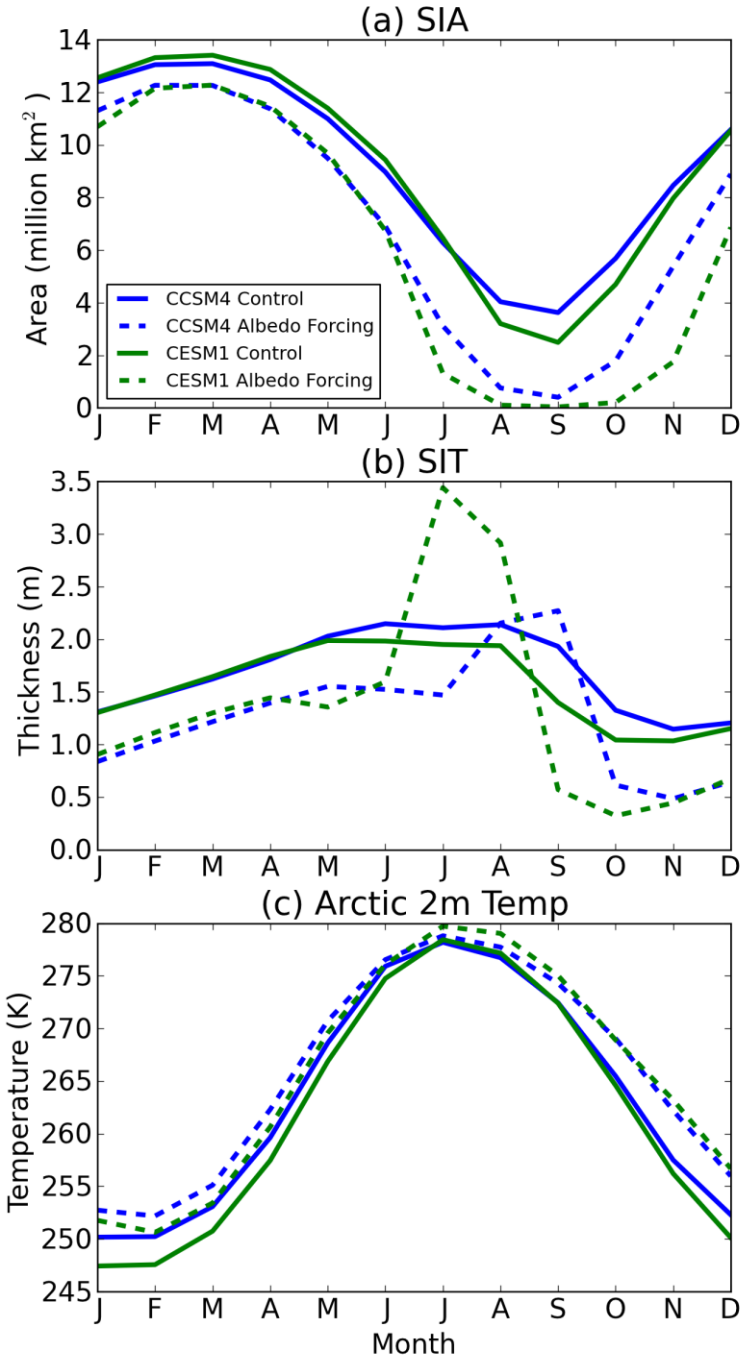

Figure A1: (a) The seasonal cycle of SIA (10^6 km^2) for the control (solid) and sea ice albedo forcing simulations(dashed) in CCSM4 (blue) and CESM1 (green). (b) As in (a) but for SIT (m). (c) as in (a) but for Arctic 2 meter temperature(°C) averaged from 65°N to 90°N.

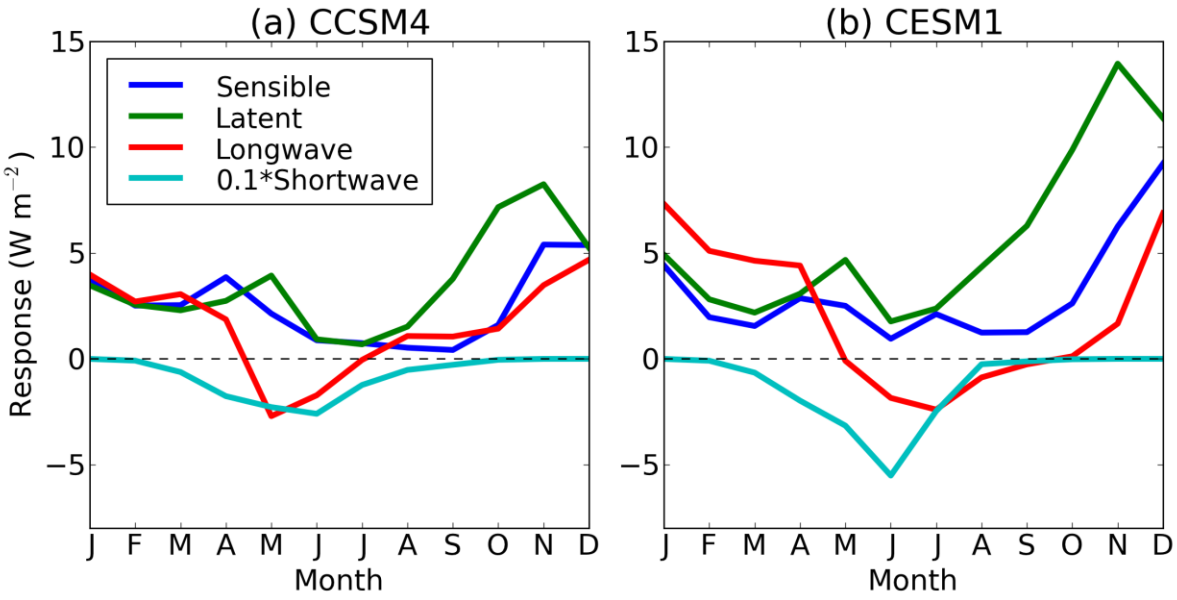

Figure A2. (a) The seasonal cycle of the sensible (blue), latent (green), longwave (red) and shortwave (cyan) heatflux (W m^{-2}) response (sea ice albedo forcing minus control) for CCSM4. The shortwave response is multiplied by 0.1. This reproduces Figure 3a in Blackport and Kushner (2016). (b) As in (a) but for CESM1.

References

Alexander, M.A., U.S. Bhatt, J.E. Walsh, M.S. Timlin, J.S. Miller, and J.D. Scott, 2004: The atmospheric response to realistic Arctic sea ice anomalies in an AGCM during winter. *J. Climate*, **17**, 890-905.

Bader, J., M. Flugge, N.G. Kvamsto, M.D.S. Mesqauita, and A. Voigt, 2013: Atmospheric winter response to a projected future Antarctic sea-ice reduction: a dynamical analysis. *Clim. Dyn.*, **40,** 0:2707–2718.

Barnes, E.A., 2013: Revisiting the evidence linking Arctic amplification to extreme weather in midlatitudes. *Geophys. Res. Lett*., **40**, 4734-4739, doi: 10.1002/grl.50880.

Barnes, E.A. and J.A. Screen, 2015: The impact of Arctic warming on the midlatitude jet-stream: Can it? Has it? Will it? *WIREs Clim Change* 2015, **6**, 277–286, doi: 10.1002/wcc.337.

Barnes E.A. and L.M. Polvani, 2015: CMIP5 Projections of Arctic Amplification, of the North American/North Atlantic Circulation, and of Their Relationship. *J. Climate*, **28**, 5254-5271, DOI: 10.1175/JCLI-D-14-00589.1

Blackport, R and P. J. Kushner, 2016: The Transient and Equilibrium Climate Response to Rapid Summertime Sea Ice Loss in CCSM4. *J. Climate*, **29**, 401–417. DOI: 10.1175/JCLI-D-15-0284.1

Butler, A. H., D. W. J. Thompson, and R. Heikes, 2010: The steady-state atmospheric circulation response to climate change–like thermal forcings in a simple general circulation model. *J. Climate*, **23**, 3474–3496, doi: 10.1175/2010JCLI3228.1.

Chiang J.C.H., and C.M. Bitz, 2005: Influence of high latitude ice cover on the marine Intertropical Convergence Zone. *Clim. Dyn*. **25**, 477-496. DOI 10.1007/s00382-005-0040-5

Cohen, J. and Coauthors, 2014: Recent Arctic amplification and extreme mid-latitude weather. *Nat. Geosci.*, **7**, 627-637, doi: 10.1038/NGEO2234.

Coumou, D., V. Petoukhov, S. Rahmstorf, S. Petri, and H.J. Schellnhuber, 2014: Quasi-resonant circulation regimes and hemispheric synchronization of extreme weather in boreal summer. *Proc. Natl. Acad. Sci.*, **111**, 12331-12336, doi: 10.1073/pnas.1412797111.

Coumou, D., J. Lehmann, and J. Beckmann, 2015: The weakening summer circulation in the Northern Hemisphere mid-latitudes. *Science*, **348**, 324-327, doi:10.1126/science.1261768

Cvijanovic, I. and K. Caldeira, 2015: Atmospheric impacts of sea ice decline in CO2 induced global warming. *Clim. Dyn.*, **44**, 1173-1186 doi:10.1007/s00382-015-2489-1.

Deser, C., G. Magnusdottir, R. Saravanan, and A. Phillips, 2004: The effects of North Atlantic SST and sea ice anomalies on the winter circulation in CCM3, Part II: Direct and indirect components of the response. *J. Climate*, **17**, 877-889.

Deser, C., R. Tomas, M. Alexander, and D. Lawrence, 2010: The Seasonal Atmospheric Response to Projected Arctic Sea Ice Loss in the Late Twenty-First Century. *J. Climate*, **23**, 333-351. doi: 10.1175/2009JCLI3053.

Deser, C., R. A. Tomas, and L. Sun, 2015: The role of ocean-atmosphere coupling in the zonal-mean atmospheric response to Arctic sea ice loss. *J. Climate*, **28**, 2168-2186.

Deser, C., L. Sun, R. A. Tomas, and J. Screen, 2016: Does ocean coupling matter for the northern extratropical response to projected Arctic sea ice loss? *Geophys. Res. Lett*., **43**, doi:10.1002/ 2016GL067792

Eade, R., D. Smith, A. Scaife, E. Wallace, N. Dunstone, L. Hermanson, and N. Robinson, 2014: Do seasonal-todecadal climate predictions underestimate the predictability of the real world? *Geophys. Res. Lett*., **41**, 5620–5628, doi:10.1002/2014GL061146.

Eisenman, I., 2010: Geographic muting of changes in the Arctic sea ice cover, *Geophys. Res. Lett*., **37**, L16501, doi:10.1029/2010GL043741.

Feldstein, S. B. and S. Lee, 2014: Intraseasonal and Interdecadal Jet Shifts in the Northern Hemisphere: The Role of Warm Pool Tropical Convection and Sea Ice, *J. Climate*, **27**, 6497-6518.

Forster, P.M., and Coauthors, 2011: Stratospheric changes and climate, Chapter 4 in *Scientific Assessment of Ozone Depletion: 2010*, Global Ozone Research and Monitoring Project-Report No. 52, 516 pp., World Meteorological Organization, Geneva, Switzerland.

Francis, J. A., and S. J. Vavrus, 2012: Evidence linking Arctic amplification to extreme weather in midlatitudes. *Geophys. Res. Lett.*, **39**, L06801, doi: 10.1029/2012GL051000.

Francis, J. A., and S. J. Vavrus, 2015: Evidence for a wavier jet stream in response to rapid Arctic warming, *Environ. Res. Lett.*, **10**, 014005, doi: 10.1088/1748-9326/10/1/014005.

Gastineau, G., F. D'Andrea, and C. Frankignoul, 2013: Atmospheric response to the North Atlantic Ocean variability on seasonal to decadal time scales, *Clim. Dyn*., **40**, 2311–2330, doi:10.1007/s00382-012-1333-0.

Gent, P. R., and Coauthors, 2011: The Community Climate System Model version 4. *J. Climate*, **24**, 4973–4991, doi:10.1175/2011JCLI4083.1.

Graversen R.G., M. Wang ,2009**:** Polar amplification in a coupled climate model with locked albedo. *Clim. Dyn.* **33**, 629-643. doi:10.1007/s00382-009-0535-6

Harvey, B. J., L. C. Shaffrey, and T. J. Woollings, 2014: Equator-to- pole temperature differences and the extra-tropical storm track responses of the CMIP5 climate models. *Clim. Dyn*., **43**, 1171–1182, doi: 10.1007/s00382-013-1883-9.

Harvey, B. J., L. C. Shaffrey, and T. J. Woollings, 2015: Deconstructing the climate change response of the Northern Hemisphere wintertime storm tracks. *Clim. Dyn*., **45**, 2847-2860 doi:10.1007/s00382-015-2510-8.

Hassanzadeh, P., Z. Kuang, and B. F. Farrell, 2014: Responses of mid-latitude blocks and wave amplitude to changes in the meridional temperature gradient in an idealized dry GCM. *Geophys. Res. Lett*., **41**, 5223–5232, doi: 10.1002/2014GL060764.

Hassanzadeh, P., and Z. Kuang, 2015: Blocking variability: Arctic amplification versus Arctic oscillation, *Geophys. Res. Lett*., **42**, 8586–8595, doi:10.1002/2015GL065923.

Holland, M. M., and C. M. Bitz, 2003: Polar amplification of climate change in coupled models. *Clim. Dyn*., **21**, 221–232, doi: 10.1007/s00382-003-0332-6.

Honda, M., J. Inoue, and S. Yamane, 2009: Influence of low Arctic sea ice minima on anomalously cold Eurasian winters. *Geophys. Res. Lett*., **36**, L08707, doi: 10.1029/2008GL037079.

Hunke, E. C., and W. H. Lipscomb, 2008: CICE: The Los Alamos sea ice model, documentation and software, version 4.0. Los Alamos National Laboratory Tech. Rep. LA-CC-06-012, 76 pp.

Hurrell, J.W. and coauthors, 2013: The Community Earth System Model: A Framework for Collaborative Research. *Bull. Amer. Meteor. Soc*., **94** 1339-1360, doi: 10.1175/BAMS-D-12-00121

Inoue, J., M.E. Hori, and K. Takaya, 2012: The Role of Barents Sea Ice in the Wintertime Cyclone Track and Emergence of a Warm-Arctic Cold-Siberian Anomaly. *J. Climate*, **25**, 2561-2568, doi: 10.1175/JCLI-D-11-00449.1.

Katz, R. and, B. G Brown, 1992: Extreme events in a changing climate: Variability is more important than averages. *Clim. Change*, **21**, 289-302.

Kay, J.E., M.M. Holland, C.M. Bitz, E. Blanchard-Wrigglesworth, A. Gettelman, A. Conley, and D. Bailey, 2012: The Influence of Local Feedbacks and Northward Heat Transport on the Equilibrium Arctic Climate Response to Increased Greenhouse Gas Forcing. *J. Climate*, **25**, 5433–5450. doi: 10.1175/JCLI-D-11-00622.1

Kay, J.E., and coauthors, 2015: The Community Earth System Model (CESM) Large Ensemble Project: A Community Resource for Studying Climate Change in the Presence of Internal Climate Variability. *Bull. Amer. Meteor. Soc*., **96**, 1333-1349. doi: 10.1175/BAMS-D-13-00255.1

Kidston, J., A.S. Taschetto, D.W.J. Thompson and M.H. England, 2011: The influence of Southern Hemisphere sea-ice extent on the latitude of the mid-latitude jet stream. *Geophys Res Lett*, **38**, L15804. doi: 10.1029/2011GL048056

Kim, B.M., S.W. Son, S.K. Min, J.H. Jeong, S.J. Kim, X.D. Zhang, T. Shim, and J.H Yoon, 2014: Weakening of the stratospheric polar vortex by Arctic sea ice loss. *Nat. Commun*., **5**, 4646. doi: 10.1038/ncomms5646.

King, M.P., M. Hell, and N. Keenlyside, 2015: Investigation of the atmospheric mechanisms related to the autumn sea ice and winter circulation link in the Northern Hemisphere. *Clim. Dyn*. doi:10.1007/s00382-015-2639-5.

Laîné, A., M. Yoshimori, and A. Abe-Ouchi, 2016: Surface Arctic amplification factors in CMIP5 models: land and oceanic surfaces and seasonality. *J. Climate*, **29**, 3297-3316, doi:10.1175/JCLI-D-15-0497.1.

Laliberte, F. and P.J. Kushner, 2013: Isentropic constraints by midlatitude surface warming on the Arctic midtroposphere. *Geophys. Res. Lett.*, **40**, 606-611, doi: 10.1029/2012GL054306.

Laliberte, F. and P.J. Kushner, 2014: Midlatitude Moisture Contribution to Recent Arctic Tropospheric Summertime Variability. *J. Climate*, **27**, 5693-5707, doi: 10.1175/JCLI-D-13-00721.1.

Laxon, S. W., and Coauthors, 2013: CryoSat-2 estimates of Arctic sea ice thickness and volume. *Geophys. Res. Lett*., **40** , 732–737, doi:10.1002/grl.50193.

Liptak, J. and C. Strong, 2014: The Winter Atmospheric Response to Sea Ice Anomalies in the Barents Sea. *J. Climate.* **27**, 914-924, doi:10.1175/JCLI-D-13-00186.1

Liu, J., J.A. Curry, H. Wang, M. Song and R.M. Horton, 2012: Impact of declining Arctic sea ice on winter snowfall. *Proc. Natl. Acad. Sci.*, **109**, 4074–4079, doi: 10.1073/pnas.1114910109.

Liu, J.P., M.R. Song, R.M. Horton and Y.Y. Hu, 2013: Reducing spread in climate model projections of a September ice-free Arctic. *Proc. Natl. Acad. Sci*., **110**, 12571-12576.

Meehl, G. A., and Coauthors, 2012: Climate system response to external forcings and climate change projections in CCSM4. *J. Climate,* **25**, 3661–3683.

Magnusdottir, G., C. Deser and R. Saravanan, 2004: The effects of North Atlantic SST and sea ice anomalies on the winter circulation in CCM3, Part I: Main features and storm-track characteristics of the response. *J. Climate*, **17**, 857-876.

Mahlstein, I. and R. Knutti, 2012: September Arctic sea ice predicted to disappear near 2°C global warming above present. *J. Geophys. Res.* , **117**, D06104, doi:10.1029/2011JD016709.

Manzini, E., and Coauthors 2014: Northern winter climate change: Assessment of uncertainty in CMIP5 projections related to stratosphere-troposphere coupling, *J. Geophys. Res. Atmos*., **119**, 7979–7998, doi:10.1002/2013JD021403.

Mori, M., M. Watanabe, H. Shiogama, J. Inoue, And M. Kimoto 2014: Robust Arctic sea ice influence on the frequent Eurasian cold winters in past decades, *Nat. Geosci.*, **7**, 869–873, doi:10.1038/ngeo2277.

Morrison, H., and A. Gettelman, 2008: A new two-moment bulk stratiform cloud microphysics scheme in the NCAR Community Atmosphere Model (CAM3). Part I: Description and numerical tests. *J. Climate*, **21**, 3642–3659.

Mudryk, L.R. and P.J. Kushner, 2011: A method to diagnose sources of annular mode time scales. *J. Geophys. Res. Atmos*., **116**, D14114, doi: 10.1029/2010JD015291

Nakamura, T., K. Yamazaki, K. Iwamoto, M. Honda, Y. Miyoshi, Y. Ogawa, and J. Ukita, 2015:, A negative phase shift of the winter AO/NAO due to the recent Arctic sea ice reduction in late autumn. *J. Geophys. Res. Atmos*., **120**, 3209–3227, doi:10.1002/ 2014JD022848.

Nakamura, T., K. Yamazaki, K. Iwamoto, M. Honda, Y. Miyoshi, Y. Ogawa, Y. Tomikawa, and J. Ukita ,2016: The stratospheric pathway for Arctic impacts on midlatitude climate. *Geophys. Res. Lett*., **43**, 3494–3501, doi:10.1002/2016GL068330.

Neale, R. B. J. Richter, S. Park, P. H. Lauritzen, S. J. Vavrus, P. J. Rasch, and M. Zhang, 2013: The mean climate of the Community Atmosphere Model (CAM4) in forced SST and fully coupled experiments. *J. Climate*, **26**, 5150 –5168.

Newson, R. L. Response of a general circulation model of the atmosphere to removal of Arctic ice-cap, 1973: *Nature*, **241,** 39-40, doi: 10.1038/241039b0

Oleson, K. W., and Coauthors, 2010: Technical description of version 4.0 of the Community Land Model (CLM). NCAR Tech. Note NCAR/TN-478+STR, 257 pp.

Orbe, C., P. A. Newman, D. W. Waugh, M. Holzer, L. D. Oman, F. Li, and L. M. Polvani, 2015: Airmass origin in the Arctic. Part I: Seasonality. *J. Climate,* **28**, 4997–5014, doi:10.1175/JCLI-D-14-00720.1.

Overland, J.E. and M. Wang, 2013: When will the summer Arctic be nearly sea ice free? *Geophys. Res. Lett*., **40**, 2097–2101, doi:10.1002/grl.50316.

Peings, Y. and G. Magnusdottir, 2014: Response of the Wintertime Northern Hemisphere Atmospheric Circulation to Current and Projected Arctic Sea Ice Decline: A Numerical Study with CAM5. *J. Climate,* **27**, 244-264, doi: 10.1175/JCLI-D-13-00272.1

Petoukhov, V. and V. Semenov, 2010: A link between reduced Barents- Kara sea ice and cold winter extremes over northern continents. *J. Geophys. Res*., **115**, D21111, doi: 10.1029/2009JD013568.

Rahmstorf, S., J.E. Box, G. Feulner, M.E. Mann, A. Robinson, S. Rutherford, and E.J. Schaffernicht, 2015: Exceptional twentieth-century slowdown in Atlantic Ocean overturning circulation. *Nat. Clim. Change,* **5**, 475–480 doi: 10.1038/NCLIMATE2554

Santer, B. D., T. M. L. Wigley, M. E. Schlesinger, and J. F. B. Mitchell, 1990: Developing climate scenarios from equilibrium GCM results. MPI Rep. 47, 29 pp.

Schneider, T., T. Bischoff, and H. Plotka, 2015: Physics of changes in synoptic midlatitude temperature variability. *J. Climate,* **28**, 2312-2331.

Schweiger, A., R. Lindsay, J. L. Zhang, M. Steele, H. Stern, and R. Kwok, 2011: Uncertainty in modeled Arctic sea ice volume. *J. Geophys*. Res., **116**, C00D06, doi:10.1029/2011JC007084.

Scinocca, J. F., M.C. Reader, D.A. Plummer, M. Sigmond, P.J Kushner, T.G. Shepherd and A.R. Ravishankara, 2009: Impact of sudden Arctic sea ice loss on stratospheric polar ozone recovery. *Geophys. Res. Lett*., **36**, L24701, doi: 10.1029/2009GL041239.

Screen, J.A., and I. Simmonds, 2010: The central role of diminishing sea ice in recent Arctic temperature amplification. *Nature*, **464**, 1334–1337, doi: 10.1038/nature09051

Screen, J.A., C. Deser and I. Simmonds, 2012: Local and remote controls on observed Arctic warming. *Geophys. Res. Lett*., **39**, L10709, 10.1029/2012GL051598.

Screen, J.A., I. Simmonds, C. Deser and R. Tomas, 2013: The atmospheric response to three decades of observed Arctic sea ice loss. *J. Climate*, **26**, 1230-1248, 10.1175/JCLI-D-12-00063.1.

Screen, J.A. and I. Simmonds, 2013: Exploring links between Arctic amplification and mid-latitude weather. *Geophys. Res. Lett*., **40**, 959–964, doi:10.1002/grl.50174.

Screen, J.A., C. Deser, I. Simmonds and R. Tomas, 2014: Atmospheric impacts of Arctic sea ice loss, 1979-2009: separating forced change from atmospheric internal variability. *Clim. Dyn*., **43**, 333-334, doi: 10.1007/s00382-013-1830-9

Screen, J.A., 2014: Arctic amplification decreases temperature variance in northern mid- to high-latitudes. *Nat. Clim. Change*, **4**, 577-582, doi: 10.1038/nclimate2268

Screen, J.A. and I. Simmonds, 2014: Amplified mid-latitude planetary waves favour particular regional weather extremes. *Nat. Clim Change*, **4**, 704–709, doi:10.1038/nclimate2271.

Screen, J.A., C. Deser and L. Sun, 2015: Reduced risk of North American cold extremes due to 720 continued sea ice loss. *Bull. Amer. Met. Soc.*, **96**, 1489–1503, doi:10.1175/BAMS-D-14-00185.1.

Screen, J.A., J. A. Francis, 2016: Contribution of sea-ice loss to Arctic amplification regulated by Pacific Ocean decadal variability, *Nat. Clim. Change.*, doi:10.1038/nclimate3011

Seierstad, I.A., and J. Bader, 2009: Impact of a projected future Arctic Sea Ice reduction on extratropical storminess and the NAO. *Clim. Dyn.* **33**, 937–943. doi: 10.1007/s00382-008-0463x

Serreze, M. C., and A. P. Barrett, 2008: The summer cyclone maximum over the Central Arctic Ocean, *J. Climate*., **21**, 1048–1065.

Smith, R. D., and Coauthors, 2010: The Parallel Ocean Program (POP) reference manual: Ocean component of the Community Climate System Model (CCSM) and Community Earth System Model (CESM). Los Alamos National Laboratory Tech. Rep. LAUR-10-01853, 141 pp.

Snape, T. J., and P. M. Forster, 2014: Decline of Arctic sea ice: Evaluation and weighting of CMIP5 projections, *J. Geophys. Res. Atmos*., **119**, 546–554, doi:10.1002/2013JD020593.

Stocker, T., and Coauthors ,2013: Climate Change 2013: The Physical Science Basis. Contribution of Working Group I to the Fifth Assessment Report of the Intergovernmental Panel on Climate Change. Cambridge University Press, Cambridge, United Kingdom and New York, NY, USA

Stroeve, J.C., V. Kattsov, A. Barrett, M. Serreze, T. Pavlova, M. Holland and W.N. Meier, 2012: Trends in Arctic sea ice extent from CMIP5, CMIP3 and observations. *Geophys. Res. Lett*., **39**, L16502, doi: 10.1029/ 2012GL052676.

Strong, C., G. Magnusdottir, and H. Stern, 2009: Observed feedback between winter sea ice and the North Atlantic Oscillation. *J. Climate*, **22**, 6021–6032, doi:10.1175/2009JCLI3100.1.

Sun, L., C. Deser and R. A. Tomas, 2015: Mechanisms of stratospheric and tropospheric circulation response to projected Arctic sea ice loss. *J. Climate*, **28,** 7824-7845 DOI: 10.1175/JCLI-D-15-0169.1

Sun, L., J. Perlwitz, and M. Hoerling ,2016: What caused the recent "Warm Arctic, Cold Continents" trend pattern in winter temperatures*?, Geophys. Res. Lett.*, **43**, doi:10.1002/2016GL069024.

Tebaldi, C., and J. M. Arblaster, 2014: Pattern scaling: a review of its strengths and 6 limitations, and an update on the latest model simulations. *Clim. Change*, **122**, 3, 459-471.

Thompson, D. W. J., and J. M. Wallace, 1998: The arctic oscillation signature in the wintertime geopotential height and temperature fields. *Geophys. Res. Lett.*, **25**, 1297-1300.

Tomas, R.A., C. Deser, and L.Sun. 2016: The role of ocean heat transport in the global climate response to projected Arctic sea ice loss. *J. Climate*, in press.

Turner, J., J. S. Hosking, T. J. Bracegirdle, G. J. Marshall, and T. Phillips, 2015: Recent changes in Antarctic sea ice, *Philos. Trans. R. Soc. A*, **373**, 20140163, doi:10.1098/rsta.2014.0163.

Vavrus, S. J., M. M. Holland, A. Jahn, D. A. Bailey, and B. A. Blazey, 2012: Twenty-first-century Arctic climate change in CCSM4. *J. Climate*, **25**, 2696–2710.

Walker, G. T., and E. W. Bliss, 1932: *World Weather V. Mem. Roy. Meteor. Soc*., **4**, 53-84

Wallace, J. M., and D. S. Gutzler, 1981: Teleconnections in the geopotential height field during the Northern Hemisphere winter. *Mon. Wea. Rev*., **109**, 784-812.

Watt-Meyer, O. and P. J. Kushner, 2015: Decomposition of atmospheric disturbances into standing and traveling components, with application to Northern Hemisphere planetary waves and stratosphere-troposphere coupling. *J. Atmos. Sci*., **72**, 787-802.

Winton, M., 2011: Do climate models underestimate the sensitivity of Northern Hemisphere sea ice cover? *J. Climate*, **24**, 3924–3934.

Wu, Y., and K. L. Smith, 2016: Response of Northern Hemisphere midlatitude circulation to Arctic amplification in a simple atmospheric general circulation model. *J. Climate* , **29**, 2041–2058, doi:10.1175/JCLI-D-15-0602.1.